UNIVERSITY OF WASHINGTON
College of Engineering
DEPARTMENT OF CIVIL ENGINEERING

and

PHOTOGRAMMETRIC BRANCH
WASHINGTON STATE DEPARTMENT OF HIGHWAYS

COOPERATIVE PHOTOGRAMMETRIC STUDY

Final Technical Report
Research Report 16.1
1974

Prepared by

S. A. Veress D.Sc., Principal Investigator
A. A. Aramaki M.S., Research Assistant
J. K. Hall M.S., Research Assistant
and
T. Takamoto M.S., Research Assistant

Research conducted for Washington State Highway Commission, Department of Highways, in cooperation with U.S. Department of Transportation - Federal Highway Administration, under Agreement No. Y-1431.

The Project was developed and carried out as a cooperative study. The field work and logistic support was done by the Photogrammetric Branch, Washington State Department of Highways, under the supervision of Mr. D. A. Yates.

The opinions, findings and conclusions expressed in this publication are those of the authors and not necessarily those of the Washington State Highway Department or Federal Highway Administration.

TECHNICAL REPORT STANDARD TITLE PAGE

1. Report No.	2. Government Accession No.	3. Recipient's Catalog No.

4. Title and Subtitle

COOPERATIVE PHOTOGRAMMETRIC STUDY

5. Report Date

6. Performing Organization Code

7. Author(s)

S.A. Veress; A.A. Aramaki; J.K. Hall;
T. Takamoto, of University of Washington

8. Performing Organization Report No.

9. Performing Organization Name and Address

University of Washington, Seattle, Washington 98195

Washington State Highway Department
Photogrammetric Branch, Tumwater, Washington 98504

10. Work Unit No.

11. Contract or Grant No.
Y-1431

12. Sponsoring Agency Name and Address

Washington State Highway Commission
Department of Highways, Highway Administration Bldg.
Olympia, Washington 98504

13. Type of Report and Period Covered
Final Report

14. Sponsoring Agency Code

15. Supplementary Notes

This study was conducted in cooperation with the U.S. Department of Transportation, Federal Highway Administration.

16. Abstract

This research project was to evaluate the different variables in photogrammetric practice, which include targeting, film and development process, camera platform and achievable accuracy.

Design criteria and standards have been established, which include the manufacturing of camera suspension for helicopter from both a theoretical and practical point of view.

The testing of these standards and design criteria includes a large number of data. Thus, they have a high statistical probability of being correct.

The project has proved that an all-time photography is possible with the proper selection of camera platform, and that the use of very low flight photography will enable the Highway Department to extend the use of photogrammetric measurement.

17. Key Words	18. Distribution Statement
helicopter, camera suspension, target, shutter, vibration, accuracy, air speed, residual errors	

19. Security Classif. (of this report)	20. Security Classif. (of this page)	21. No. of Pages	22. Price
unclassified	unclassified	146	

Form DOT F 1700.7 (8-69)
HWY FORM 341-004 6/72

TABLE OF CONTENTS

LIST OF FIGURES

page

LIST OF TABLES

ABSTRACT

The purpose of the research project was to evaluate the different variables in photogrammetric practice. These variables include targeting, film and development process, camera platform and achievable accuracy.

Design criteria and standards have been established. The design criteria include the manufacturing of camera suspension for helicopter from both a theoretical and practical point of view.

The testing of these standards and design criteria includes a large number of data. Thus, they have a high statistical probability of being correct.

The project has proved that an all-time photography is possible with the proper selection and design of camera platforms, and that the use of very low flight photography will enable the Highway Department to extend the use of photogrammetric measurement.

CONCLUSIONS AND RECOMMENDATIONS

It was found during the course of this research that the resolution in general, and the dynamic resolution in particular, are adequate to use for evaluation of a photogrammetric system. It is recognized that the resolution is largely dependent on the type of target used, and thus it is difficult to make uniform for all the Departments of Highways. In spite of this disadvantage, the use of resolution is suggested for the following reasons: 1) the system is uniform within an organization; 2) no special instrument is required for evaluation; and 3) a fairly reliable comparison system is provided among various organizations.

Considering the various types of aircraft as camera platforms, it was concluded that the helicopter and the fixed-wing aircraft are complementary rather than competitive to each other. The effect of the vibration of these aircraft can be minimized and partially eliminated by proper design of the camera suspension system; i.e., the camera mounting system must have a natural frequency much lower than the disturbing frequency supplied by the camera platform (helicopter) and the damping factor must be large. The design criteria and methods are given in the text. With a properly designed camera suspension system it is possible to achieve a minimum shutter speed of 1/60 sec., as compared to the theoretical 1/50 sec. The recommended minimum shutter speed for practical work is 1/100 sec.

The photographic process and proper exposure time have a major influence on the achievable accuracy. These influences are found to be considerably larger than in any research reported earlier. It was found that the exposure level, in the region of underexposure, is the primary factor influencing the achievable accuracy. This influence is so pronounced that the phenomenon was investigated by using the modulation transfer function. The final

conclusion drawn is that the use of proper exposure and processing are more important than the resolution of the film used. Thus the film to be used must be selected so that its sensitivity will provide the proper exposure level.

A variety of targets were constructed and it was found that the circular target provides the best results. Some of the targets were constructed so that they would serve for photographs taken at various elevations. These targets were regarded as multiple-purpose targets. It has been found that the multiple-purpose targets will not provide the expected accuracy unless they are designed for photographs of considerable scale difference. For example, one can design common targets for a 1" = 50' and 1" = 150' photographic scale (that is, for three times of scale difference), but any intermediate scale is not advisable. The design criteria for such targets are given in the text.

The standard for design of flight for various speeds has been determined and a chart has been developed. The design chart has been tested for helicopter as well as for fixed-wing aircraft and found to be correct. Therefore, its use is recommended.

During the course of research it was found that a reliable relationship can be obtained by expressing the achievable accuracy as a function of resolution. The relationship is a polynomial one. Its constant should be determined by the individual organizations. The polynomial function is found to be correct only at the proper exposure level. If the exposure level falls below that recommended, the relationship is disturbed by the fact that the major influence is shifted from the resolution to the exposure level.

In summary, during the research a number of parameters were examined. A set of procedures has resulted concerning the proper determination of

various parameters. If one takes these parameters and their standards, a proper specification of photogrammetric work can be obtained which covers all the phases of work at the Department of Highways.

INTRODUCTION

Doyle (1960) pointed out, "Whenever one puts together a camera in a mount in an aircraft, one has a system." This is partially true in the engineering use of photogrammetry where a wide variety of problems and purposes should be solved and satisfied.

Large scale photography (1/600 - 1/2,000) and its various applications are being used to a larger extent today than ever before: the highway engineer uses large scale photography for volume determinations on construction projects, highway pavement and retaining wall deformations, and bridge and landslide monitoring; the forest engineer uses it for tree volume estimates; the hydrographic engineer employs it in charting shorelines, reefs, and shoals; the geological engineer finds it useful for identifying soil and rock types; and the urban planning engineer uses it for traffic studies, property assessment, and general planning and development. These are but a few of the many possible applications of large scale photography.

For the photogrammetric engineer concerned with large scale photography, one of the major problems is that this type of photography necessitates relatively low altitude flying. However, the conventional airplane is restricted by the Federal Aviation Administration to a minimum flying height of 1,000 feet for congested areas, and to a relatively high speed, which causes large image motion distortions on the photograph under these conditions. Thus, with the conventional aircraft, the large scale and quality photographic reproduction which is desired may not be mutually possible. The helicopter, on the other hand, due to its lower flying height allowances under the F.A.A. regulations, and slow speed capabilities

(which extends to hovering), would seem to be the logical aerial platform for this large scale photography.

A study of the current literature on helicopter photography applied to photogrammetry indicates that only limited research has been conducted in this field. Research has been conducted by R. N. Colwell (1956), F. B. Robison and L. I. Withem (1967), W. H. Scott (1968), and O. W. Cheffins (1969), on single camera mount helicopter systems; while G. Avery (1956) and E. H. Lyons (1961 and 1964) have done research on twin camera mount systems. Possibly, the relatively high cost of helicopter flights has deterred researchers and private industries from a wider use of the helicopter for aerial photography applications. In many cases, though, high accuracy and fine quality from large scale photography necessitates the consideration of an aerial platform such as a helicopter. Thus, more research in this field of helicopter photography is needed to define the limitations and use characteristics.

There has been practically no research study concerning the helicopter as an aerial platform being complementary, rather than competitive, to the fixed-wing aircraft. The comparison must be made on achievable accuracy and feasible economy.

1.0 BACKGROUND STUDIES

1.1 The Colwell Study

One of the first attempts at using the helicopter system, however, was done by R. N. Colwell, published in Photogrammetric Engineering, September, 1956, and entitled "The Taking of Helicopter Photography for Use in Photogrammetric Research and Training."

The primary concern was with the taking of still photographs, and the feasibility of the helicopter for this specialized role. There was no emphasis placed on the analysis of photographic quality obtained.

The helicopter chosen was the Hiller, Model HTE-2, and the camera, a K-17 aerial camera with focal length of 12 inches. A camera mounting system was not even attempted; the aerial camera was hand held during exposure. It was felt that in this way image blur due to aircraft vibration might be minimized. The qualitative results of this method proved acceptable.

1.2 The Robison and Withem Study

F. B. Robison and L. I. Withem published "Helicopter Photography and Mapping" in Photogrammetric Engineering, October, 1967, describing their experimentation in this field dating back to 1963. The primary criterion for this analysis was to bring vertical error into the hundredths place.

The first step was in picking a helicopter, with the Bell J-2 chosen. The Wild RC-8 camera formed the second part of the system, as its universality of use and camera control placements makes it quite readily adaptable. The camera was then attached to the frame through the vibration-dampening mounts. This set-up is similar to the initial system utilized in our project.

The methodology following was primarily an attempt to determine only the feasibility of helicopter photography. No attempt was made to correlate any of the numerous variables, but only to determine the typical accuracy that might result from this form of system.

The initial flight was in 1964 under overcast skies, which is somewhat less than optimum conditions. Flying heights were 300, 600 and 900

feet, with flying speed slightly under 25 m.p.h. The conclusions reached were relative in nature: 5X enlargements of the 300-foot flying height photographs were "very sharp and showed no evidence of vibration transmitted to the camera."

The major concern was in compilation accuracy, rather than the maximum attainable accuracy that is sought in our project. As such, the following figures are based on instrumental rather than analytical methods, but still provide favorable results. The test figures are from a project done by the Photogrammetry Section of the California State Division of Highways.

Note from Table 1 the standard error of spot elevations on a bituminous surface. The value of ±0.084 feet is quite adequate for many applications, and is promising of better accuracies as further studies are made. The arithmetic mean has little value, however, in determining worth of the system.

Surface Type	Contours			Spot Elevations		
	No. of Points	Arithmetic Mean	Standard Error	No. of Points	Arithmetic Mean	Standard Error
Bitum	43	+.027	±.162	63	+.055	±.084
PCC	21	+.050	±.143	8	-.006	±.116
Dirt	87	-.033	±.245	48	+.009	±.111
Grass	22	-.034	±.149	59	+.001	±.094

Scale: 1" = 20'

Table 1. Accuracy Data, Robison and Withem.

One concern noted with the use of a helicopter was the rotational element. It proved very difficult to keep the helicopter at the correct altitude. A second problem was in holding a constant flying height. Both of these parameters must be kept in control for plotter applications. Their final conclusions were quite favorable, however, and predicted much wider utilization of this system in the future.

1.3 The Scott Study

An additional study was initiated as a result of the success of the attempt by Robison and Withem. It was entitled "Helicopter Photography" by William H. Scott, and published in Photogrammetric Engineering, September, 1968. The immediate objective of this project was mapping at a scale of 100 feet per inch with 5-foot contour intervals. The helicopter system was utilized due to a breakdown in their higher-altitude equipment. Further, they also evaluated the system flying as low as 300 feet.

The camera chosen for the helicopter was the Fairchild Cartographic camera. Orientation parameters did not become a paramount concern in their system. To overcome this problem, the camera controls were held fixed, and the altitude of the helicopter itself was adjusted by use of level bubbles in the cockpit to conform to the camera position. Initially, the camera was leveled relative to the ground. This method appears to keep the orientation values within the limits of the instrument used for plotting, a Kelsh plotter.

The average residual in this case is 0.8 feet, and corresponds to an accuracy of approximately 1:3750. Further, by taking the largest residual noted (1.5 feet), this amounts to only 30% of the mapped contour interval, and quite acceptable.

Of the lower flown helicopter flights, one in particular was done to a scale of 20 feet per inch, and accepted by the courts as an exhibit for an automobile accident case.

1.4 The Cheffins Study

The final system summarized was done by O. W. Cheffins, entitled "Accuracy of Heighting from Vertical Photography Obtained by Helicopter," and published in The Photogrammetric Record of London, England, dated October, 1969. The basic attempt here was to find the maximum achievable accuracy of height measurement obtainable by any photogrammetric means.

He notes that the largest feasible scale in civil engineering projects as being 1:500, with a minimum contour interval of 1 foot. These parameters have been accurately plotted by use of wide-angle photography in fixed-wing aircraft flying at 1500 feet. What if, however, contour plotting must be done to, say, 1 inch? This might be applicable to as-built surveys of roads and airport runways. The cost of ground surveys to this accuracy would be quite high, and in fact may not even be possible with conventional techniques.

The system utilized consisted of a Wild RC-8 survey camera, with a 150 mm focal length wide-angle Aviogon lens, mounted to a Bell J-2 helicopter. The isolaters consisted of four "Faireymounts," each comprising helical springs designed for low frequency/large amplitude vibrations. A series of models were designed with 60 per cent forward overlap and a flying height of 250 feet. Control points were on concrete, with measurement done by spirit leveling.

Instruments utilized for plotting were the Zeiss Stereoplanigraph C8 and the Wild Autograph A8. Absolute orientation was achieved by use of

five or six control points per model located on the perimeters of the respective test areas.

The mean square error ranged from 0.37 inches to 0.61 inches, or from 1/8,000 to 1/5,000 of flying height accuracy. Maximum errors were in the range of +1.08 inches to -1.32 inches. Out of the 490 photogrammetric height checks, only 8 were in error by more than one inch, or a proportion of 1.6 per cent.

The final conclusion reached by all mentioned articles, and particularly that by Cheffins, was to the positive future of the system. We also concur with their findings, and hope to establish some further quantitative approach to the various problem parameters involved in its use.

There has been no report in the literature on research or studies concerning the system approach to the helicopter and the fixed-wing aircraft, i.e., the two camera platforms being complementary to each other rather than competitive.

2.0 THE EVALUATION PROBLEM

Historically, the primary performance measurement for an optical system was the resolving power (l/mm). Today, the resolution as widely accepted by photogrammetrists is almost regarded as a fundamental quality parameter. Besides the above advantage, the measure of resolution requires minimum equipmentation because it allows one to measure the combined effect of various parameters: vibration, film performance, exposure, film processing, observer, etc. No other indicator covers this many aspects in one measurement. For these reasons, the resolution was chosen as a main unit of measurement of the results. It must be pointed out, however, that the

simplicity and the all-encompassing power of the resolution proves also to be the greatest drawback in its use.

The modulation transfer function (MTF) provides a more meaningful indicator of resolution than line-pairs per millimeter. The advantage of the MTF is that the effect of individual parameters can be evaluated. Perhaps even more importantly, this evaluation transcends the problem of human observer inaccuracies and becomes dependent on the established microdensitometer. Because of these advantages, part of the research is also evaluated by the use of MTF as a complementary system to the resolution.

2.1 Resolution

Historically, the primary performance measure for an optical system was resolving power (see Jensen, 1968). In the context of the photogrammetrist, this usually means noting the smallest group of bars of a resolution target on a photograph that appears separate and distinct. The reciprocal of the width of a line and space of this smallest group is then the resolution value of the photograph (see Figure 1). This concept is well accepted in practice, and is one of the foremost stipulators of a system's worth. But as with so many other good scientific definitions, there appears to be a major problem in putting resolution to work.

The foremost problem associated with resolution is in its standardization. It is dependent totally on the type of target used. When quoting resolution values, therefore, one must also stipulate all parameters that were involved in arriving at some particular value. As mentioned previously, this limits the useful results of a study to only that particular system, and adaptation to other systems is only possible with identical evaluations.

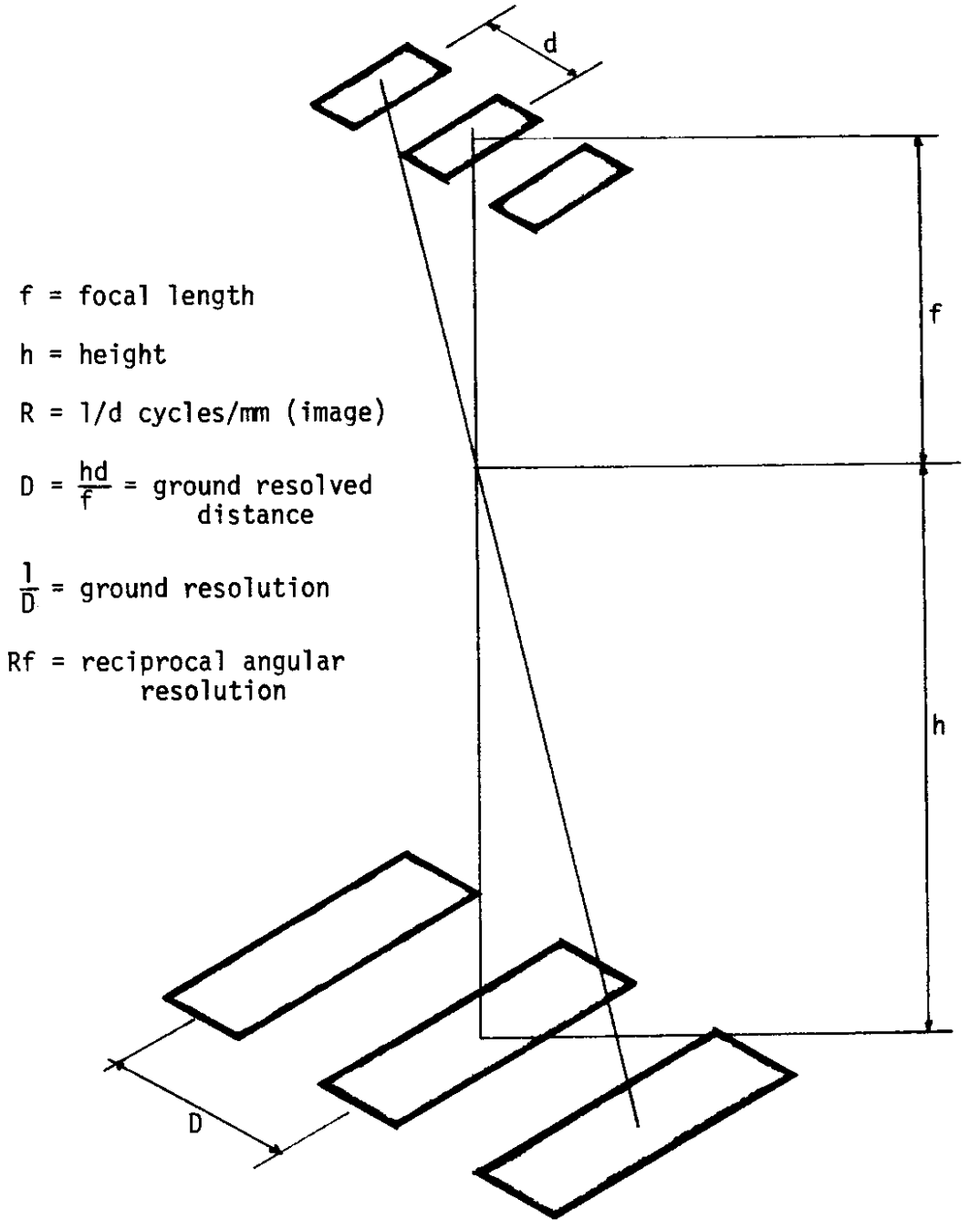

Figure 1. Defining resolution.

Phase I of this project includes a study of many of these parameters. The resolution values given in aerial camera calibration are essentially only guide lines in practice. They do show the trend of resolution decrease away from the center of the photograph, but the absolute numbers given are not applicable. The need for faster aerial films, particularly in aerial photography, greatly differs from the slow speed films utilized in calibration. Further, light scattering in the lens is much greater in practice (see Manual of Photogrammetry, 3rd Edition). In fact, there is even a difference due to artificial versus diffusely reflected sunlight. They also do not include the practical variables of vibration, image motion, atmospheric haze, and temperature differential.

The most obvious drawback associated with standardizing resolution is that of the human observer, who is a critical component of this approach. The measurement is made by the observer's ability to distinguish line pairs of the target. Whenever a human observer is given an opportunity to make this type of value judgment, all mathematical means of establishing absolute quantities are lost. Observations depend upon visual acuity, degree of visual astigmatism, personal judgment, and various other subjective criteria (see Rosenberg, 1971). This alone makes resolution a non-reproducible commodity.

A survey of the literature indicates that Carmen and Brown (1970) and Perrin and Altman (1953) advocate the use of an annular pattern for a resolution target. However, for this experiment the conventional three bar pattern would be more appropriate because the resolution number in this experiment is not an experimental variable, but is the prime criterion for judging a system's quality of reproduction; and, therefore, an accepted pattern which is widely used in practice today was desired. It should also

be mentioned that this resolution target was designed for the purpose of assigning a resolution number to a test photographic system containing the experimental variables (vibration, image motion, and photographic process), and to compare it with the resolution number of a ground control system in which the effect of the variables was minimized. Thus, it was not designed for calibration purposes; and, therefore, for economic and spatial reasons, the size of the bars and the spaces between them was varied from the largest group, of 95 lines/mm, by a factor of 2.5 lines/mm instead of the conventional sixths or fourth root of two, which would have involved more groups. Perrin and Altman (1953) showed that resolving power increases as the length-width ratio of the bars increases. Therefore it was necessary to maintain a constant length-width ratio for each group. The conventional length-width ratio is 5:1.

A numerical example for determining the resolution bar sizes at different scales is calculated as follows:

Given a resolution of 5 l/mm:

$$\text{space + bar width on photograph} = \frac{1}{\text{Resolution}} = 0.2 \text{ mm}$$

$$\text{space or bar width on a target for a scale of 1/600} = \frac{0.2}{2} \times 600 = 60 \text{ mm}$$

A resolution bar of this size, distinguishable at a scale of 1/1,200 or 1/1,800, would yield a resolution of:

$$\text{Resolution (1/1,200)} = 5 \times \frac{(1/600)}{(1/1,200)} = 10 \text{ l/mm}$$

$$\text{Resolution (1/1,800)} = 5 \times \frac{(1/600)}{(1/1,800)} = 15 \text{ l/mm}$$

A computer flow chart for calculating resolutions from 5 to 95 lines/mm is shown in Appendix I. A computer output is displayed in Table 2. It should be noted that the bar sizes are calculated for a resolution target placed

Table 2

3-LINE RESOLUTION TARGET DESIGN
AT A SCALE OF 1/600

TARGET (L/MM)	TARGET SPACE OP BAR WIDTH (MM)	RESOLUTION 1/1200 (L/MM)	RESOLUTION 1/1800 (L/MM)
5.0	60.000	10.0	15.0
7.5	40.000	15.0	22.5
10.0	30.000	20.0	30.0
12.5	24.000	25.0	37.5
15.0	20.000	30.0	45.0
17.5	17.143	35.0	52.5
20.0	15.000	40.0	60.0
22.5	13.333	45.0	67.5
25.0	12.000	50.0	75.0
27.5	10.909	55.0	82.5
30.0	10.000	60.0	90.0
32.5	9.231	65.0	97.5
35.0	8.571	70.0	105.0
37.5	8.000	75.0	112.5
40.0	7.500	80.0	120.0
42.5	7.059	85.0	127.5
45.0	6.667	90.0	135.0
47.5	6.316	95.0	142.5
50.0	6.000	100.0	150.0
52.5	5.714	105.0	157.5
55.0	5.455	110.0	165.0
57.5	5.217	115.0	172.5
60.0	5.000	120.0	180.0
62.5	4.800	125.0	187.5
65.0	4.615	130.0	195.0
67.5	4.444	135.0	202.5
70.0	4.286	140.0	210.0
72.5	4.138	145.0	217.5
75.0	4.000	150.0	225.0
77.5	3.871	155.0	232.5
80.0	3.750	160.0	240.0
82.5	3.636	165.0	247.5
85.0	3.529	170.0	255.0
87.5	3.429	175.0	262.5
90.0	3.333	180.0	270.0
92.5	3.243	185.0	277.5
95.0	3.158	190.0	285.0

at 300 feet (at f = 6 inch). Thus this target size is suitable for a camera of focal length, "f," if the resolution board is placed at a distance of 600f from the camera.

Although greater resolution is obtainable from a high contrast target than from a low contrast target, it must be emphasized that the only concern in this test is that relative resolution numbers should be derived. Thus, the absolute contrast of the target was inconsequential when the ground control photography and in-flight test photography were based on the same contrast resolution targets, and when atmospheric conditions were approximately the same. Density measurements directly on the resolution board gave values of 1.7 for the black, and 0.03 for the white. This yields a contrast, or density, ratio of 57:1, which is a high contrast.

2.2 Manufacture and Evaluation of Resolution Targets

The resolution target was drafted on a square sheet of plywood (4' X 4' X 1/2"). The resolution bars were drafted by a Faul/Coradi coordinatograph on a black background and the white bars (Con-tact) were drafted with an Exacto-knife and were peeled off.

The opposite of this arrangement - i.e., white background with black bars - was first tried with negative results due to the halation effect of the white background. The process of manufacturing the target is presented in Figure 2. The resolution pattern with white bars on black background gave slightly higher resolution values, which would indicate that this pattern would be more readily distinguishable, and would provide a better pointing accuracy.

But besides a better pointing accuracy, high contrast targets also show increase in absolute resolution values. Figure 3 notes two test

Figure 2. The drafting of the resolution board on the Faul/Coradi Coradograph.

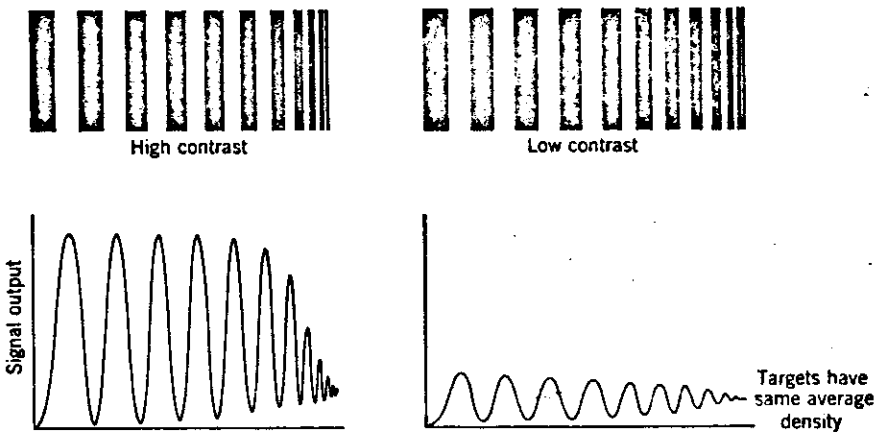

Figure 3. Microdensitometer scan output for varying contrasts (see Jensen, 1968).

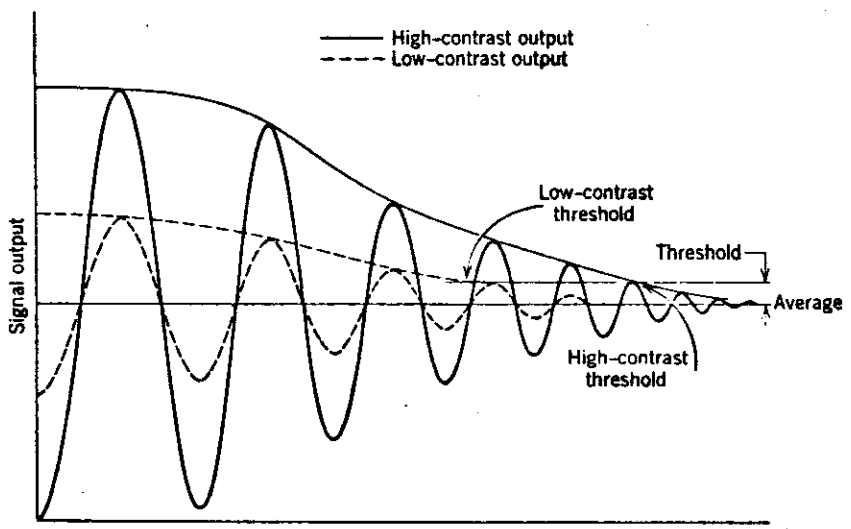

Figure 4. Contrast effects on threshold resolution (see Jensen, 1968).

targets with identical average density, except that one is a high-contrast target and the other is low-contrast. Each target increases in spatial frequency to the right. A microdensitometer trace is made of each target, and notes a frequency similar to that of the target, but with decreasing amplitudes. The amplitude becomes indistinguishable when it reaches some "threshold" value.

From comparison of the two traces, it is concluded that contrast is simply the analog of scale factor (see Jensen, 1968). Further, Figure 4 shows the low-contrast curve envelope intersecting the threshold at a lower spatial frequency than the high-contrast curve envelope. The conclusion, then, is to maintain a high contrast for both better pointing accuracies on target and higher resolution values - a relationship basic to accuracy analysis.

The problem, however, again occurs when applying this theory to practice. High contrast targets must be maintained as long as the effects of halation are avoided. On bright days, the infringement of black and white bars on each other becomes immense, and must be avoided even to the degradation of resolution.

One final factor affecting the resolution of the system is exposure level. It has been noted by Zweig, Higgins, and MacAdam that peak resolution occurs when exposure yields a density of about 0.85 above the base density of the film, where density is defined as the $\log_{10}$ of the reciprocal of the transmission of the film. This can be shown by observing the typical D-log E curve of Figure 5. It is obvious there can be no resolution at very high and very low exposures due to the lack of slope to the curve. Between these limits is the characteristic constant slope of the curve.

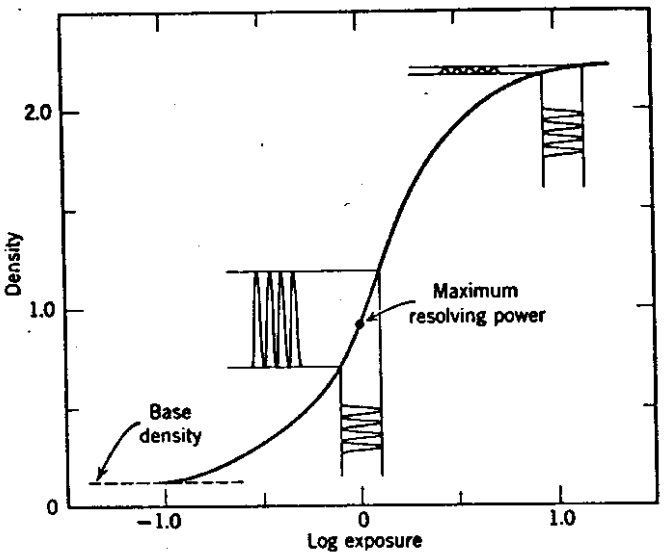

Figure 5. Typical D-log E curve for film (see Jensen, 1968).

A question arises as to the validity of one point on the curve producing maximum resolution, particularly from a practical standpoint. From the previous discussion, it can be concluded that a specific resolution value is given only for the sake of simplicity. In reality, this specific value denotes only the central tendency of the system's data (see Brock, 1966). Even under identical conditions, the values may vary. A sample plot of this characteristic is shown in Figure 6, and resembles the well-known Gaussian distribution. For this reason, and the fact that variances are inherent within the photographic material, it seems feasible to conclude that the prime criterion for exposure is to maintain values between the upper and lower limits of the curve.

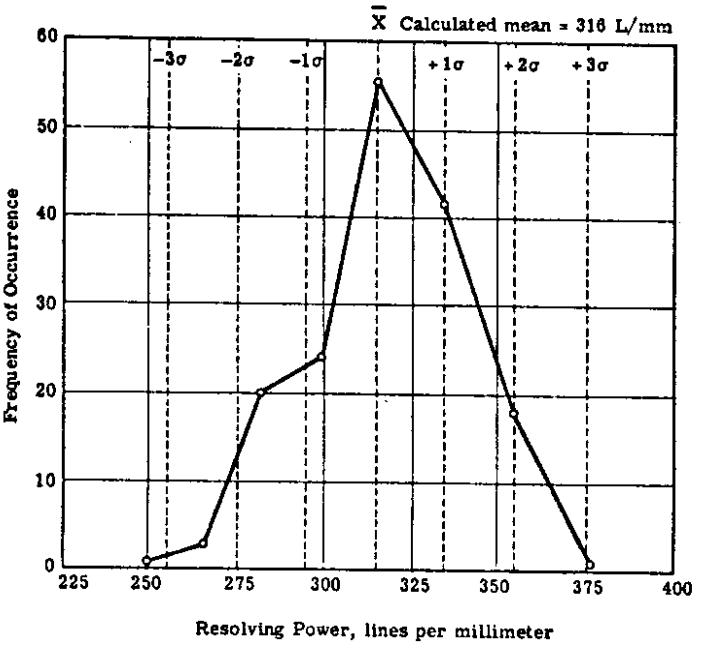

Figure 6. Typical plot of frequency of occurrence vs. resolving power (see Brock, 1966).

Combining all these effects, then, produces the familiar equation (see Manual of Photogrammetry, 3rd Ed.):

$$\frac{1}{R_o^n} = \frac{1}{R_1^n} + \frac{1}{R_2^n} \cdots \frac{1}{R^n} \quad \text{.....2.1}$$

where

R_o = system resolution

R_1, R_2, etc. = various resolution values for the system's components

n = exponential power factor

Our main function is just to observe the final R_o value and compare it to the attained accuracy. If someone wishes to build this system, however, he must evaluate the various individual parameters involved, an almost impossible task under this approach. Firstly, one must determine a value

for "n," which in itself seems open to a great debate. A somewhat more recent, and easier, approach to this particular problem is by use of the sine-wave theory for quantifying the resolution parameters.

2.3 Sine-wave Theory

The modulation transfer function (MTF) provides a more meaningful indicator of resolution than line-pairs per millimeter. MTF is a response of the optical system as a function of spatial frequency. In this approach, optical images are analyzed in a manner quite similar to that of electrical signals (see Jensen, 1968). Rather than current or voltage varying with time, brightness is a function of linear dimensions. Instead of frequency expressed as cycles per second, spatial frequency is expressed as cycles per millimeter. Corresponding to this approach, one can then estimate the net system performance simply by taking the initial value of target energy and successively multiplying it by the transfer values of the other components of the system. This falls in line with the theory behind high-fidelity sound systems (see McDonald, 1961).

One drawback of this method, however, is that MTF values do not give any indication as to film sensitivity, as they assume correct film exposure and development to a linear input. As will be mentioned, this same exposure assumption was made in the classical method utilized in this project. Optical system response is then determined for various waveforms and are known as spread functions. MTF shows response of amplitude as a function of spatial frequency. A more encompassing approach is to describe response of any spatial frequency, and is known as the Optical Transfer Function (OTF). OTF is not popular, however, as it is more complex, and amplitude is the only primary concern.

Specifically, MTF represents the modulus of the Fourier transform of a line spread function. This is the natural diffusion effect which occurs when a narrow line is projected on an emulsion surface. This, then, mathematically describes image quality, as it specifies light distribution caused by scattering. MTF is defined by (see Brock, 1966):

$$T_n = \frac{M_m^e}{M_n^i} \quad \text{.....2.2}$$

where

T = modulation transfer function

n = spatial frequency

M^i = modulation in image falling on emulsion

M^e = modulation in effective image within emulsion during exposure

An example of a spread function and corresponding MTF relationship is shown in Figure 7.

The most direct method of measuring MTF is based on use of sinusoidal targets. In this context, the standard bar charts can be adapted to this purpose. The transmittance, T, varies sinusoidally with the distance in one direction but is constant at right angles to that direction. Figure 3 represents a trace of a sinusoidal target, and modulation is then defined in terms of intensity (amplitude) and varies between 0 and 1:

$$M = \frac{I_{max} - I_{min}}{I_{max} + I_{min}} = \% \quad \text{.....2.3}$$

It must be noted here of the relation between modulation to other representations of contrast. The ratio of maximum to minimum transmittance (density differences) are commonly expressed for bar charts. The correspondence to modulation as given by Brock, 1966, is:

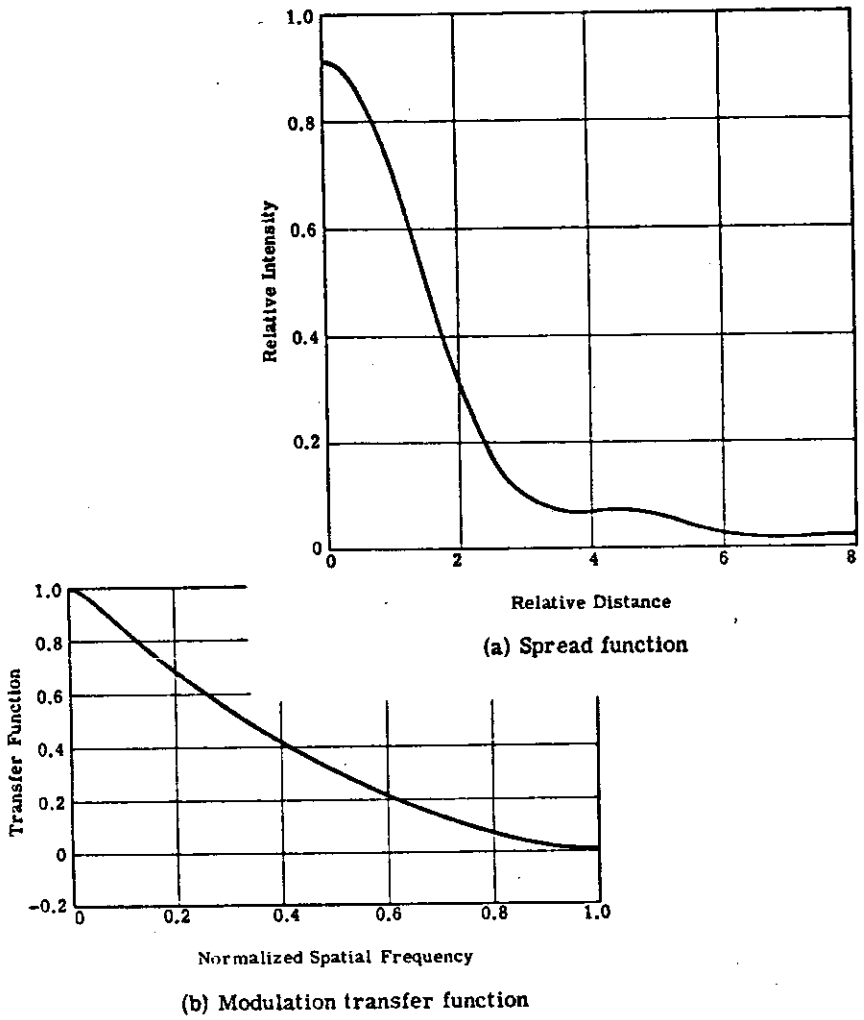

Figure 7. Spread function and corresponding modulation transfer function for an optical system (see Brock, 1966).

$$M = \frac{C-1}{C+1} = \frac{10^{D}-1}{10^{D}+1} \quad \text{.....2.4}$$

where D = density

Figure 8 graphically shows this density relationship for increasing values of resolution. Note the decrease in contrast of images for increasing values of resolution. Further, Figure 9 shows a similar modulation (response) curve for a typical photo-optical image (see Yost, 1961).

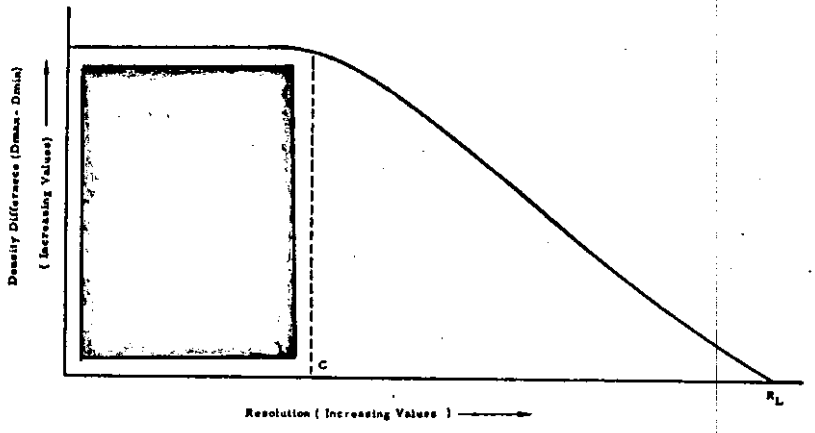

Figure 8. Typical graph of density difference vs. increasing values of resolution (see Yost, 1960).

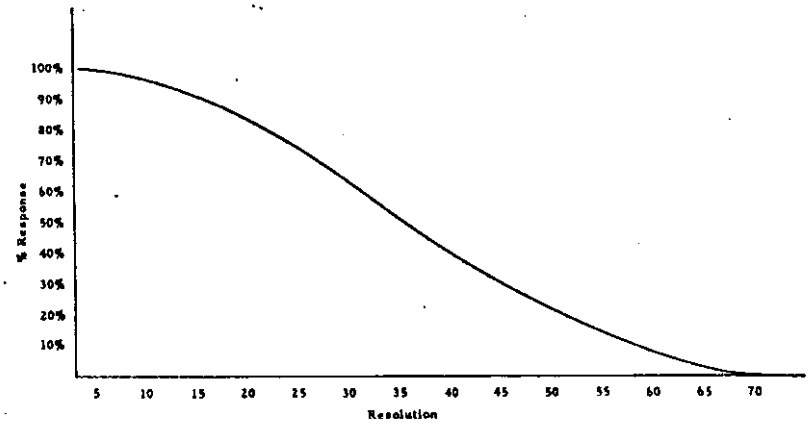

Figure 9. Typical graph of sine-wave response vs. increasing values of resolution (see Yost, 1960).

Note the similarity in curve shapes for the standard resolution pattern and the sine-wave pattern. However, note also that Figure 9 is continuously changing, whereas no change in contrast occurs in Figure 8 until a point "C" is reached. Point "C" in this case denotes the resolution value at which spreading reduces space density and increases bar density.

The use of MTF can become an integral part of photographic quality determinations. Evaluation has transcended the problem of human observer inadequacies, and now becomes dependent on the established microdensitometer. Even more important is that distinct elements of a system can be readily combined to give effects of the entire system. The MTF plot is sufficiently reproducible under standardized conditions for use as a tool in design. In regard to our project, there is a definite problem in correlating the resolution values observed and the actual targets used for pointing. Even if contrast consistency is maintained, differences in spatial frequency between targets is inherent, and therefore makes reproduction of the system quite difficult. But it would seem that the basic relationship between resolution target and pointing target is constant. With an MTF plot, then, a ratio can be established with the frequency of the pointing target, making correlation much stronger.

The concept of quantifying resolution is quite exciting, and perhaps may be further developed in Phase III of this project. For the present, however, the basic evaluation in "line-pairs per millimeter" resolution is sufficient. In fact, it may be preferable at this stage. The fact that MTF is a curve also is a disadvantage in that it is yet to be readily understood, and makes a finite resolution number presently more acceptable. Further, from a practical standpoint again, Figures 8 and 9 show that possibly resolution in terms of classical methods are more appropriate. The

authors would assume that Figure 8 represents a more general case in that there is no appreciable decrease in contrast, at least to the observer, until the images are close together (point "C").

3.0 VIBRATION AND IMAGE MOTION

3.1 Background

The aircraft vibration effects on a camera can cause extreme loss of quality and resolution in the resulting photographs if the camera is not properly stabilized. Much research has been conducted to determine both the qualitative and quantitative deterioration of the image recorded by a camera mounted in a conventional airplane. The result of this research has been the design of vibration-isolated camera mounts for these aircraft. The vibrations caused by a helicopter (predominant frequency range of 8.5 to 24 cycles/second) are of a greater amplitude than those caused by the airplane. Thus, the camera mounts which have been designed for the higher frequency vibration in airplanes may not be suitable for the lower frequency vibration occurring in the helicopter. As well as vibration, image motion causes a degradation of the resulting photographs. Before designing a vibration-isolated mount for a helicopter, an investigation of the literature on the camera stabilization problems (vibration and image motion) in the airplane and helicopter is warranted.

Doyle, in his article, "Problems in the Integration of Stabilized Mounts in Photo Systems" (1956), mentions that angular motions of the camera cause a loss of resolution in the image, especially for longer focal lengths. He discovered that serious degradation of resolution occurs for only a few seconds of arc of angular motion, and cautions that vibration

isolators must be designed so that their deflection is uniform and does not introduce an angular rotation. Alter (1956) recommends silicon rubber or steel wool wound inside of an ordinary helical spring as the vibration isolator. In the article, "Camera Mounting for Photogrammetric Purposes" by Pallme (1956), graphs of the effect on resolution of both angular motion and linear motion are displayed. These graphs are Shown in Figure 10 and Figure 11. The resolution loss with increasing motions is adequately displayed in these graphs. Pallme also introduces the importance of supporting the camera at the center of gravity of the airplatform. In the article, "The Effects of Motion on Resolution," Trott (1960) theorizes that the reduction of the exposure period, "T," reduces the motion occurring as a result of vibration only for frequencies below T/2 c.p.s. According to this theory, the maximum exposure period for a helicopter should be (twice the maximum helicopter frequency = 2 X 24 c.p.s.) 48 (i.e., about 1/50 second). This and faster exposures are quite feasible for helicopter work. Jackson, in his article, "Factors Affecting the Interpretability of Air Photos" (1959), also mentions that image motion due to ground speed and scale can be reduced, either by reducing the time of exposure or by image motion compensation. He feels that if the image motion is kept less than 0.3 times the resolved distance, there will be no effect on resolution. The tolerable motion in microns is given as 300/resolution. Thus, for a Wild RC-8 camera (wide angle f5.6 Aviogon lens) the minimum tolerable motion would be approximately 12 microns. This is equivalent to an angular rotation of about 17". Jackson also feels that by using an exposure time, "T," greater than one tenth of the r.p.m. of the aircraft engine, rotation of the camera during exposure could be reduced by half. For the Model 47G-3B-1 helicopter used in this research

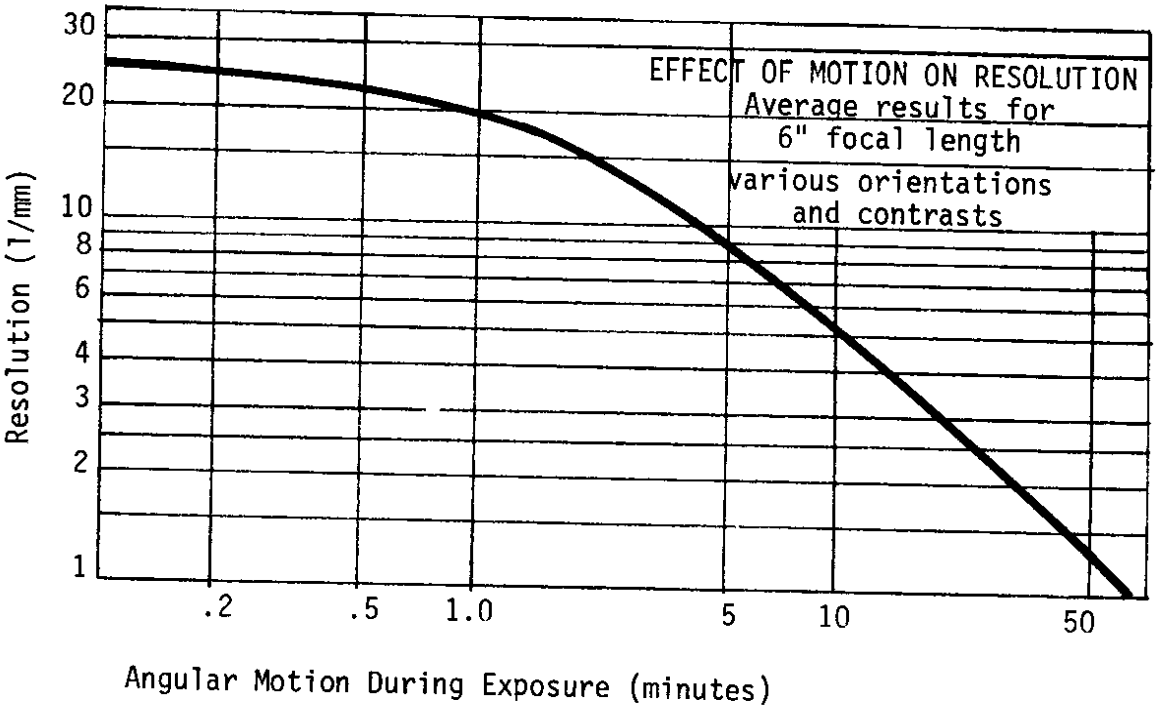

Figure 10. After Fig. 2, "Camera Mounting for Photogrammetric Purposes," p. 902.

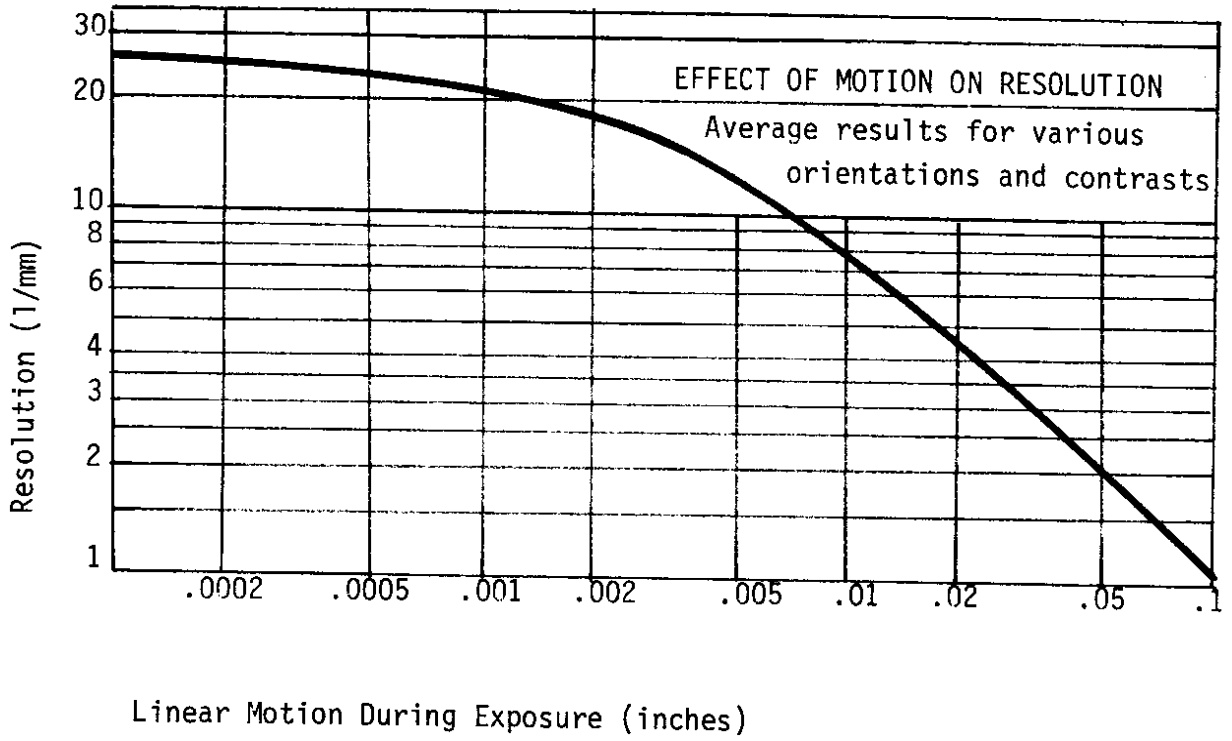

Figure 11. After Fig. 3, "Camera Mounting for Photogrammetric Purposes," p. 902.

this would be: T = 3200/10 = 320, or a 1/320 second exposure. This exposure speed will also reduce vibration effects, as previously mentioned by Trott.

An excellent article on vibration is given by H. Brown in "Vibration of Air Survey Cameras" (1959). Brown found that image plane motion due to the movement of the shutter mechanism was observed to be less than five microns at any shutter speed. This effect is practically negligible when compared to vibration effects. Concerning the camera mount, Brown recommends supporting the camera near the horizontal plane containing the aircraft's center of gravity. He also mentions that the mount should be of such resilience that the natural frequencies of the assembly are as low as possible. He further recommends sufficient damping of the mount, as sudden shocks which could occur in rough air might cause a camera in a resilient mount to oscillate, which could cause serious image motion during exposure. Brown recommends foam or sponge rubber loaded uniformly to about 1 p.s.i. because of the low natural frequency and good damping factor of these materials. A very good article on vibration presented by Richard Casper is "Resolution of Vibration Isolated Cameras " (1964). To the previously mentioned points Casper adds that the longer the isolator base, the smaller will be the angular rotation due to an imbalance. This is an important fact to remember for the design of a suspension system.

Kawachi, in his article, "Image Motion Due to Camera Rotation" (1965), agrees that the result of an aircraft's random motion upon photographic quality is the degradation of resolution. He states that the degradation is directly influenced by the distance of image motion blur and the stationary lens-film resolution. This degradation is represented by his formula for small blur distances:

$$1/R^2 = 1/R_o^2 + D^2 \quad \text{.....3.1}$$

where

R = dynamic resolution in 1/mm

R_o = static lens-film resolutions in 1/mm

D = blur distance (image velocity x exposure time) in mm

For example, assuming a blur distance "D" on the photograph equal to 0.112 mm and a static resolution of 22.5 1/mm, the dynamic resolution "R" is computed as 8 1/mm. The formulae for image velocity due to rotations are given in Table 3. These are developed for the case when the camera is coincident with the center of gravity (rotational center) of the aircraft.

Table 3. Image Velocities after Table II, "Image Motion Due to Camera Rotation," p. 865.

	$\dot{x}$	$\dot{y}$
Pitch (ϕ)	$(\frac{f^2 + x^2}{f})\,\dot{\phi}$	$\frac{xy}{f}\,\dot{\phi}$
Roll (ω)	$\frac{xy}{f}\,\dot{\omega}$	$(\frac{f^2 + y^2}{f})\,\dot{\omega}$
Yaw (κ)	$y\dot{\kappa}$	$x\dot{\kappa}$

The importance of target blur is expounded in J. C. Trinder's article, "Pointing Accuracies to Blurred Signals" (1971). He found that, of several variables tested, target blur had the most significant effect on pointing accuracies. Thus, the camera should be mounted so that the effects of image motion and vibration are reduced.

3.2 Angular and Linear Motions

Kawachi has previously derived the equations for image motions due to rotations about the center of gravity of the airplatform. There will be a larger image motion effect (blur) if the camera is mounted eccentric to the center of aircraft rotation. Besides the given rotational elements, there will also be an effect due to translation. The blur, or image motion, is caused by the previously developed image rotational velocities and the translational motions. The calculations for the resulting blur, with reference to Figure 12, are as follows:

$$A = \frac{(e_z + f)}{\cos \omega} - (e_z + f) = (e_z + f)\left(\frac{1}{\cos \omega} - 1\right)$$

$$B = \frac{A}{\tan \omega}$$

$$C = e_y - B = e_y - \frac{(e_z + f)(1/\cos \omega - 1)}{\tan \omega}$$

$$e_z = C \sin \omega = e_y \sin \omega - (e_z + f)(1/\cos \omega - 1)\cos \omega$$

$$= e_y \sin \omega - (e_z + f)(1 - \cos \omega)$$

$$\Delta e_y' = e_z \tan(\alpha - \omega)$$

$$\Delta = e_y - e_y \cos \omega$$

$$\Delta e_y = (e_z + f)\sin \omega + \Delta = (e_z + f)\sin \omega + e_y (1 - \cos \omega)$$

A good approximation for θ is, with reference to Figure 13, as follows:

$$D = \Delta e_y + \Delta e_y'$$

$$E = D \cos(\alpha - \omega)$$

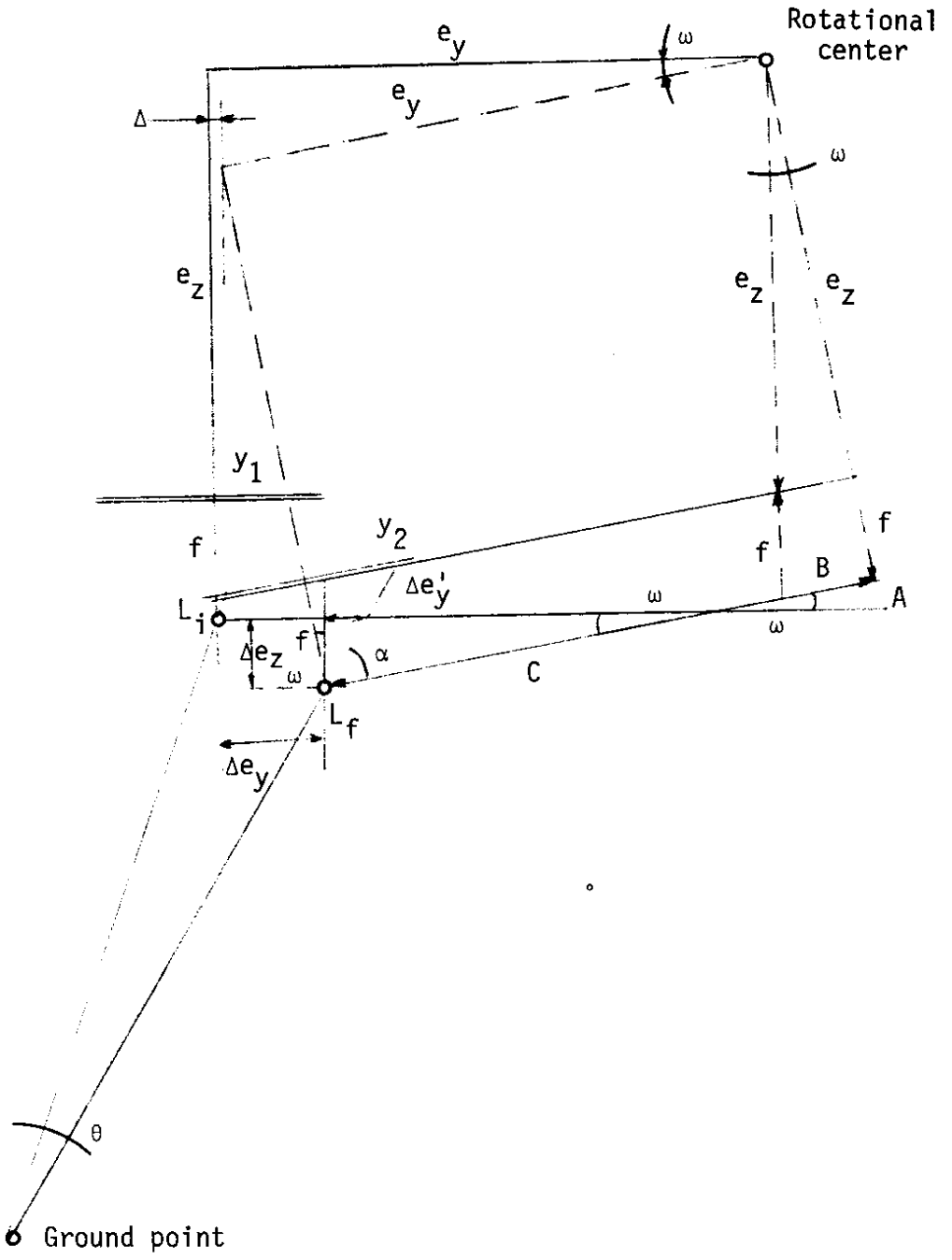

Figure 12. Effects of a roll (ω) on a camera mounted eccentric to the rotational center of the aircraft.

e_y = horizontal component of eccentricity in "Y" direction

e_z = vertical component of eccentricity in "Z" direction

L = camera lens

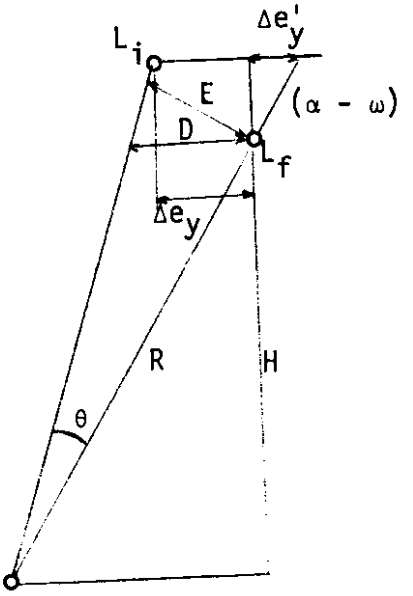

Figure 13. Approximation for θ.

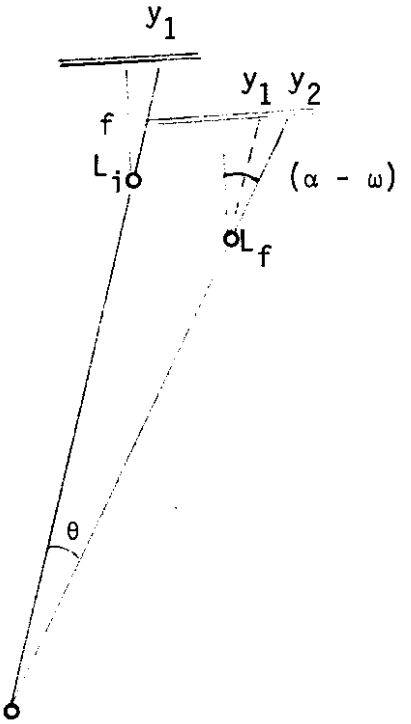

Figure 14. Blur geometry.

$$R = H/\cos(\alpha-\omega)$$

$$\theta = \frac{E}{R} = \frac{D\cos(\alpha-\omega)}{H/\cos(\alpha-\omega)} = \frac{D}{H}\cos^2(\alpha-\omega)$$

Assuming ω is small: $\cos\omega - 1$ and $\sin\omega = \tan\omega = \omega$

$$\theta = \{[(e_z + f)\omega + e_y(1 - 1)] + [e_y\omega - (e_z + f)(1 - 1)]$$

$$X \tan(\alpha-\omega)\} \frac{\cos^2(\alpha-\omega)}{H}$$

$$\theta = \frac{[(e_z + f)\omega + (e_y\omega)\tan(\alpha-\omega)]\cos^2(\alpha-\omega)}{H} \quad \text{.....3.2}$$

With reference to Figure 14, blur due to translation is given as:

$$\text{Blur} = y_1 - y_2 = f\tan(\alpha-\omega-\theta) - f\tan(\alpha-\omega)$$

With reference to Table 3, blur due to rotation was given previously as:

$$\text{Blur} = \dot{y}t = \left(\frac{f^2 + y^2}{f}\right)\omega$$

For the worst case, where the rotation and translation effects combine, the blur is given by:

$$\text{Blur} = \left|f[\tan(\alpha-\omega-\theta) - \tan(\alpha-\omega)]\right| + \left|\left(\frac{f^2 + y^2}{f}\right)\omega\right|$$

The blur resulting from a roll motion (ω) of the helicopter has the greatest detrimental effect when computing the relative positions of two distant points on the photograph. The images of the two most distant points in a model area occur for "y" = 0 ($\alpha = 0^\circ$) and "y" = 4.5 inches ($\alpha \cong 37^\circ$) for a constant "x". Thus, total positional error (blur) is given by:

$$\text{Blur}_{(y = 4.5)} - \text{Blur}_{(y = 0)} = \{f[\tan(\alpha-\omega-\theta) - \tan(\alpha-\omega)] + \left(\frac{f^2 + y^2}{f}\right)\omega\}$$

$$- \{f[\tan(-\omega-\theta) - \tan(-\omega)] + f\omega\}$$

$$\Delta \text{ Blur} = f[\tan(\alpha-\omega-\theta) - \tan(\alpha-\omega) + \tan(\omega+\theta) - \tan(\omega)] + \frac{y^2}{f}\omega \quad \ldots 3.3$$

The given variables for the Wild RC-8 camera mounted on the right side of a Model 47G-3B-1 helicopter are: "f" is 6 inches, "e_y" is 40 inches, and "e_z" is 40 inches. From (3.2) and (3.3), and assuming a roll (ω) of 0.8 seconds and an altitude of 300 feet, the relative positional error is given as 13.2×10^{-6} inches on the photograph. For large scale photography at a scale of 1/600 this would represent an error of 0.008 inches on the ground. This error would be attenuated if these images occur in subsequent overlap areas. Using the formulae in Table 3, and assuming a scale of 1/600, the maximum blur for a pitch (ϕ) of 1.5 seconds about the center of gravity of the helicopter is calculated as 0.015 inches on the ground; while a blur of 0.016 inches results from a yaw (κ) of 1.2 seconds.

In addition to these angular motions, there is a blur induced from a purely linear motion of the helicopter. This forward image motion, "M", is given as:

$$M = 1.467\ Vtf/H \quad \ldots\ldots\ldots\ldots\ldots\ldots\ldots\ldots\ldots\ldots\ldots\ldots\ldots\ldots 3.4$$

where

V = image velocity in m.p.h.

t = exposure period in seconds

H = flying height above ground in feet

f = focal length in inches

Assuming that "V" equals 30 m.p.h., "t" equals 1/400 second, "f" equals 6 inches, and "H" equals 300 feet, the resulting blur is calculated as 1.32 inches on the ground for a scale of 1/600.

For a flying height of 900 feet with the same variables as before, the blurs on the ground are calculated as: 0.024 inches for a roll, 0.045

inches for a pitch, 0.048 inches for a yaw, and 1.32 inches for a forward velocity. From these results it can be seen that the major effect for low altitude, large scale photography is the image motion due to the forward velocity of the helicopter. If the helicopter is in a hovering position (V = 0 m.p.h.), the effects caused by angular motions of the helicopter are essentially negligible.

3.3 Vibration

For a better understanding of the variables involved in the vibration problems in designing a camera suspension system, the following proof is presented from Wiley (1966, p. 144):

A system of one degree of freedom can be described completely by one coordinate (i.e., by one physical datum such as a displacement or an angle) as shown in Figure 15.

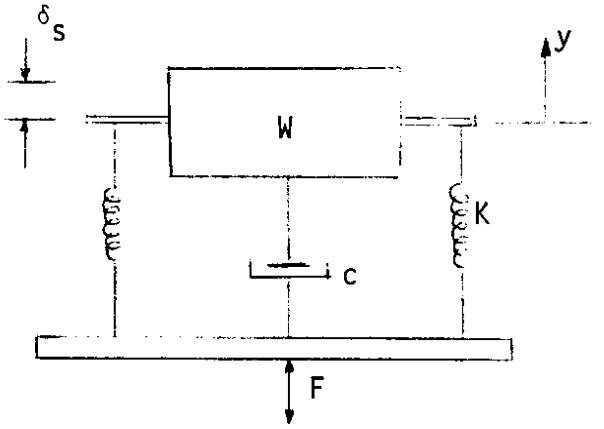

Figure 15. Vibration system.
W = weight of camera
δ_s = static deflection
K = spring modulus
c = friction coefficient
F = disturbing force

Assumption: the weight is guided, so that vertical motion, without swinging, is possible. The forces acting on the system are given as:

1. Gravitational force = -W.
2. Spring force = Ky'. The spring is already compressed by δ_s, where δ_s = W/K. Thus y', which is measured from the equilibrium position, equals W/K - y. Therefore
3. Friction force = -c X (velocity of the mass)

   = -c (dy/dt)

   Resistance acts in opposition to velocity.
4. Disturbing force - F_o cos ωt. This is a periodic function.

From Newton's Law:

$$ma = F$$

$$(m)\ d^2y/dt^2 = -W + (W - Ky) - (c)\ dy/dt + F_o \cos \omega t$$

Rearranging this equation gives:

$$(m)\ d^2y/dt^2 + (c)\ dy/dt + Ky = F_o \cos \omega t \quad \ldots\ldots\ldots\ldots\ldots\ldots 3.5$$

From this differential equation, forced motion, which is the case for an aerial camera is represented by the Particular Integral, which describes the response of the system to a specific influence external to the system (helicopter). Assuming that:

$$Y = A \cos \omega t + B \sin \omega t \quad \ldots\ldots\ldots\ldots\ldots\ldots\ldots\ldots\ldots\ldots 3.6$$

then $dy/dt = (-A\omega) \sin \omega t + B\omega \cos \omega t$

$$d^2y/dt^2 = (-A\omega^2) \cos \omega t - (B\omega^2) \sin \omega t$$

and substituting into (3.5)

$$M[-A\omega^2 \cos \omega t - B\omega^2 \sin \omega t] + c[-A\omega \sin \omega t + B\omega \cos \omega t]$$
$$+ K[A \cos \omega t + B \sin \omega t] = F_o \cos \omega t$$

and $\cos \omega t[-mA\omega^2 + B\omega c + KA - F_o] + \sin \omega t[-mB\omega^2 - A\omega c + KB] = 0$

Setting the coefficients of "cos ωt" and "sin ωt" equal to zero respectively gives:

$$-mA\omega^2 + B\omega c + KA - F_o = 0 \quad \text{.....3.7}$$

$$-mB\omega^2 + A\omega c + KB = 0 \quad \text{.....3.8}$$

From (3.8) $A = [KB - mB\omega^2]/\omega c$

Substituting into (3.7)

$$(K - m\omega^2)[KB - mB\omega^2]/\omega c + B\omega c = F_o$$

$$B = \frac{F_o}{(K - m\omega^2)[K - m\omega^2]/\omega c + \omega c}$$

Similarly:

$$A = \frac{K - \omega^2 m}{[K - {}^2m]^2 + (\ c)^2} F_o$$

Substituting into (3.6) yields:

$$Y = \frac{K - \omega^2 m}{[K - \omega^2 m]^2 + (\omega c)^2} F_o \cos\ t + \frac{\omega c F_o \sin\ \omega t}{[K - m\omega^2] + (\omega c)^2}$$

$$= \frac{F_o\{[K. - m\omega^2] \cos\ \omega t + \omega c \sin\ \omega t\}}{[K - m\omega^2]^2 + (\omega c)^2}$$

$$= \frac{F_o}{([K - m\omega^2]^2 + (\omega c)^2)^{\frac{1}{2}}} \{\frac{[K - m\omega^2] \cos\ \omega t}{([K - m\omega^2] + (\omega c)^2)^{\frac{1}{2}}}$$

$$+ \frac{\omega c \sin\ \omega t}{([K - m\omega^2]^2 + (\omega c)^2)^{\frac{1}{2}}}\}$$

These equations are related in Figure 16.

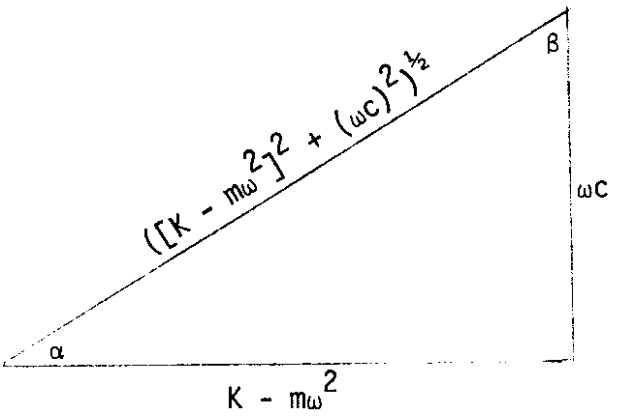

Figure 16. Phase angle relationships.

From the triangle shown in Figure 16:

$$Y = \frac{F_o}{([K - m\omega^2]^2 + (\omega c)^2)^{1/2}} (\cos\ \omega t \cos\alpha + \sin\ \omega t\ \ \sin\alpha)$$

$$Y = \frac{F_o}{([K - m\omega^2]^2 + (\omega c)^2)^{1/2}} \cos(\omega t - \alpha)$$

Rearranging and dividing by K/K:

$$Y = \frac{F_o/K}{([1 - (m/K)\omega^2]^2 + (\omega c/K)^2)^{1/2}} \cos(\omega t - \alpha)$$

But, $\delta_s = F_o/K$, $\omega_n = (K/m)^{1/2}$ which is the natural frequency of the camera mount system, and $c_c = (4Km)^{1/2}$ which is the critical damping coefficient of the system. Therefore:

$$Y = \frac{\delta_s}{([1 - \omega^2/\omega_n^2]^2 + [\omega/(K/m)^{1/2} \times 2c/(4Km)^{1/2}]^2)^{1/2}} \cos(\omega t - \alpha)$$

$$\therefore = \frac{\delta_s}{([1 - (\omega/\omega_n)^2]^2 + [2(\omega/\omega_n)(c/c_c)]^2)^{1/2}} \cos(\omega t - \alpha)$$

The magnification ratio, "M", is defined as:

$$M = \frac{1}{([1 - (\omega^2/\omega_n^2)]^2 + [2(\omega/\omega_n)(c/c_c)]^2)^{\frac{1}{2}}}$$

The quantity, $M\delta_s$, is the amplitude of vibrations which result when a constant force, "F_o", acts dynamically with frequency, "ω". The curves shown in Figure 17 demonstrate the magnification ratio, "M", of the damping ratio, "c/c_c". These curves demonstrate that to minimize "M", and thus, the amplitude of the vibrations, the mount must be designed for a $\omega/\omega_n > 1.4$ and $c/c_c > 1/\sqrt{2}$. Thus, the camera mounting system must have a natural frequency much lower than the disturbing frequency supplied by the helicopter, and the damping factor must be large. The stipulations can be accomplished using elastic damping materials in the mount. As pointed out by Brown (1959), an elastic or resilient mount subjected to sudden shocks

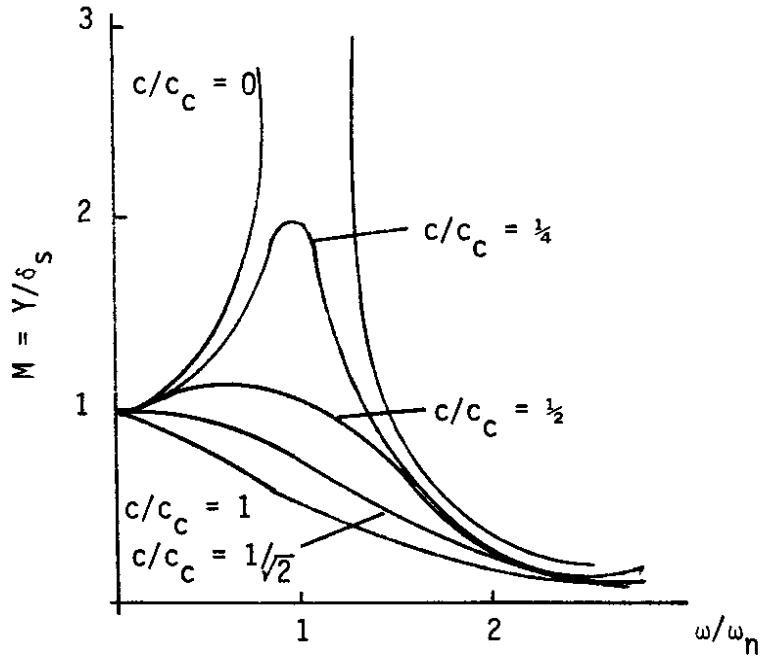

Figure 17. Vibration curves.

or accelerations would yield serious image motion. This image motion is a result of the large deflections and rocking caused by the weight of the camera. Thus, the damping material, besides causing a rapid damping of the oscillations, should also cause a reduction of the oscillation amplitudes. Phase angle, α, is a measure of the damping coefficient of a material. The phase angle (see Figure 16) is the angle of lag of the response (i.e., the displacement lags (by α) in respect to the disturbing force). With reference to Figure 16 the variables involved are related as follows:

$$\tan \alpha = \frac{\omega C}{K - m\omega^2}$$

α is the phase angle, or angle of lag of the response.

Rearranging the previous equation ($\div K$):

$$\tan \alpha = \frac{\omega C/K}{1 - m\omega^2/K} = \frac{\omega/(K/m)^{\frac{1}{2}} \times 2c/(4K/m)^{\frac{1}{2}}}{1 - \omega^2/(K/m)}$$

$$\tan \alpha = \frac{2(\omega/\omega_n)(c/c_c)}{1 - (\omega/\omega_n)^2}$$

Shown in Figure 18 are the curves of the phase angle, α, as a function of the impressed frequency ratio ω/ω_n for various amounts of damping. When there is no damping ($c/c_c = 0$), displacement is in phase with the disturbing force below ω_n, and 180° out of phase with it at higher frequencies. At ω_n there is a sudden jump in phase; with damping the process is more general.

In porous materials such as cork, wood, felt or rubber, viscous damping (damping due to air being compressed out of, or drawn into, the material's pores) is quite high for small amplitudes. For various materials the average values of loss angle (α) for a spring which is not supporting a load ($m = 0$), but is subjected to the influence of damping, are shown in Table 4.

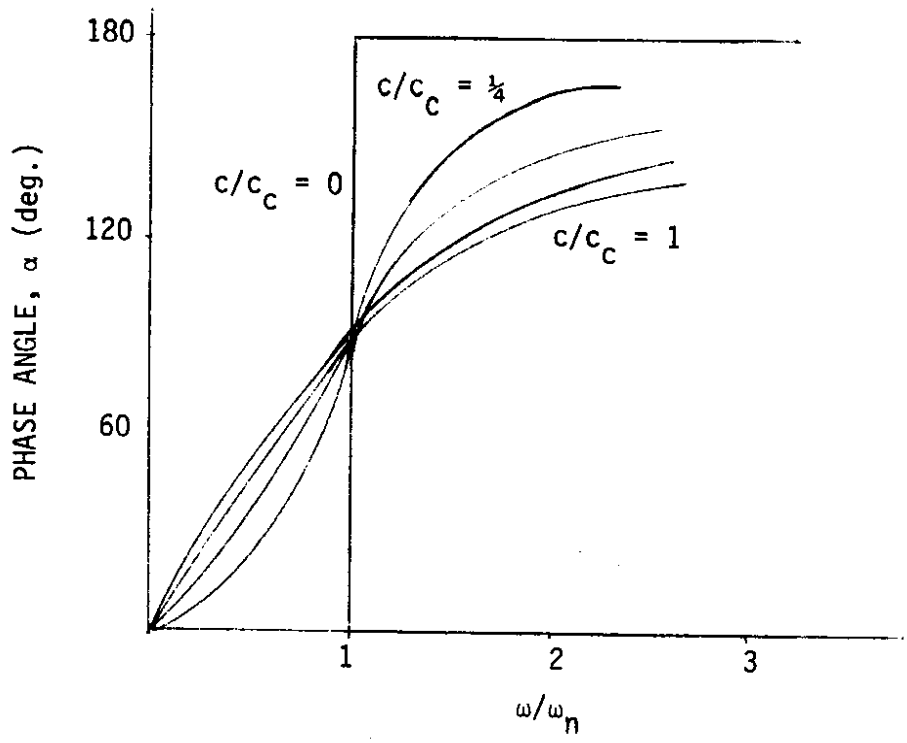

Figure 18. Phase angle as a function of the impressed frequency ratio.

Table 4. Loss angles after Table XIV, Introduction to a Study of Mechanical Vibration, p. 185.

Material	α in deg.
Wood	1.2
Cork	4.0
Rubber	6.0

This table indicates that rubber is the best damping material of those tested. It should also be noted that the mass of the camera acts to reduce the magnitude of vibrations. This is evidenced in equation (3.9). An increase in "m" decreases ω_n, and thus decreases "M". Therefore the mass or inertia of the camera will act as a self stabilizer.

Brown mentioned that rubber loaded uniformly under a compression of 1 p.s.i. was best for decreasing the effects of vibration. The effect of initial compression (or deflection) of the damping material was studied by L. T. Wilson in his article, "Resilient Cushioning Materials" (1957). Wilson felt that, for his conditions (disturbing frequency of 8 - 60 c.p.s.; 0.06 inch displacement; system natural frequency 10 - 20 c.p.s.; shock forces of 10 - 15 g.'s; unit weights of 100 - 200 lb.), which very nearly duplicate helicopter conditions, a resilient cushioning material was less complicated than a spring and damper system. He found that initial compression increased the damping capabilities for all materials tested (polyvinylchloride, modified polyvinylchloride, rubber foam, latex foam, vinyl foam, polyurethane, cellulose, glass fibers, felt, and bound hair) except for rubber foam and 10 p.c.f. fiberglass. He cautions that this increased damping capability also causes an increase in shock mitigation. Wilson recommends a static stress of 1.2 p.s.i. for rubber foam.

3.4 Camera Mount Systems

The important facts to consider in the camera mount suspension system are:

1. Helicopters are characterized by low frequency, high amplitude vibrations (thus, suspension should be resilient, with a large damping factor);

2. Helicopters are subject to rapid accelerations due to air turbulence (thus, suspension should not be too resilient);
3. There is a less detrimental effect if the camera is mounted near the center of gravity of the helicopter;
4. The reducing of the exposure period reduces the effect of vibration; and
5. The longer the isolator base, the smaller will be the angular motion of the camera.

Various suspension systems have been tested in helicopters. Lyons (1964) used 5/8 inch industrial felt pads preloaded to 30 lbs. pressure and a shutter speed of 1/200 second. Cheffins (1969) used isolators comprising a number of helical springs, which support the load and incorporate accurately controlled viscous damping especially designed for the isolation of low frequency, large amplitude vibrations.

Based on the vibration theory and previous research literature, it was felt that rubber pads would be the best material for isolating the camera. The pads used were the regular rubber buffers which are built into the Wild RC-8 camera mount. These pads provide effective damping in the range of frequencies of 15-100 c.p.s. with an amplitude of 0.7 mm. Another more costly material considered was hydraulic fluid. A third system considered was the D.A.V.I. (Dynamic Antiresonant Vibration Isolator). The theory on which the D.A.V.I. is based is presented in the article "Application of the Dynamic Antiresonant Vibration Isolator to Helicopter Vibration Control" by Robert Jones and William G. Flannelly (1968).

As shown in Figure 19, due to the isolated mass, "m_2", the natural frequency of the D.A.V.I. is less than a conventional isolator with the

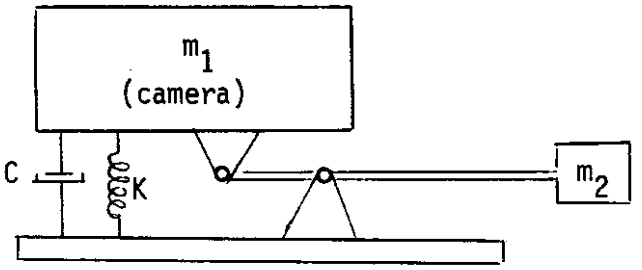

Figure 19. D.A.V.I.

same spring rate. The natural frequency and transmissibility are given by:

$$\omega_n^2 = \frac{K}{m_1 + m_2(R/r - 1)^2 + I/r^2}$$

$$|T|^2 = \frac{\{K - \omega^2[I/r^2 + m_2R/r(R/r - 1)]\}^2 + \omega^2c^2}{\{K - \omega^2[m_1 + m_2(R/r - 1)^2 + I/r^2]\}^2 + \omega^2c^2}$$

Experimental results from an input of approximately 1.0 g. acceleration at a frequency of 10.5 c.p.s. showed a 98% effective isolation. A comparable isolation from a conventional isolator at this frequency would require a minimum static deflection of five inches, or thirty-five times the deflection required for the D.A.V.I.

The three isolating systems to be tested in order of increasing cost were rubber pads, hydraulic fluid, and D.A.V.I. It was hoped that the rubber pads, due to their lower cost, would prove satisfactory, thus negating the need for developing and testing the remaining two more expensive systems.

4.0 CAMERA SUSPENSION SYSTEM

4.1 Manufacture

A camera suspension system must be designed with consideration for all

the variables which may cause a loss in the qualitative and quantitative reproduction capacity of a system. These variables have been mentioned previously as vibration and angular motions.

With consideration for these variables, ideally the camera should be mounted near the center of gravity of the aircraft. This is usually impossible in a helicopter, due to the location of the engine and the wiring. The logical place on the helicopter for the placing of the camera would seem to be between the skids, slightly to one side of the helicopter body. By properly aligning the camera mount along the side, the only displacement from the center of gravity would occur along the "Y" axis. The effect of this eccentricity on angular motions was demonstrated in the previous chapter.

The air-frame was constructed from aluminum angles bolted together. There are three positions on the air-frame where isolators may be applied to reduce the helicopter vibrations. These are:

1. The U-shaped threaded bolt connecting the air-frame to the skid,
2. The bolted connection between the angle cross-bars and the angle support between the skids, and
3. The connection between the camera mount and the air-frame cross-bars.

Blade turbulence whips up dust from the ground, so it was felt that a sleeve should be built onto the air-frame and under the camera to protect the camera lens on take-offs and landings. This aluminum sleeve was pulled forward to uncover the lens after take-off by pushing back on the attached rod. This rod was easily accessible to the photographer in the cockpit. For landings, the rod was again pulled forward to cover the lens. Figure 20 gives the dimensions of the air-frame.

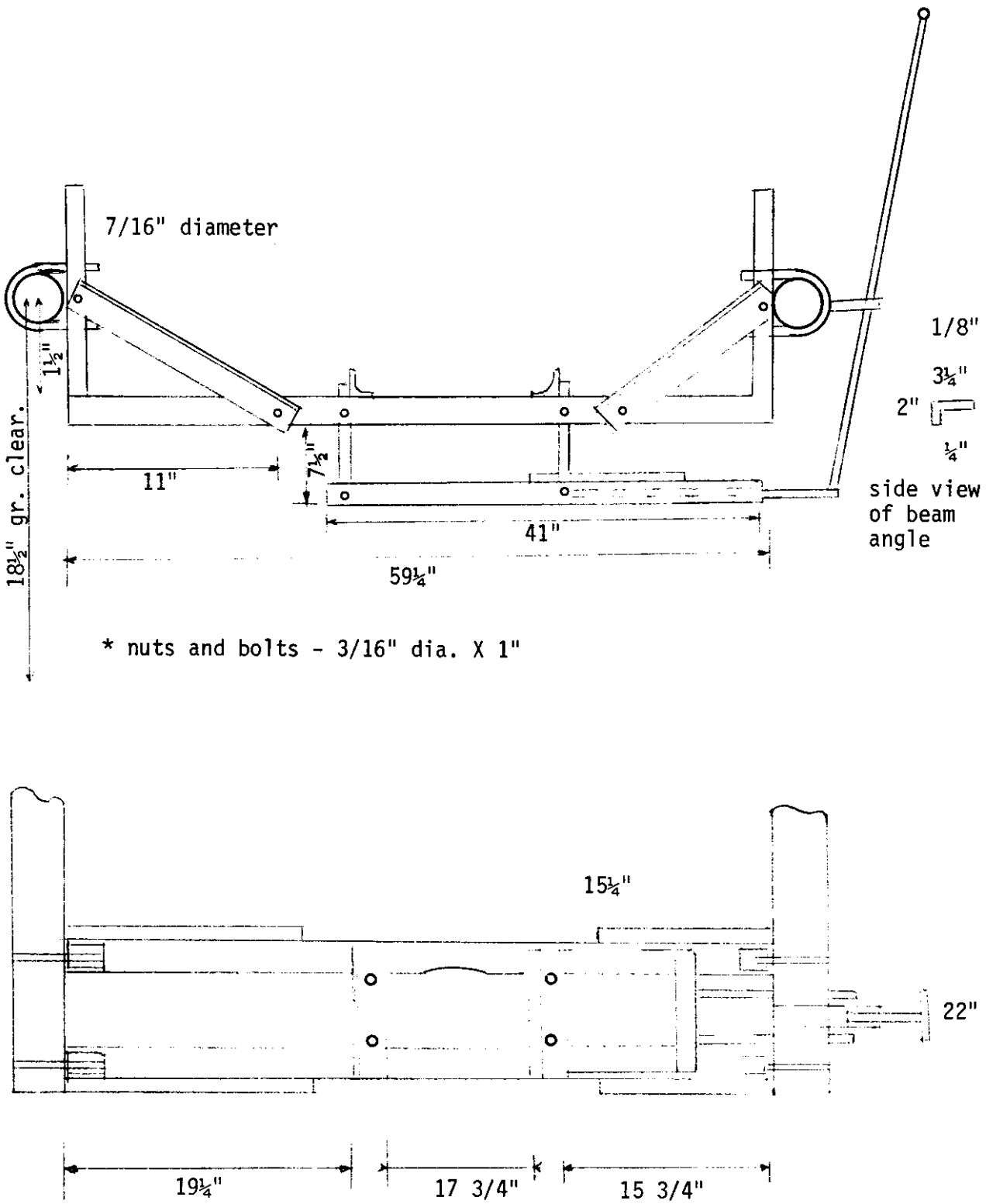

Figure 20. Aluminum angle air-frame.

The orientation of the camera during flight was adjusted by turning the various orientation control knobs on the camera, with a special rod used by the photographer from the cockpit. To facilitate ease in operation, a special knob was attached to the camera to control fore and aft tips. The photographer could easily reach the knob for side tilts. The intervalometer, vacuum pump, and viewfinder were set up in the helicopter cockpit.

4.2 Effects of the Air-frame

The air-frame, besides acting as a support for the camera, may act as a form of beam spring and thus reduce vibration effects. The vibration effects of the air-frame must be checked to make sure resonance ($\omega = \omega_n$) is not encountered. Hopefully the design is such that vibration effects are reduced. With reference to Figure 21, the moment of inertia about the Y-Y axis (I_y) for the aluminum angle beams is determined as follows:

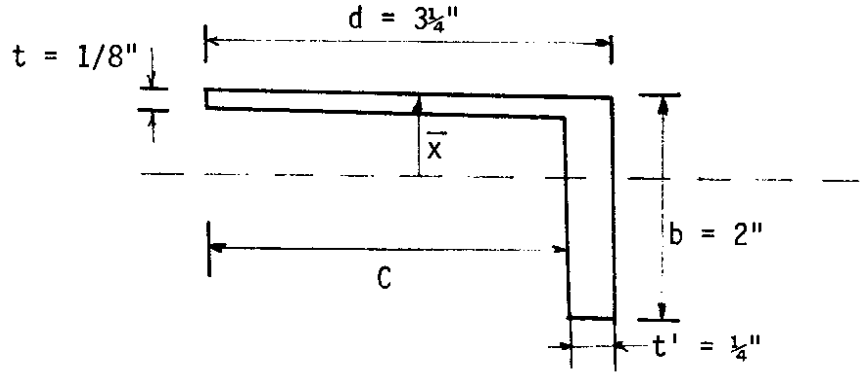

Figure 21. Angle dimensions.

d = length of horizontal flange (in.)
t = thickness of horizontal flange (in.)
b = length of vertical flange (in.)
t'= thickness of vertical flange (in.
$\bar{x}$ = vertical distance from Y-Y axis to top of horizontal flange (in.)

The moment of area about the Y-Y axis is calculated as:

$(3)(1/8)(\bar{x} - 1/16) + (\bar{x})(1/4)(\bar{x}/2) = (\bar{x} - 2)(1/4)(\bar{x} - 2)^{1/2}$

Thus, $\bar{x} = 0.598$ inches.

The moment of inertia is calculated as:

$I_y = 1/3[t'(b - \bar{x})^3 + d\bar{x}^3 - c(\bar{x} - t)^3] = 0.355 \text{ inches}^4$

Assumptions for the calculations of the air-frame natural frequency, ω_n, are:

1. half the camera weight, P, is applied to the beam, of length, L, at its center;
2. the beam is essentially fixed-end due to its joints;
3. rotor disturbing frequency, ω, for the Model 47G-3B-1 helicopter is 340 r.p.m. or 5.7 c.p.s.

With reference to Figure 22, the calculations for ω_n are as follows:

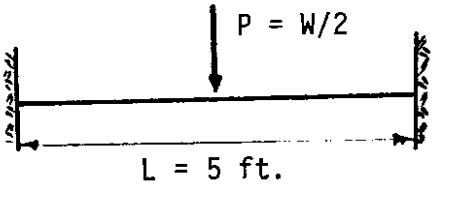

Figure 22. Aluminum angle beam.

The beam's maximum deflection is given as:

$$\Delta_{max} = \frac{PL^3}{192EI} = 0.032 \text{ inches}$$

and, $\omega_n = 1/2\ \pi\ (K/m)^{1/2} = 3.14/(\Delta_{max})^{1/2} = 17.6$ c.p.s.

This would yield a ω/ω_n ratio of 0.3, and as evidenced in Figure 17, a "M" value of approximately 1. These results indicate that the aluminum air-frame does not reduce the effect of rotor vibration to any degree; but,

on the other hand, the air-frame does not induce larger amplitudes due to resonance. The air-frame would, however, reduce the higher frequency (3,200 r.p.m.) engine vibrations (M = 0.2). Also, the air-frame, because of its large spring constant, provides a rigidity to the otherwise resilient mount, and would thus protect the camera under conditions of sudden accelerations.

5.0 PHOTOGRAPHIC MATERIAL AND PROCESS

5.1 Photographic Process

The photographic process is the relationship between the exposure of an aerial scene, which is the input, and the resulting photograph, which is the output. The variables involved in the photographic process are: film emulsion, exposure, developing time, and developer.

Research has been done on all of these variables. Ray A. Kelsey, in his article, "Resolution Experiments in Contact Printing Through the Film Base" (1955), stated that there was no differentiation in output (resolution) with different developers. He studied several developers: hydroquinone with sodium hydroxide, elon-hydroquinone with sodium carbonate, and elon-glycin with borax. James, in the book The Theory of the Photographic Process (1966), states that resolving power increases to a constant value with an increasing relative aperture, although there was a drop in resolution with very large relative apertures. Jensen, in his book Optical and Photographic Reconnaissance Systems (1968), reasons that films containing larger grains in the emulsion are more sensitive, and thus have a high speed rating. But with larger grains there is an encroachment of lines upon their neighbors, which produces a lower resolution. Thus, for high resolution capabilities, a slower, fine grain film is best. There is a compromise, however, in that

with a slow speed film, there is a greater chance of degradation of the image due to image motion. With the helicopter in a hovering position (no forward motion), the slow film would be best because it will yield images of high resolution, which will not be subjected to image motion. Yost, in his article "Resolution and Sinewave Response as Measures of Photo-Optical Quality" (1960), mentions that overdevelopment causes a decrease in resolution as a result of a spread in image edges. An excellent article, "Resolution of Four Films in a Survey Camera," by P. D. Carman and H. Brown (1970), demonstrates that resolution is improved by stopping down the lens (i.e., increase the aperture) and using slower, high resolution films.

5.2 Tests of the Photographic Process

To test the findings of the previously mentioned researchers, a series of experiments were conducted on the photographic process. Photographs were exposed on Metallographic Plates (format size 9 X 12 X 0.127 cm glass), with the Officine Galileo Camera Verostat Phototheodolite (f = 100 mm). These orthochromatic, antihalation plates have a high resolving power. The resolving power of this camera is shown in Table 5, where "r" is the radial distance from the principal point.

For the experimental conditions, the targets, placed at 125 feet, which yielded a photographic scale of 1/375, were two resolution boards: one with black bars on a white background and the other with white bars on a black background. These were situated to coincide with the principal point of the glass plate. In this first test, an attempt was made to test the effect on resolution of: aperture, magnification, developer, and resolution boards (i.e., white bars on black background versus black bars on a white background).

Table 5. Verostat Resolution Test.

r(mm) / f-stop	-30	-25	-20	-15	-10	0	+10	+15	+20	+25	+30
6.3	34	28	34	34	34	28	34	40	40	28	20
9	24	20	28	34	28	24	17	28	34	40	40
12.5	40	40	40	28	28	28	28	28	40	40	40
18	40	40	40	28	28	28	28	40	40	40	40
25	40	40	40	40	28	28	28	40	40	40	40
36	40	40	40	28	28	28	28	40	40	34	40

It was theorized that a resolution target consisting of white bars on a black background would yield slightly higher resolution values than one of opposite color scheme due to the halation, or image spread effect. The exposures, all at 1/125 second, and developer used on each plate are given in Table 6. The two developers used were Microdol-X and Dektol. Microdol-X

Table 6. Test Conditions.

Plate	Exposure as a function of f-stops	Developer
1	f22	Microdol-X
2	f22	Dektol
3	f16	Microdol-X
4	f16	Dektol
5	f11	Microdol-X
6	f11	Dektol
7	f 8	Microdol-X
8	f 8	Dektol
9	f 5.6	Microdol-X
10	f 5.6	Dektol

is a fine grain developer for films, and contains p-methyl-aminophenol sulfate. Dektol contains monomethyl-p-aminophenol sulfate and hydroquinone. The results for two observers are shown in Figures 23 and 24.

The resolution target of white bars on a black background gave slightly higher resolution values than did the resolution target of black bars on a white background. This would make this target color scheme more readily distinguishable (as discussed in the previous chapter). A more noticeable effect demonstrated in these figures is the loss of resolution for the larger apertures. This is found to agree with James' findings of a decrease in resolution with increasing apertures (in excess of design value). Table 5 indicates that varying the f-stop should produce a nearly constant resolution at the principal point. Because the resulting resolution was not constant for the varying apertures, it would appear that exposure is the cause for the variation in resolution. The overexposure condition, which results in a loss of resolution, should therefore be avoided. From these results it was recommended that the resolution target of white bars on a black background be used in further tests; and that conditions of overexposure be minimized.

Figures 25, 26, 27 and 28, which show the results for two observers, demonstrate that the effect of magnification and developer on resolution is negligible. The detrimental effect of overexposure on resolution is again evidenced in Figures 27 and 28.

In the second test, an attempt was made to determine the effect of shutter speed, or exposure, on resolution. As evidenced in Figure 29, the overexposed plates again gave lower resolution values. A third test to determine the effect of development time on resolution was also conducted. As indicated in Figure 30, resolution increases to a constant value with

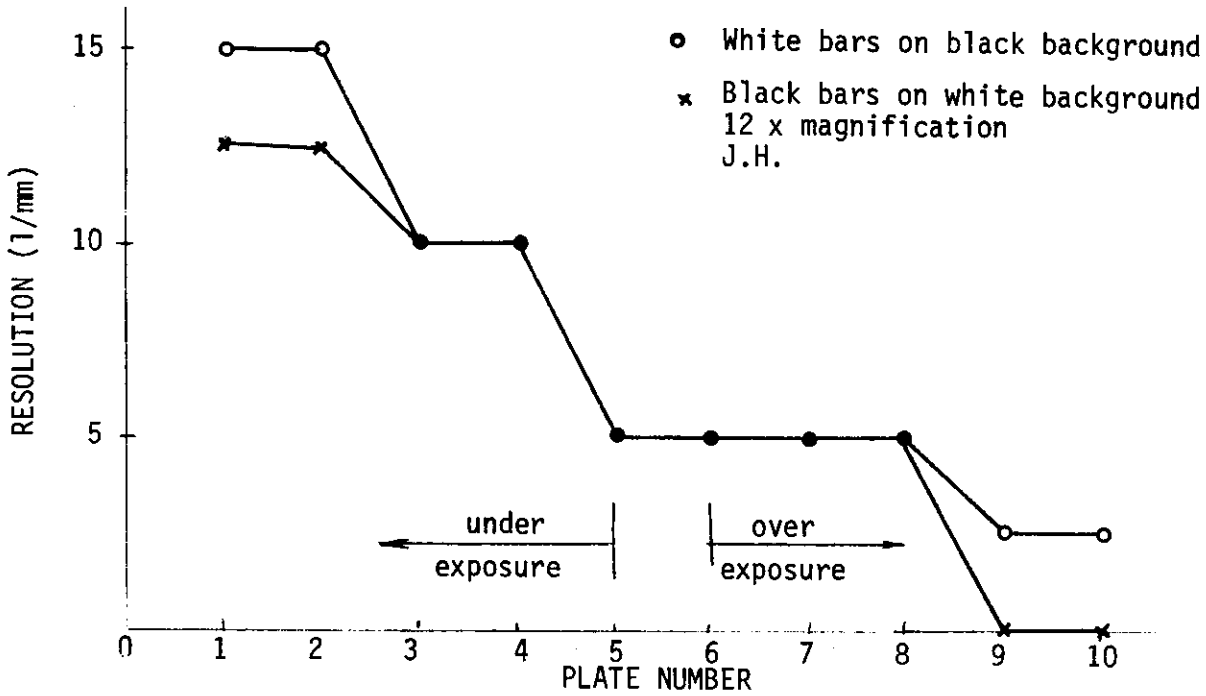

Figure 23. Resolution as a function of resolution target and exposure (controlled by varying f-stop).

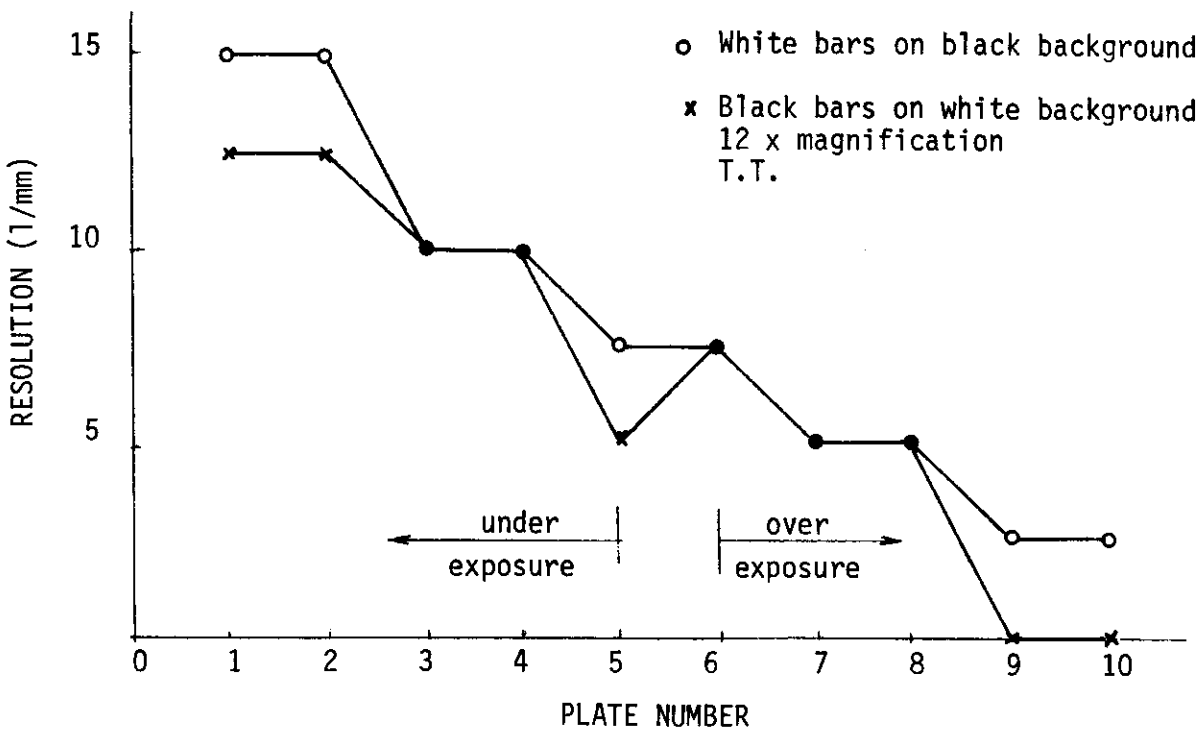

Figure 24. Resolution as a function of resolution target and exposure (controlled by varying f-stop).

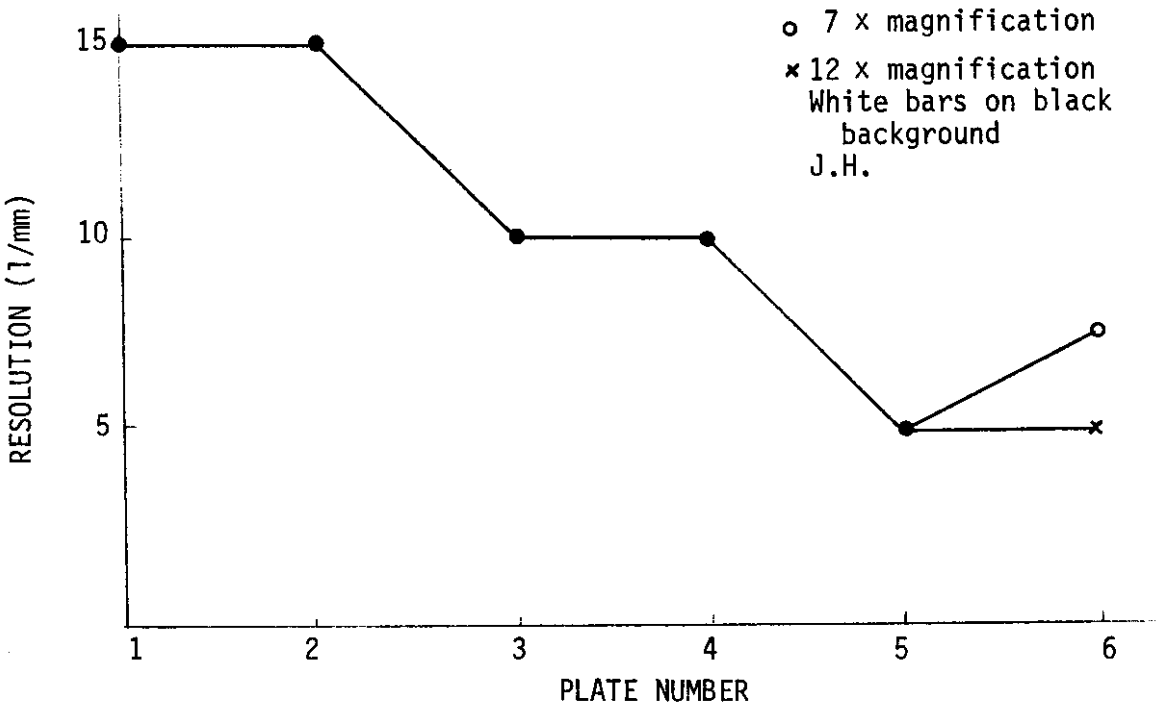

Figure 25. Resolution as a function of magnification.

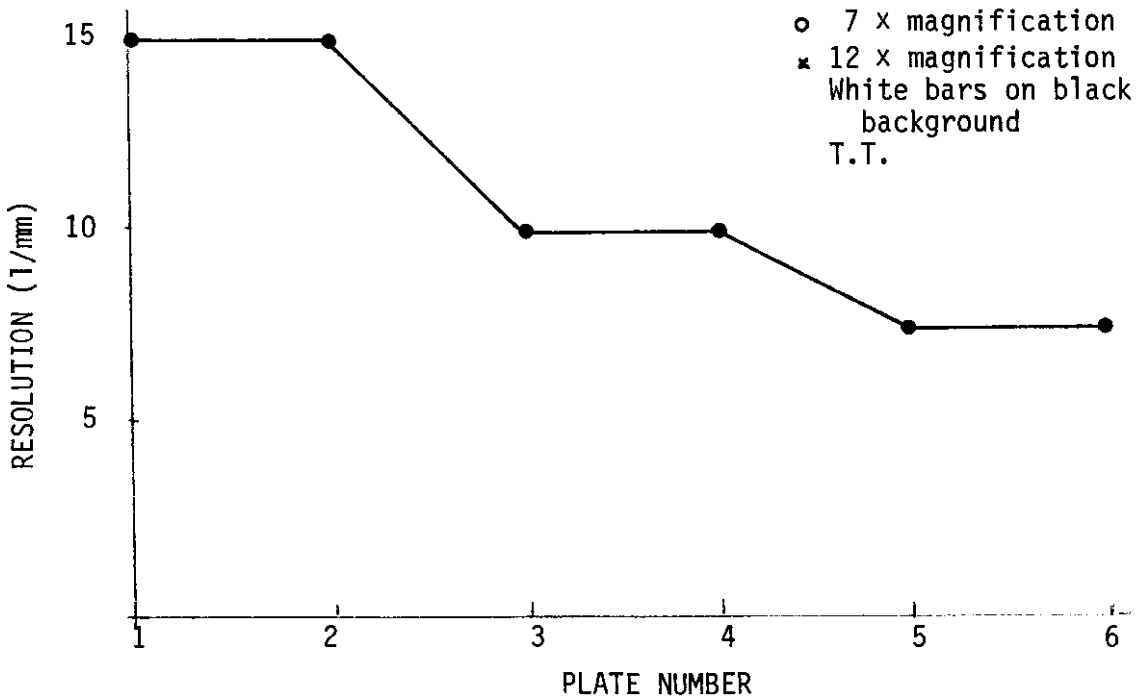

Figure 26. Resolution as a function of magnification.

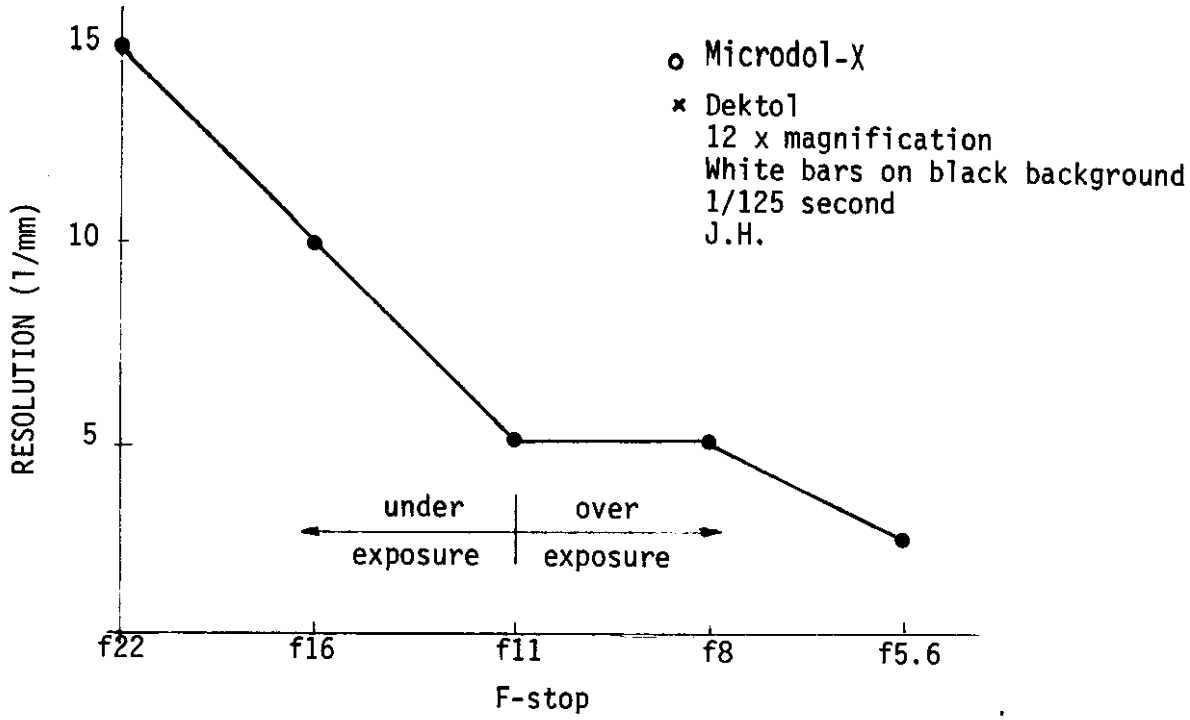

Figure 27. Resolution as a function of developer.

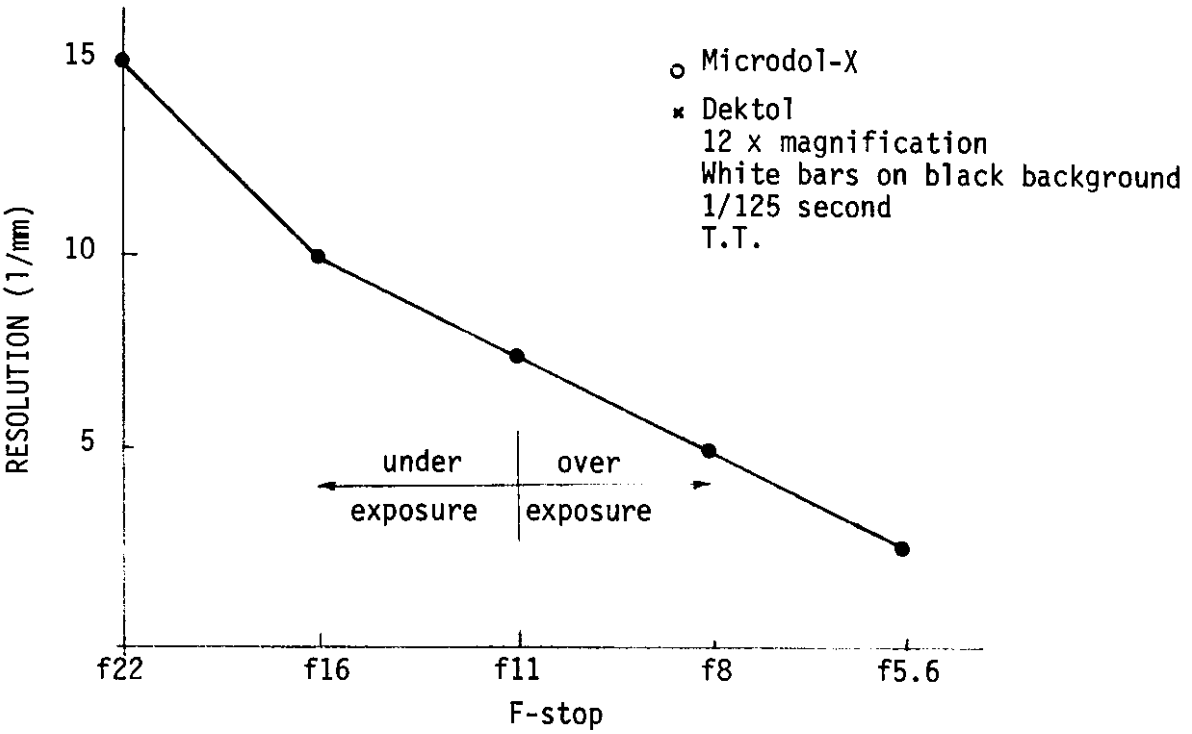

Figure 28. Resolution as a function of developer.

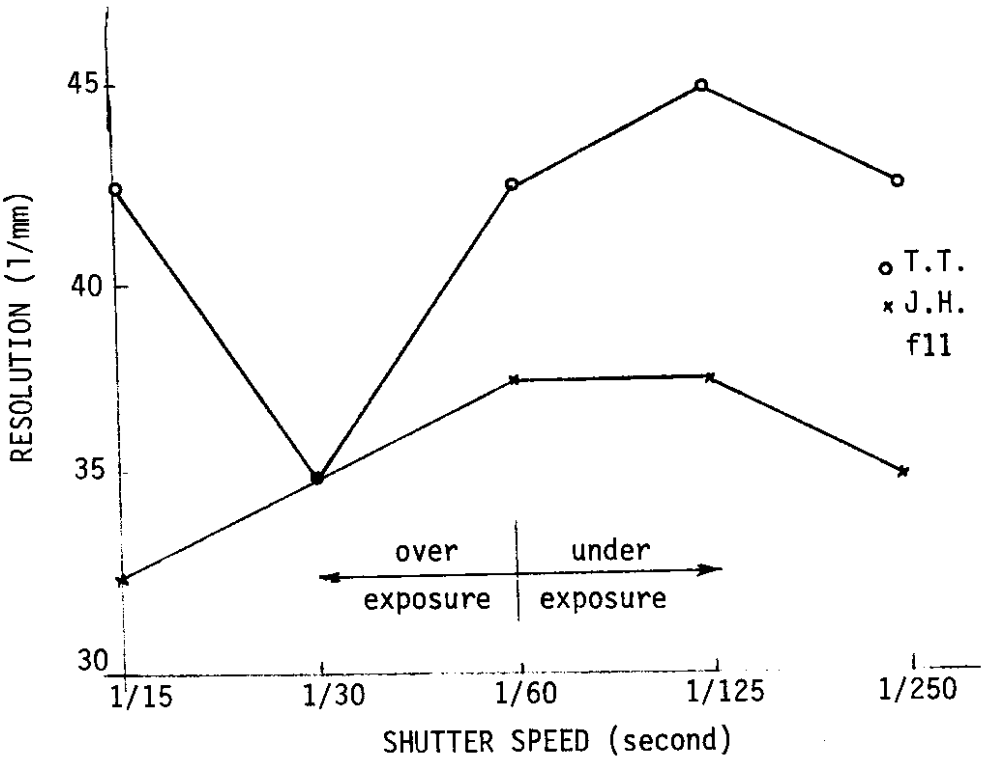

Figure 29. Resolution as a function of exposure (controlled by shutter speed).

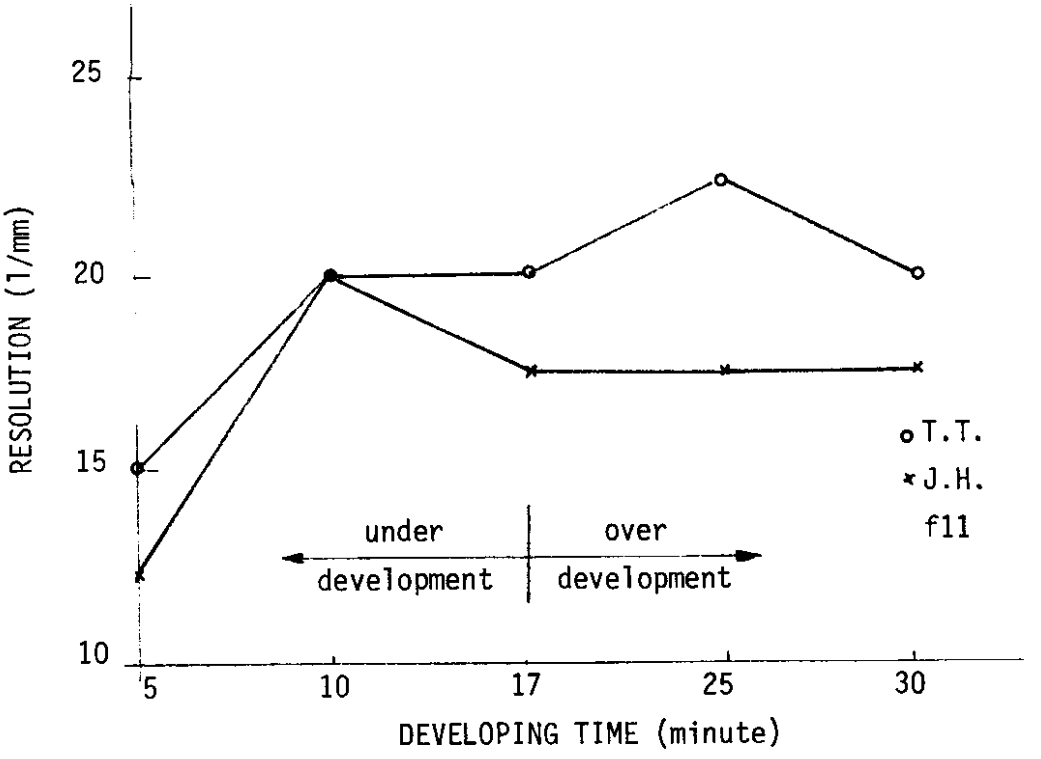

Figure 30. Resolution as a function of developing time.

increasing development time. Thus, the development condition of extreme underdevelopment should be avoided. By developing to manufacturer's specifications a good value of resolution should be obtained.

From the first two tests, it can be seen that overexposure should be avoided by either a decrease in shutter speed or a decrease in aperture size. Both conditions cannot be accomplished simultaneously, as there will not be enough light for a proper exposure if the aperture is made too small with an increased shutter speed. A test was therefore conducted with varying proper exposures, as read on an exposure meter. The results, shown in Figure 31, indicate that there is an optimum exposure for obtaining the best resolution.

These tests were conducted under sunny conditions with a target placed at a distance of 125 feet, which yields a scale of 1/375. Because of scene brightness losses through the atmosphere at the greater in-flight test altitudes, it was felt that a large aperture of f5.6 should be used for the Wild RC-8 camera. The requirement for the avoidance of overexposure would be met by increasing the shutter speed. This was also advantageous in that with a faster shutter speed, there is less detrimental effect due to vibration or image motion. Thus, the variable, photographic process, was varied in the flight tests by setting the aperture at f5.6 and varying the shutter speeds.

The experimentation with aerial films was executed in connection with the test flight. A Zeiss RMK 15/23 f = 6" format size 9" X 9" aerial camera was used with Kodak Double X Aerographic 2405 film, Aerial Film Speed (AFS) 320. A Wild RC-8 f = 6" format size 9" X 9" aerial camera was used with DuPont SR-114R aerial film, AFS 400.

The Zeiss RMK 15/23 camera has a resolution of 75-40 l/mm at the center and at the corner, respectively. The maximum resolution it was possible

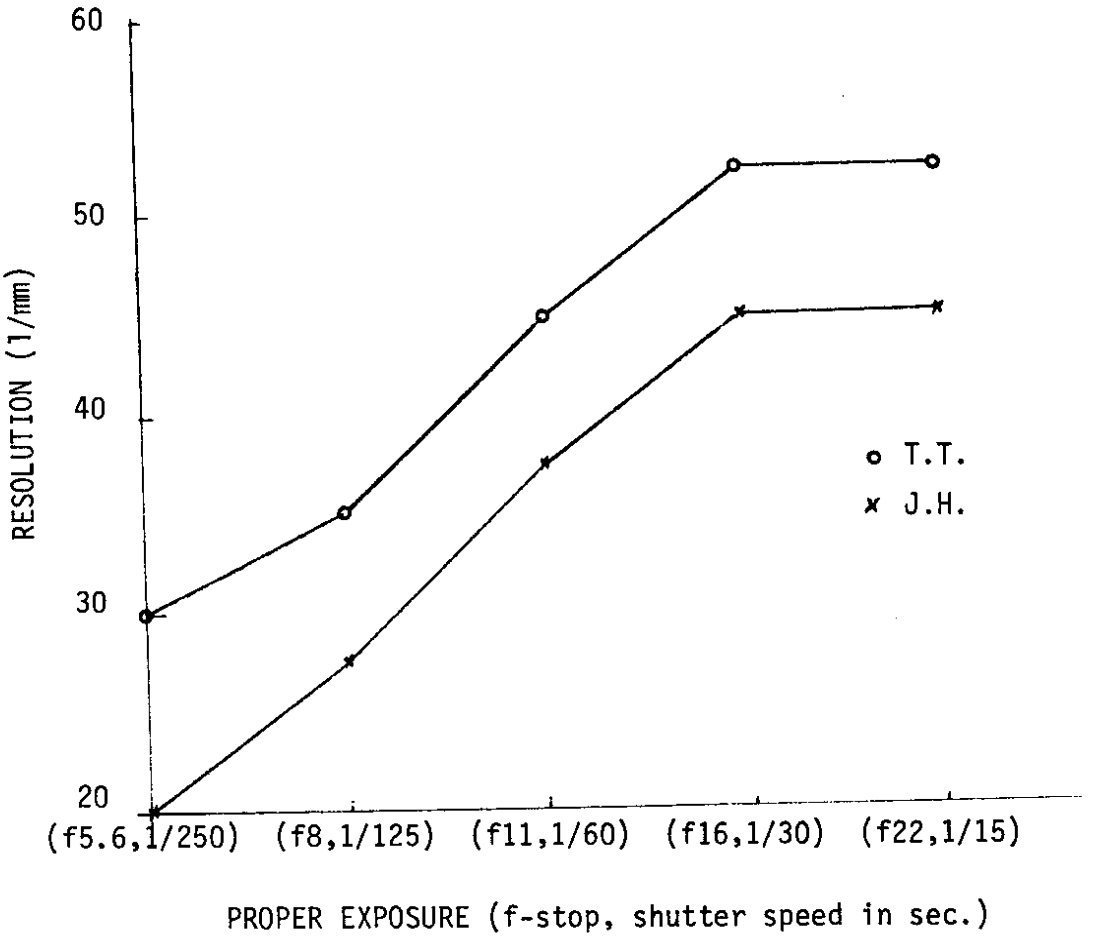

Figure 31. Optimum exposure.

to obtain with this camera and film combination is 30 l/mm.

The Wild RC-8 camera has the resolving power of 50-17 l/mm at the center and at the corner, respectively. The maximum resolving power obtained with this camera and film combination is 27 l/mm.

Several tests executed under various atmospheric and photographic processing conditions verified the above results but no improvements were obtained. The conclusion drawn was that the camera and film as a system are incompatible. In order to verify this conclusion, several tests were made using Kodak High Definition Aerial Film 3414. The resolution of this film ranges from 600 l/mm to 250 l/mm as function of the contrast. The emulsion base of the film is 0.06 mm Estar as compared to the conventional 0.1 Estar base. It was found that the resolving power with the use of the Zeiss camera was 75 l/mm and 40 l/mm at the center and at the corner as compared to 76 l/mm and 39 l/mm provided by the U.S. Bureau of Standards. It can therefore be concluded that the full capability of the cameras mentioned can only be utilized with films of higher resolution.

The 0.06 mm Estar base disqualifies the Kodak High Definition Aerial 3414 film for metric work due to the considerable film shrinkage. Therefore it is not recommended for use. This film has an AFS of only 8, which restricts its use in brilliant sunlight when the normal exposure is 1/200 seconds of f5.6.

The recommended film for use in quality metric work is Kodak Panatomic X on 0.10 mm Estar base, AFS 64, resolution 160-63 l/mm; or Kodak Plus X Aerial on 0.10 mm Estar base, AFS 200, with the resolving power of 100-40 l/mm for days of lower illumination.

6.0 CONTROL POINT TARGETS AND TEST AREA

6.1 Background

The testing at various altitudes of a photographic system's accuracy necessitates the use of ground control points. A prime consideration for these control points is the design of targets. The targets must be designed so that the accuracy of pointing to the target is the same under all test conditions. The pointing accuracy is defined as the precision of centering the black circular floating mark of a plotting machine with a mechanical or optical train on the diapositive image of the target. If there is a constant pointing accuracy for all test conditions, an additional variable will not be introduced with the other variables being tested: vibration, image motion, and photographic process.

Research on pointing accuracies and target design has been conducted by O'Connor (1967) and Colcord (1969). These authors found that the best accuracy of pointing was accomplished by centering the black floating mark inside a white circle on a target. O'Connor found that the significant geometrical variable is the width of the annulus between the edge of the centered floating mark and the edge of the light disk, which is encompassed by a black background. Gubisch (1967) found that the grating acuity of a human eye with a four mm pupil is near one minute of arc, and thus the separation of periodic stimuli can be performed only to this limit of arc. This fact is evidenced in O'Connor's curve of standard deviation of pointing versus annulus width. At a critical annulus width of 1 minute of arc, the curve changed from linear to curvilinear for larger annulus widths. Using the previously mentioned data, Colcord calculates that the target annulus width around the black floating mark should be less than ten micrometers for best

pointing accuracy. Thus, the white circle on which the black floating mark is to be centered should be of a diameter equal to the floating mark diameter plus twenty micrometers, on the photographic image.

6.2 Design

Due to varying flying heights and thus, varying scales of the photographed scene, the area of the projected floating mark on the image will also vary in size. Thus, at each scale, there is an optimum sized white circle for centering the black circular floating mark on the target. As previously mentioned, this white circle diameter, "C", was equivalent to the floating mark diameter plus twenty micrometers. For a forty micrometer diameter floating mark, the diameter of the image of the white circle on the target would be sixty micrometers. A black ring width, "R", of thirty micrometers formed the background for the central wihte circle of the target. The theoretical sizes, "R" and "C", of the target on the ground at each of the varying test scales is calculated in Table 7.

It was felt that, if all these theoretical white circles and encompassing black rings could be placed inside one another (i.e., concentric circles and rings) on one target placed over the control point, then a constant pointing accuracy would be obtained for any of the given scales. This

Table 7. Design Calculations.

	Scale				
	1/600	1/1,200	1/1,800	1/3,000	1/6,000
R (mm)	18	36	54	90	180
C (mm)	36	72	108	180	360

constant pointing accuracy is due to the circles and rings being designed relatively the same at each scale. In designing a target for the size criteria at each scale, it was found that the multi-white circles and black annuli, or rings, surrounding them became cluttered and overlapped. This is due to the black ring at one scale overlapping and thus obliterating the white circle of the next larger scale. Thus, the final target was designed only for the scales of 1/1,800 and 1/6,000.

As shown in Figure 32, the white center circle has a diameter of 108 mm with a surrounding black ring of 54 mm width. The larger white circle has a diameter of 360 mm (including the 54 mm wide black ring, and the 108 mm diameter white center circle) and a surrounding black ring of at least 180 mm width.

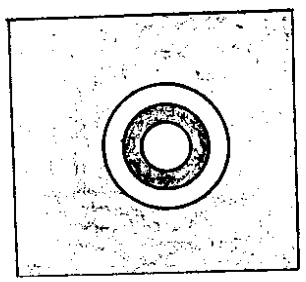

Figure 32. Control target.

Centering the relatively smaller floating marks in the design white circle (at scales 1/1,800 and 1/6,000) yields annuli larger than the ten micrometers specified by Colcord. Larger white annuli will occur at the scales 1/600, 1/900, and 1/3,000. These annuli, "A", are as calculated in Table 8 for a forty micrometer floating mark diameter ("F.M.").

Table 8. Annuli Calculations.

Scale	C_{target} (mm)	$F.M._{target}$ (mm)	A_{target} (mm)	$A_{photograph}$ (μm)	θ (minutes)
1/600	108	24	42	70	11.6
1/1,200	108	48	30	25	4.2
1/1,800	108	72	18	10	1.6
1/3,000	360	120	120	40	6.6
1/6,000	360	240	60	10	1.6

For the worst case of a measuring mark of 6.6 minutes of arc and an annulus width range from 1.6 (1/1,800 scale) to 11.6 (1/600 scale) minutes of arc, there would be an approximate range of the standard deviation of pointing of 5 seconds of arc (i.e., less than 1 micrometer). This fact is based on the curvilinear portion of O'Connor's curve of standard deviation of pointing versus annulus width. Thus, even though the annuli widths are greater than the ten micrometers specified, theoretically an approximately constant standard deviation of pointing should result.

6.3 Testing

Tests were conducted to determine the pointing accuracies at all of the five scales. Tri-X Panchromatic plates (Type B) were exposed on the Officine Galileo Camera Verostat Phototheodolite (f = 100 mm). In case the test results showed a large range of the standard deviation of pointing under the larger annulus width conditions, a black cross was positioned in the center white circle to aid in pointing at the larger scales (1/600 and 1/1,200). A conventional cross target which is used for small scale

photography and a three-legged target were also tested. The effect of tone was also determined on the cross target: a white cross on a black background was compared to a light-blue cross on a black background. It was felt that the white could cause irradiance, or image spread, and increase the size of the white areas with a reduction in size of the black areas (thus, a light-blue target was also tested). These three targets are shown in Figure 33. Also included are two other types of targets, which were found to be unsuitable because they could not be seen at the smaller 1/6,000 scale.

Pointing accuracies for the five targets (white circles with black rings with and without a black cross in the center white circle (see Figure 32), three-legged (black) on a white background, white cross on a black background, and a light-blue cross on a black background) were calculated from the pointings of two observers. The "x" and "y" plate coordinates of the floating mark centered on the target image were measured on the Nistri AP/C Analytic Plotter, which has a 7X magnification. A flow chart of a program for computing standard error of pointing on the target is shown in Appendix I. For the two observers, Figures 34 and 35 compare the standard errors of pointing on the target with the cross to the three-legged target; and Figures 36 and 37 compare the circular target (with and without the center cross) under different contrast or exposure conditions. Poor contrast resulted from underexposure.

The ideal target is the one which gives the least deviation in standard errors throughout the scale ranges, not the one which gives the least absolute value of the standard error of pointing. The results indicate that the cross gives a smaller deviation in standard errors of pointing and is therefore better than the three-legged target; and over the scales tested, the white cross is better than the light-blue one. The circular target without

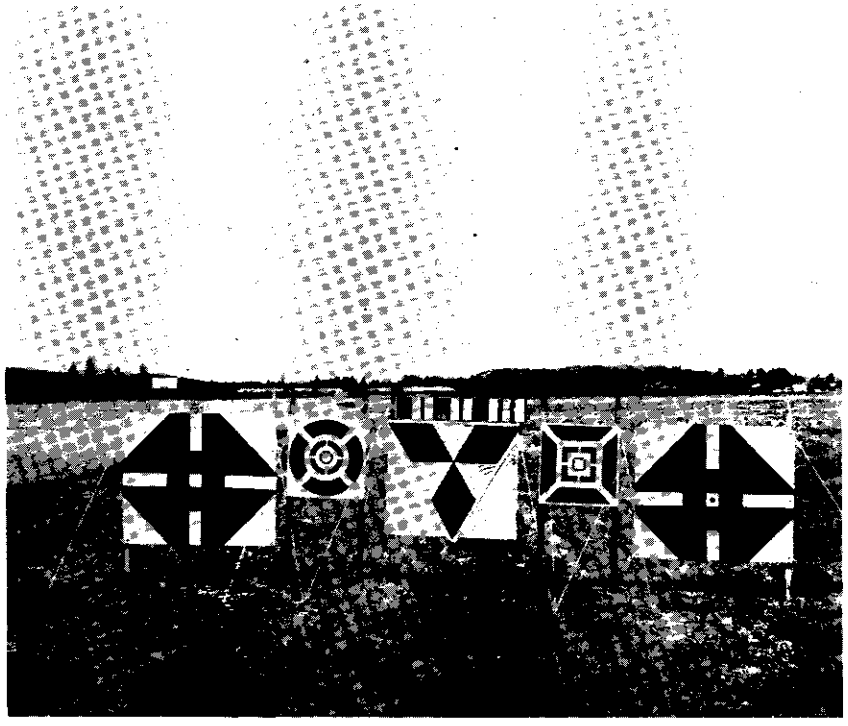

Figure 33. Test targets.

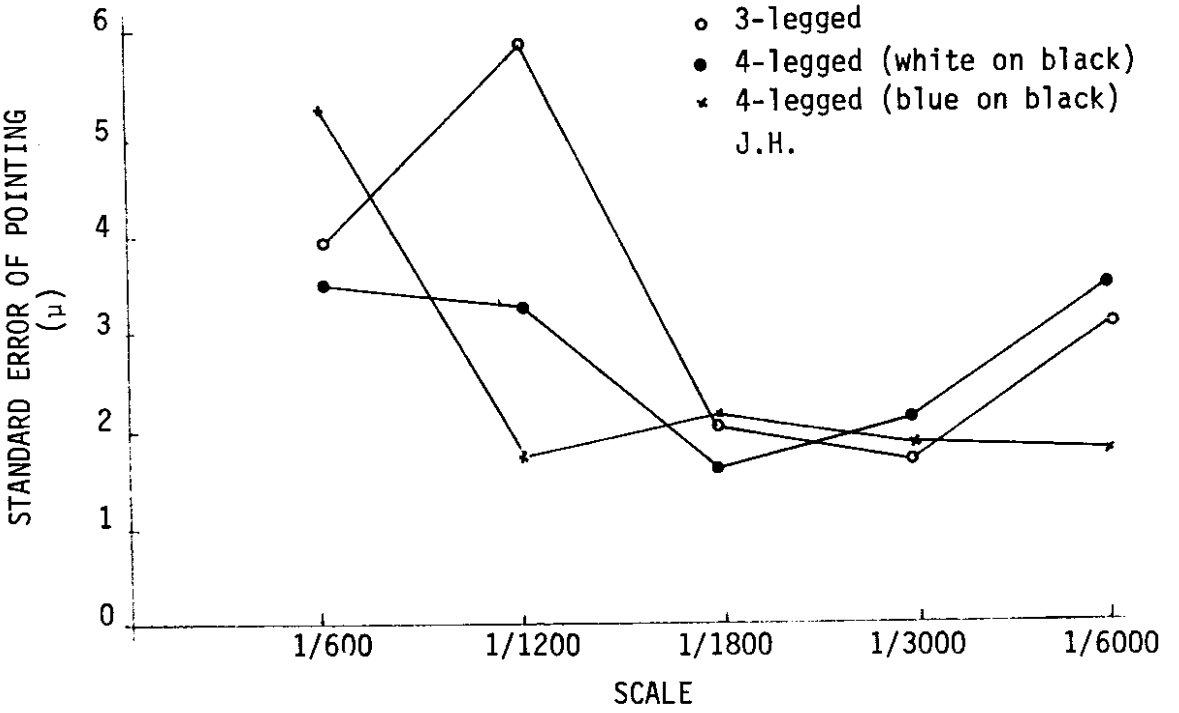

Figure 34. Standard errors of pointing for three-legged target and cross target (white and light-blue crosses).

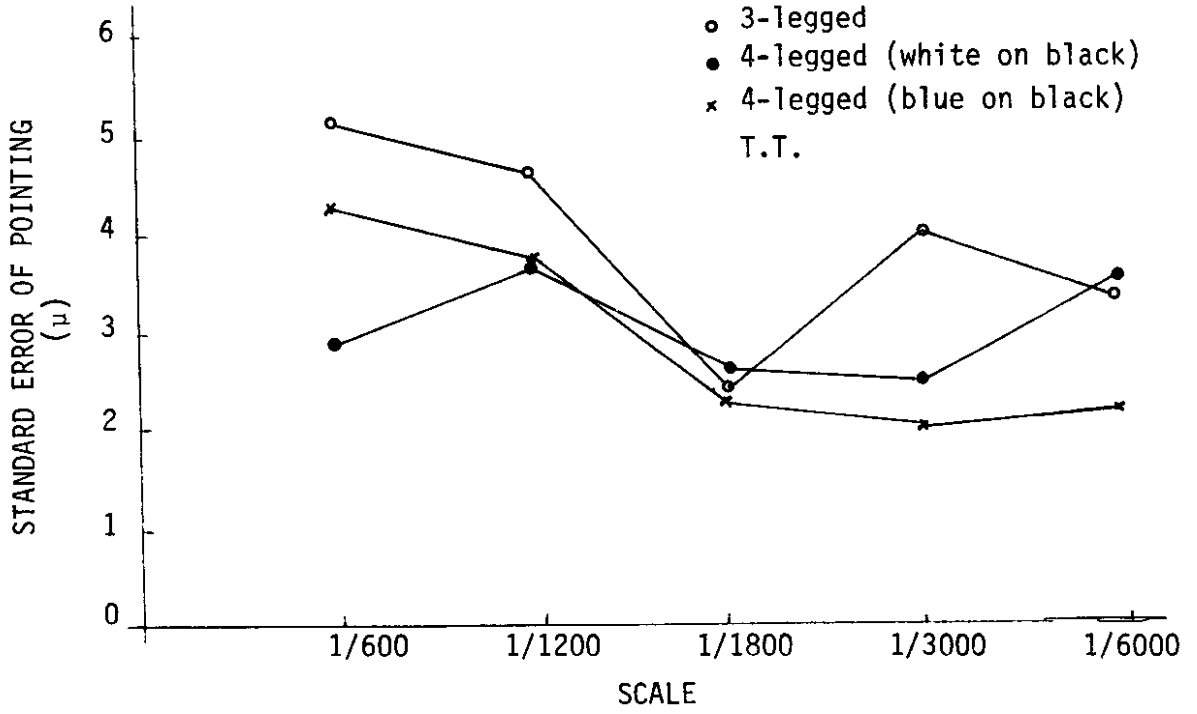

Figure 35. Standard errors of pointing for three-legged target and cross target (white and light-blue crosses).

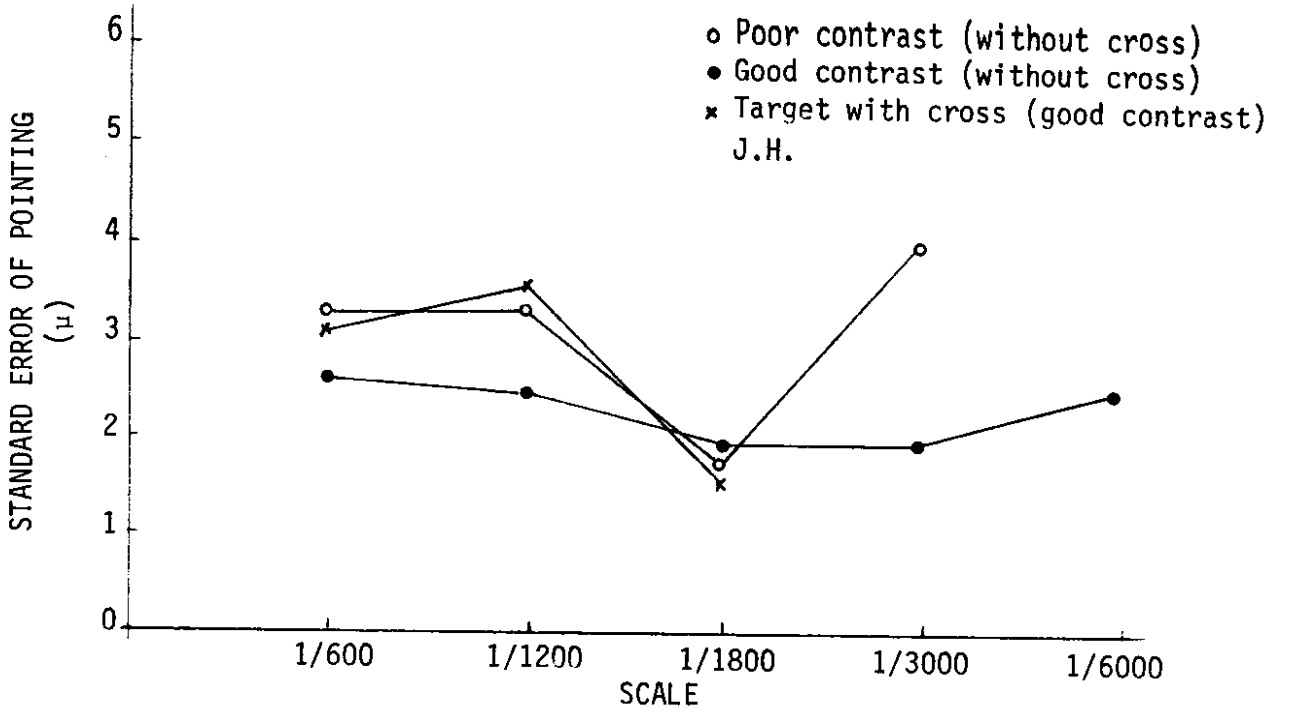

Figure 36. Standard errors of pointing for circular targets.

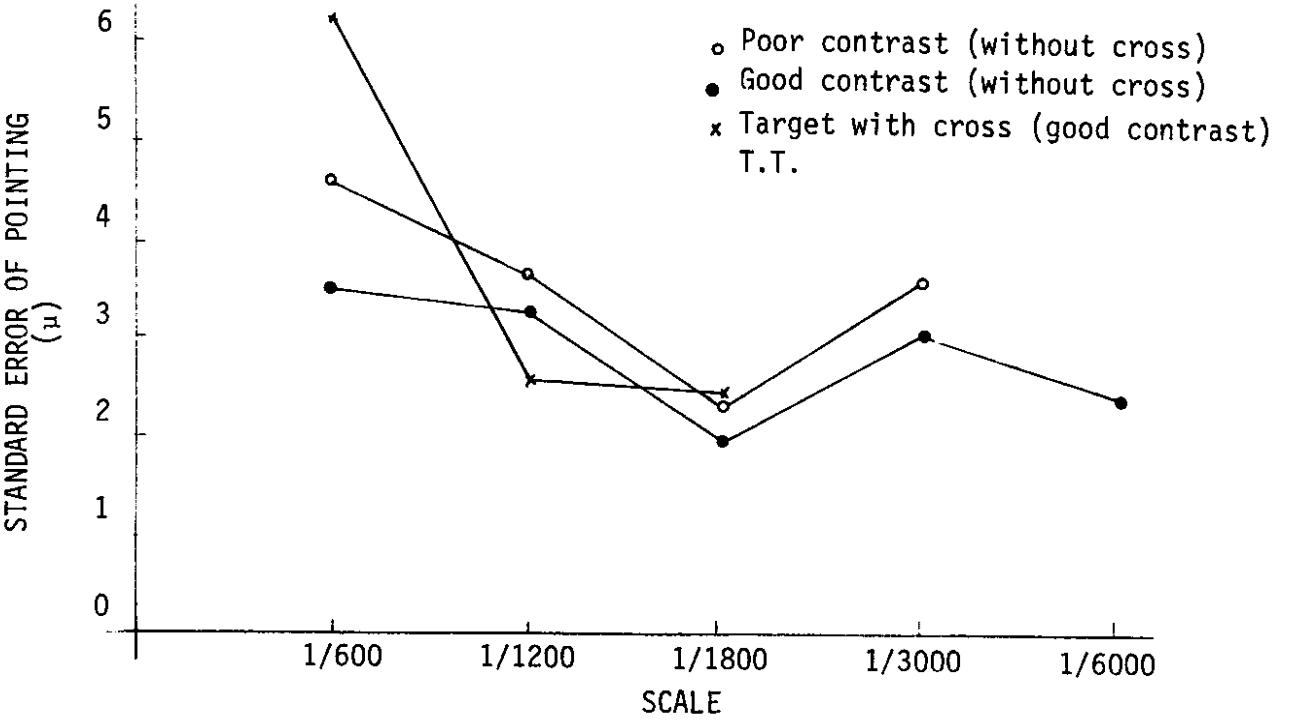

Figure 37. Standard errors of pointing for circular targets.

the cross was the best target in this test. It is interesting to note that the deviation in the standard errors of pointing for the circular target without the center cross is almost constant (as predicted from O'Connor's curve). It should also be noticed from Figures 36 and 37 that the contrast of the targets has a great effect on pointing accuracy. A greater range in standard errors of pointing results for a target of poor contrast. Thus, it was recommended that the target scheme used for in-flight tests be the one with white circles and black rings (design scales 1/1,800 and 1/6,000); and it was also recommended that good contrast be upheld in order to have an approximately constant standard error of pointing at all scales.

6.4 Test Area

The area to be used for in-flight testing of the effects of the test variables was the airport at Tumwater, Washington. Preliminary tests were conducted at flying heights of 300, 600 and 900 feet. A model of two photographs with a sixty per cent overlap was established at each flying height for each test condition. Resolution boards were placed on the ground, as shown in Figure 38, to coincide with the principal point of the photographs, and were spaced at distances equivalent to the airbase needed at each altitude for a sixty per cent overlap. These airbases were 180, 360, and 540 feet. Between these resolution boards, in the sixty per cent overlap model area, control targets were painted on the asphalt taxi-ways, as depicted in Figure 39. By suitably placing the resolution targets, which were the principal point of each photograph, the control points for the 300 foot exposures would occur in the 600 foot exposures. Similarly, both the 300 and 600 foot control points would occur in the 900 foot exposure. At least twenty control points were painted for photographing in each model. Some

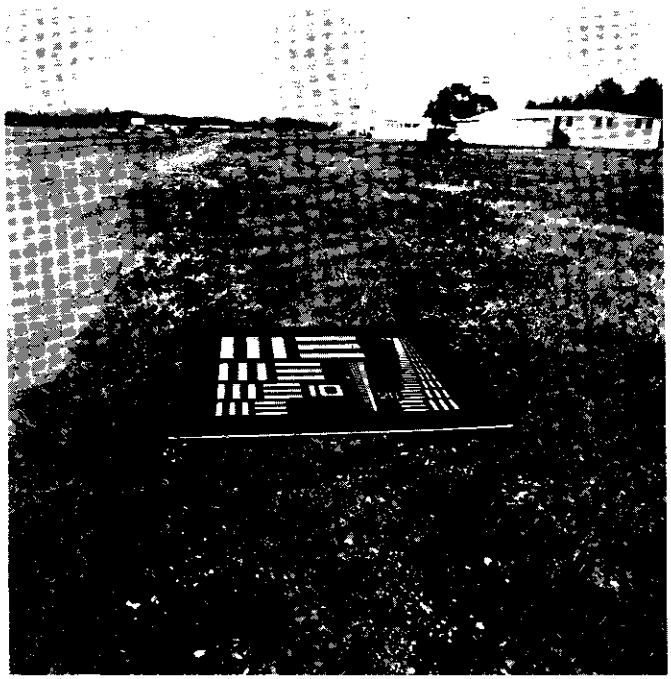

Figure 38. Resolution target in test control area.

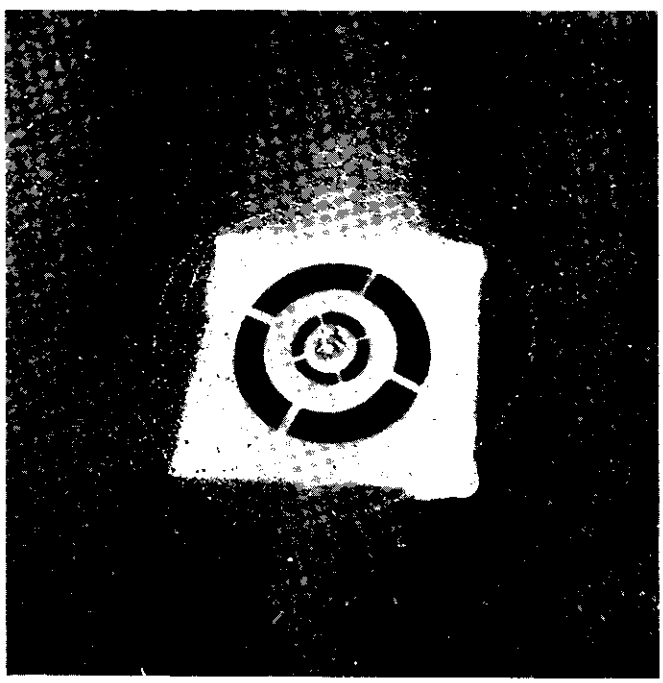

Figure 39. Control target in test control area.

of these were to serve as control targets and the remainder were to serve as accuracy checks to compare with the coordinates as determined on a photogrammetric plotter (e.g., AP/C). The "x", "y" and "z" coordinates of these control points were surveyed by intersection and traverse methods to a better than second order accuracy.

Flights over the test area were conducted at each altitude with the Model 47G-3B-1 helicopter in both a hovering and flight (30 m.p.h.) condition. The film used in the Wild RC-8 camera (f = 152 mm) was DuPont's SR-114R, ultra speed panchromatic (AFS 400). The shutter speed was varied (1/200 - 1/700 second) only at the 300 foot flying height. Vibration was also tested at this flying height by taking exposures with the camera mounted on the rubber pads and then mounted rigidly to the air-frame. The effects of image motion were tested at each flying height with the helicopter flying at a velocity of 30 m.p.h.

Thus, the control point targets were used for determining the accuracy of a system (i.e., the accuracy of the determination of the "x", "y" and "z" coordinates of the control points). The resolution targets were used for determining the effect on resolution of the variables: vibration, image motion, and the photographic process.

After the flight tests the camera was mounted, in a terrestrial position, and photographs were taken with the resolution targets spread across the photograph image. These photographs were taken with the same shutter speeds as used in the flight tests. Thus, these ground control photographs would give resolution values at any point on the photograph for all the tested exposures and without the detrimental effects of vibration and image motion. These photographs gave, in essence, the static film-lens resolution value throughout the photograph image.

6.5 Re-targeting of Control Points

The actual tests of the targets and control points provided negative results concerning the size and geometric configuration of the targets and the accuracy of control points.

The most apparent problem occurred in the pointing targets utilized. The target design for multiple scale was too large for accurate observations. Weathering of the paint bleached out the dark rings. Added to this were the halation effects, enhanced by the white background and the induced target blur.

The conclusion has been drawn that neither the painting method nor the geometry of the target were unacceptable. Further, the design of targets for multiple flying height is not practical. The target should not be designed for more than the two flying heights, so that the rings in the geometry of the targets will remain clearly distinguishable.

To overcome this problem, the targets had to be repainted, and also made smaller for the low flying heights utilized. This created an additional inconsistency, however, because now the repainting made targeting a variable, and possibly any correlations made between previous flight accuracies would be erroneous.

The new target was designed for flying heights of 600 feet and 1800 feet. Figure 40 depicts the target design. The contrast scheme was reversed from the design for previous flights. This was done to reduce the halation effects, and also added consistency to the resolution boards, as they are white bars on a black background.

The paint criteria involved a high contrast between black and white, a low per cent transmission in white to avoid halation effects, and a strong

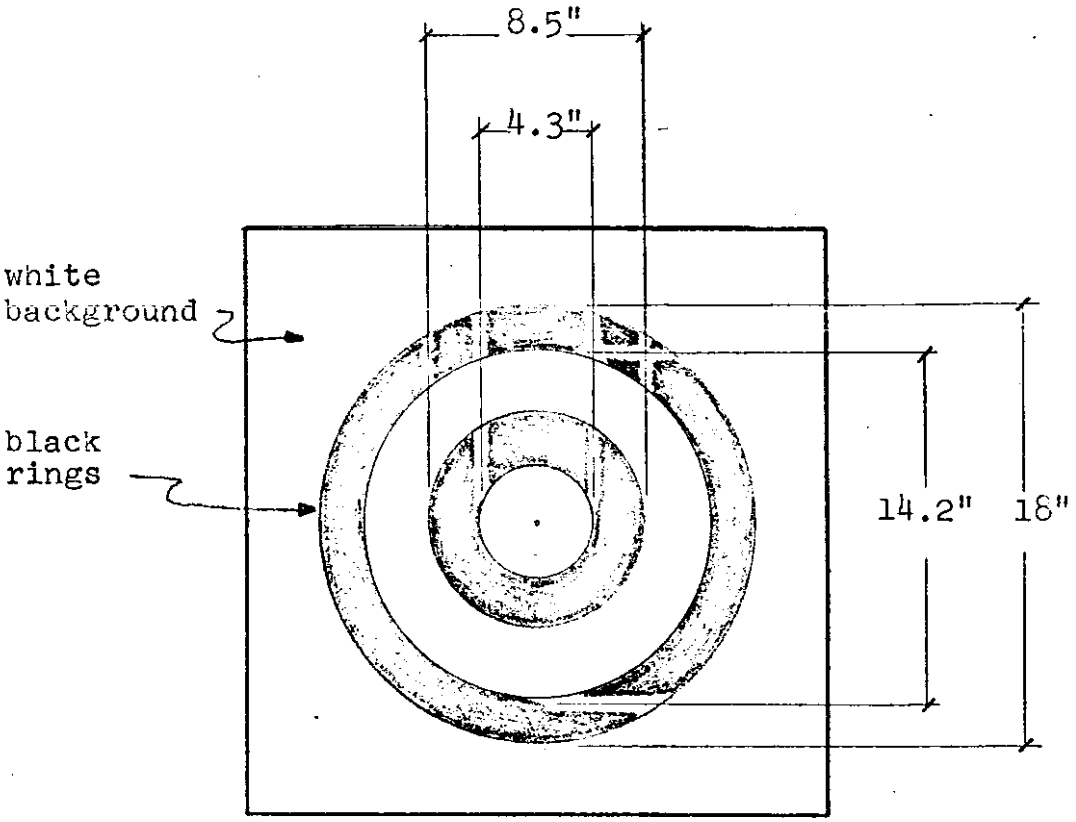

Figure 40. Point targeting.

resistance to weathering. To accomplish these parameters, chlorinated white rubber base traffic line paint and traffic black paint were used. One further stipulation involved painting the target on the asphalt surface. Sharp edges must be required to hold resolution as high as possible, and yet paint was used for permanence of controls. Since spray paint proved unsuitable, a stencil was cut from wood to be used with a brush. To maintain distinct edges, the stencil was bordered with weather-stripping to fill the small gaps in the asphalt. This proved to be both an effective and efficient means of laying ground targets.

These targets maintained their contrast and shape for two years without any noticeable deterioration.

Other targets have also been subjects of experiments and research, notably targets manufactured by Industrial Photographic Sign Corporation (10846 Myers Way South, Seattle, Washington 98168). These signs or targets can be manufactured in different colors and shapes. The targets consist of metal bases upon which the targets are coated photographically. The photographic coatings are then sealed with transparent epoxy.

These targets have been the subject of extensive experiments because it was felt that they are capable of providing "permanent" monuments for aerial photogrammetry. The most severe experiment was to use them on a road surface where traffic was moderate. These targets showed no deterioration after five winter months. The exception was on a road surface where studded tires were used. Consequently, these targets are recommended wherever permanent signalization of monuments is required.

6.6 Re-establishment of the Control Net

From the initial results, we found ourselves dealing with residuals in tenths and hundredths of a foot, as will be shown later. It seemed that with this consideration in mind, the second-order accuracy of our ground net may be unacceptable. Asphalt also has a tendency for movement, and it was therefore felt the control net should be checked. Further, some difficulty was encountered in placing the target stencil symmetrically about the tack. It seemed advisable, then, to re-measure locations about the center of the target rather than the tack coordinates. The unique procedure used to establish these new coordinates deserves mention, and the approach is herein presented.

The level net, or "Z" coordinate, was established in the conventional level-rod manner, utilizing a Zeiss self-adjusting level. Three runs were

made through the net, and the greatest closure error amounted to 0.01 feet. Therefore, the values were simply averaged.

The traverse was attempted during a hot day, and heat waves from asphalt can be intolerable. For this reason, a trilateration system was considered and finally adopted, as electromagnetic distance measuring devices (EDM) are not as affected as reading a theodolite. The largest distance in the net amounts to about 300 feet, and therefore a short-range EDM was sufficient. The choice was the Hewlitt-Packard 3800, which has a resolution of 0.002 feet and accuracy of $\pm$0.01 feet + Distance/100,000. For the short distances measured, the accuracy can be simplified to $\pm$0.01 feet. The assembly comprised an attenuator and single prism, which provided sufficient power for readout.

The procedure for measurement was to establish an outer net of three points, from which all other points were shot-gunned. Since there are 17 points in the entire model, this amounts to 46 independent observations. Points 13 and 16 were used as given ground control, thereby stabilizing the geometry of the system (see Figure 41).

The observation equation method of least squares adjustment was utilized to reduce the data, as now we have 46 observations, 30 unknowns (X and Y coordinates of 15 points). The basic equation of the observation method is:

$$V = AX - L \quad \text{in matrix}$$

$$46V_1 = 46A_{30}\ 30X_1 - 46L_1 \quad \cdots\cdots\cdots\cdots\cdots\cdots\cdots\cdots\cdots\cdots 6.1$$

The standard procedure was utilized to form the matrices, which involved a Taylor series expansion to linearize the basic distance equation. A unity weight matrix was assumed for two reasons: (1) a constant EDM error source, and (2) additional weight placed on the outer net control points is inherent in the "A" matrix.

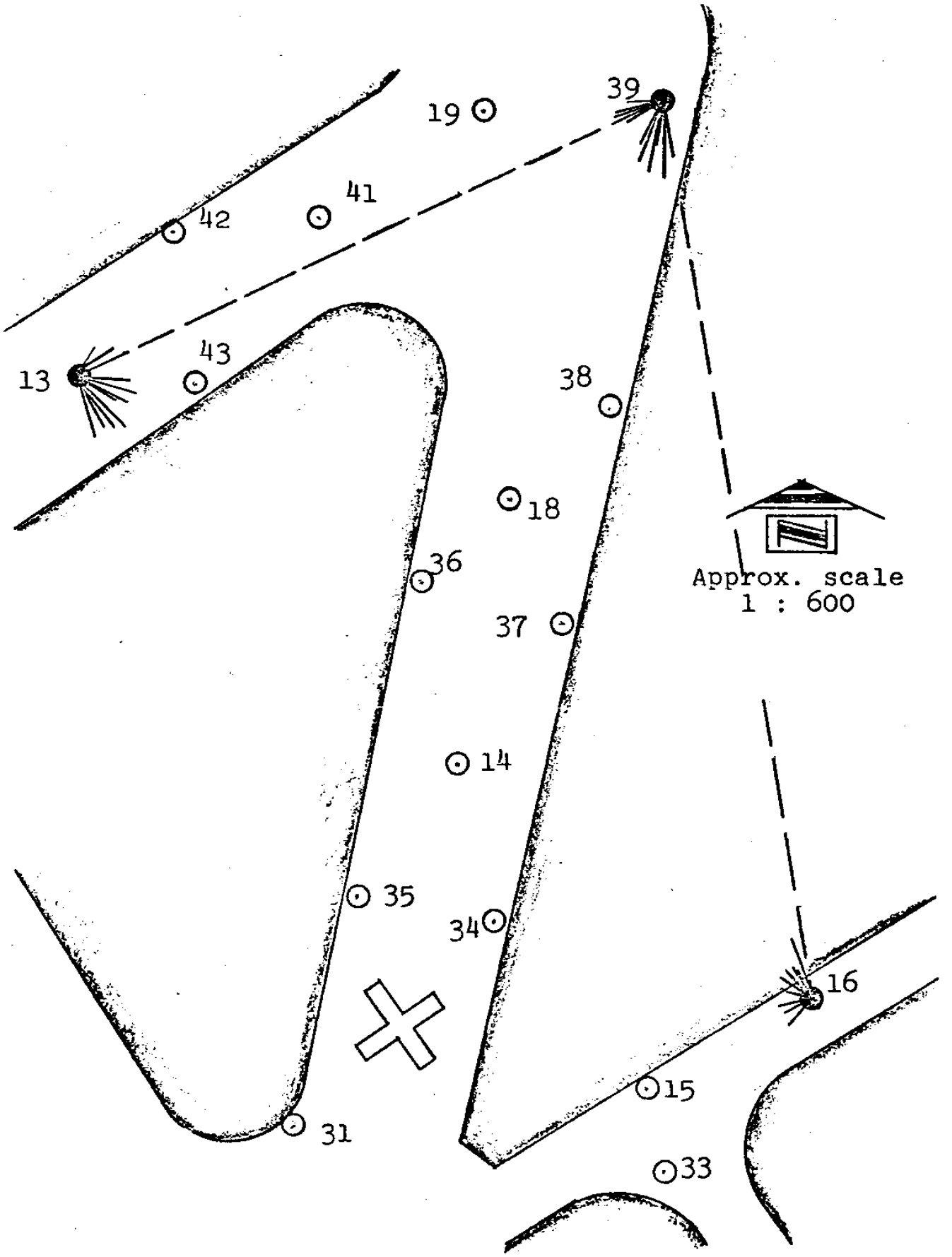

Figure 41. EDM trilateration net.

The results are quite acceptable. The value of the unit standard error squared was 0.00014. This value was then placed in the equation:

$$\sigma_i^2 = q_{xx}\,\sigma_o^2 \quad \ldots\ldots\ldots\ldots\ldots\ldots\ldots\ldots\ldots\ldots\ldots\ldots 6.2$$

to determine the standard errors of the most probable values of X and Y coordinates. The range of these standard errors was between 0.0054 feet and 0.014 feet, with a mean standard error of the net of $\pm$0.010 feet, or precisely the accuracy statement of the EDM itself. The ground control values are shown in Table 9 for future reference.

7.0 NUMERICAL EVALUATION

There were five helicopter test flights in order to determine the various parameters of use of the helicopter as a camera platform. The various flights will not be described in detail in this section. Instead, they will be grouped by the results achieved.

A typical test flight usually consists of obtaining 30-50 photographs taken under various conditions and parameters. Table 10 shows a typical arrangement for the test flight as well as the results evaluated in terms of resolving power. Tests were made to determine the minimum shutter speed and the deterioration of resolution due to image motion and vibration, to determine the variation in orientation elements, and finally, to find the achievable accuracy.

7.1 Determination of Minimum Shutter Speed

The helicopter as a camera platform is characterized by low frequency, high amplitude vibrations. The exposure time, "t", is a short period which may occur at any point during the period of oscillation. If it falls at a

Table 9. Re-established Ground Network.

POINT	X (ft)	Y (ft)	Z (ft)
13	308.780	685.960	192.725
14	425.409	569.635	193.694
15	489.290	474.141	194.145
16	533.930	503.180	194.036
18	438.319	653.792	193.080
19	424.252	770.075	192.320
31	383.873	453.705	194.504
33	495.872	448.656	194.410
34	440.309	522.634	194.097
35	397.209	527.788	194.010
36	412.265	625.766	193.318
37	454.958	617.050	193.415
38	466.155	684.314	192.966
39	478.612	775.512	192.378
41	376.746	735.412	192.459
42	334.807	734.038	192.426
43	342.662	683.460	192.776

NOTE: X and Y values are $\pm$0.011 feet
Z values are $\pm$0.030 feet

Grid system: X coordinates - 1,401,500.0
Y coordinates - 607,000.0

Table 10. Results of First Flight.

Photo No.	Altitude (feet)	Exposure (sec.)	Flight *	Resolution (l/mm)		Mean Resolution (l/mm)
				J.H.	T.T.	
1	300	1/200	H	20	20	20
2	"	"	H	25	25	25
3	"	"	F	7.5	7.5	7.5
4	"	"	F	7.5	10	9
10	"	1/400	H	25	25	25
11	"	"	H	22.5	20	21
4A	"	"	F	17.5	17.5	17.5
5	"	"	F	25	27.5	26
30	"	"	RH	27.5	27.5	27.5
31	"	"	RH	22.5	25	24
32	"	"	RF	12.5	12.5	12.5
33	"	"	RF	10	12.5	11
8	"	1/700	H	27.5	30	29
9	"	"	H	27.5	25	26
6	"	"	F	25	27.5	26
7	"	"	F	27.5	30	29
12	600	1/400	H	15	10	12.5
13	"	"	H	25	25	25
14	"	"	F	25	30	27.5
15	"	"	F	20	20	20
20	900	"	H	30	37.5	34
21	"	"	H	22.5	22.5	22.5
18	"	"	F	22.5	22.5	22.5
19	"	"	F	22.5	15	19
16	"	"	F	15	22.5	19
17	"	"	F	22.5	22.5	22.5
34	T	1/200	TL	12.5	10	11
"	"	"	TC	22.5	22.5	22.5
"	"	"	TR	12.5	15	14
"	"	"	TFR	15	15	15
35	"	1/400	TL	15	17.5	16
"	"	"	TC	25	22.5	24
"	"	"	TR	15	17.5	16
"	"	"	TFR	15	17.5	16
36	"	1/700	TL	20	22.5	21
"	"	"	TC	30	27.5	29
"	"	"	TR	12.5	17.5	15
"	"	"	TFR	17.5	20	19

* H = hover
F = flight (30 m.p.h.)
T = terrestrial
RH = rigid hover
RF = rigid flight (30 m.p.h.)

TL = terrestrial (left side of photo)
TC = terrestrial (center of photo)
TR = terrestrial (right side of photo)
TFR = terrestrial (far right side of photo)

time when the sine function of oscillation is at its peak, the motion will be minimum, and when the sine function is zero the motion will be at its maximum. Considering this phenomenon, Troth (1960) pointed out that "The reduction of exposure period reduces the motion occurring as a result of vibration only for frequencies below ½ t c.p.s. For these frequencies the effect of the motion is essentially the same as that produced by a 'uniform motion.'" For a helicopter with maximum frequency of 24 c.p.s., the maximum exposure will be:

$$t_{max} = 2 \times 24 \text{ c.p.s.} \simeq 1/50 \text{ sec.} \quad \ldots\ldots\ldots\ldots\ldots\ldots 7.1$$

This equation indicates that for a helicopter with low frequency vibration, 1/50 second exposure is possible. If such a long exposure is proved practible, then an "all-weather" photography is possible. In order to test this equation, a Hasselblad 70 mm (f = 50 mm) camera was used because neither the Wild nor the Zeiss aerial cameras have a shutter speed of 1/50 second. In order to imitate the same conditions involving the use of a standard aerial camera, the Hasselblad was placed in the Wild RC-8 camera mount between two steel ballasts, thus allowing the same weight used with the other camera. Figure 42 shows this solution with the air-frame over the helicopter pad.

Photographs were taken as the helicopter hovered over the resolution target at a 100 foot altitude. The photo scale of 1:600 corresponds to a photograph taken with a standard aerial camera at a 300 foot altitude. The shutter speeds were varied from 1/500 to 1/15 second. Several photographs were evaluated and the average results are listed in Table 11.

Table 11

Shutter speed	1/500	1/250	1/125	1/60	1/30	1/15
Resolution 1/mm	27.5	24.0	27.5	10.0	10.0	5

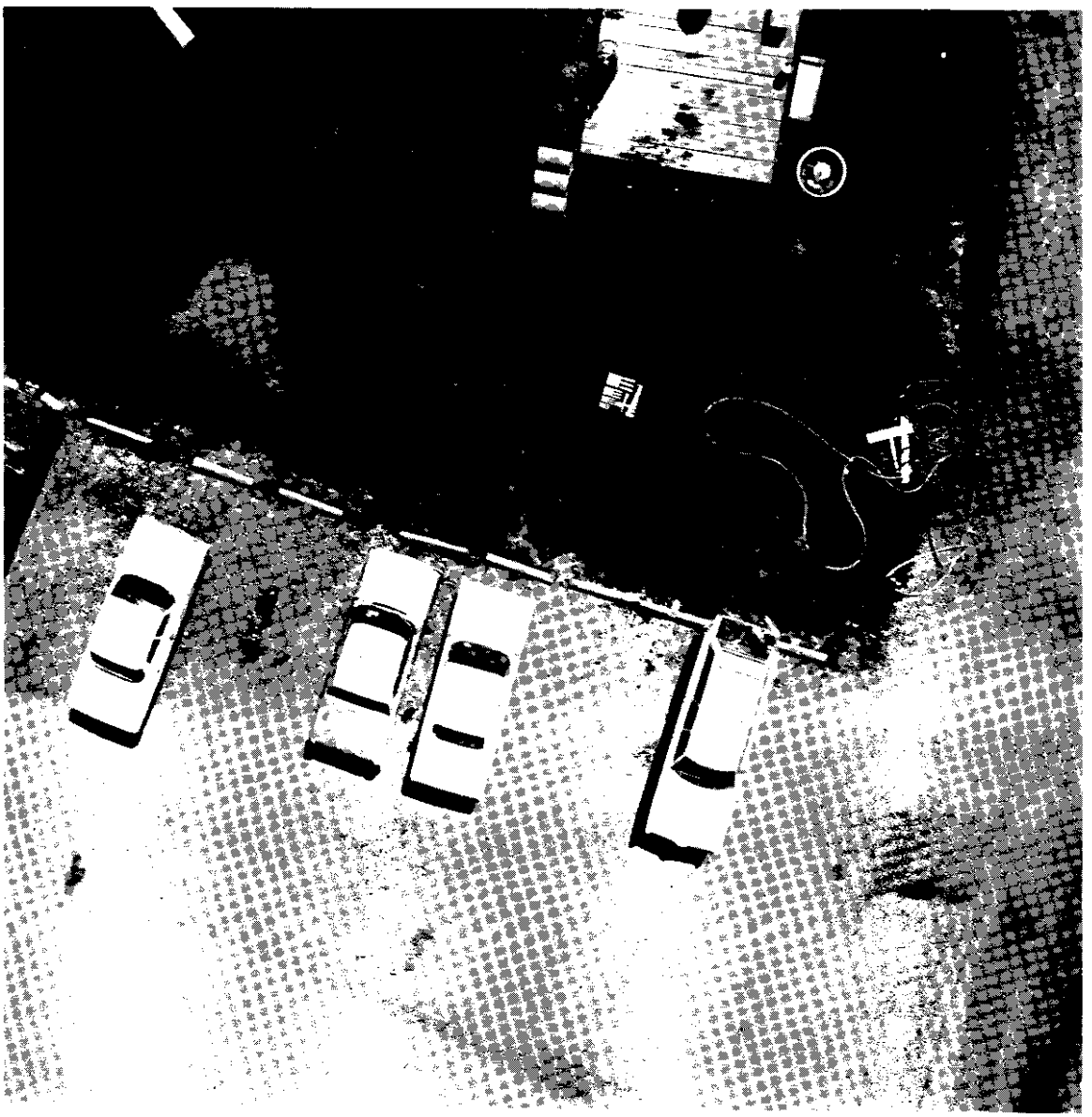

Figure 43.

It can be seen from this table that the maximum exposure time is around 1/60 second as indicated by equation (7.1). To illustrate the worst results obtained from this experimentation, the photographs taken at 1/60 second exposure are given in Figure 43. This photograph indicates that some bars on the resolution target are blurred while others exhibit sharp edges. The sharp images are parallel to the direction of flight while the blurred ones are perpendicular to it. Therefore it can be concluded that the blur resulted from the forward motion of the helicopter.

The final conclusion from these experiments is that the minimum possible exposure time recommended is 1/100 second, which permits "all-weather" photography.

7.2 Deterioration of Resolution

The initial step in analyzing the resulting test photography was a determination of the resolution. This resolution was read off the resolution boards situated at the approximate centers of the photographs. As an example, Table 10 lists the resolution values which were read, for all conditions tested, by two observers. The apparent differences in resolution between two stereo pairs of photographs is partially due to the inability of the pilot to keep the helicopter at a constant flying height. The results from these resolution determinations can be listed as follows:

1. For the ground control (terrestrial) photographs, there was an increase in resolution as the shutter speed increased (i.e., 1/700 second shutter speed gave the best resolution). There was also a drop-off in resolution from the center of the photograph.

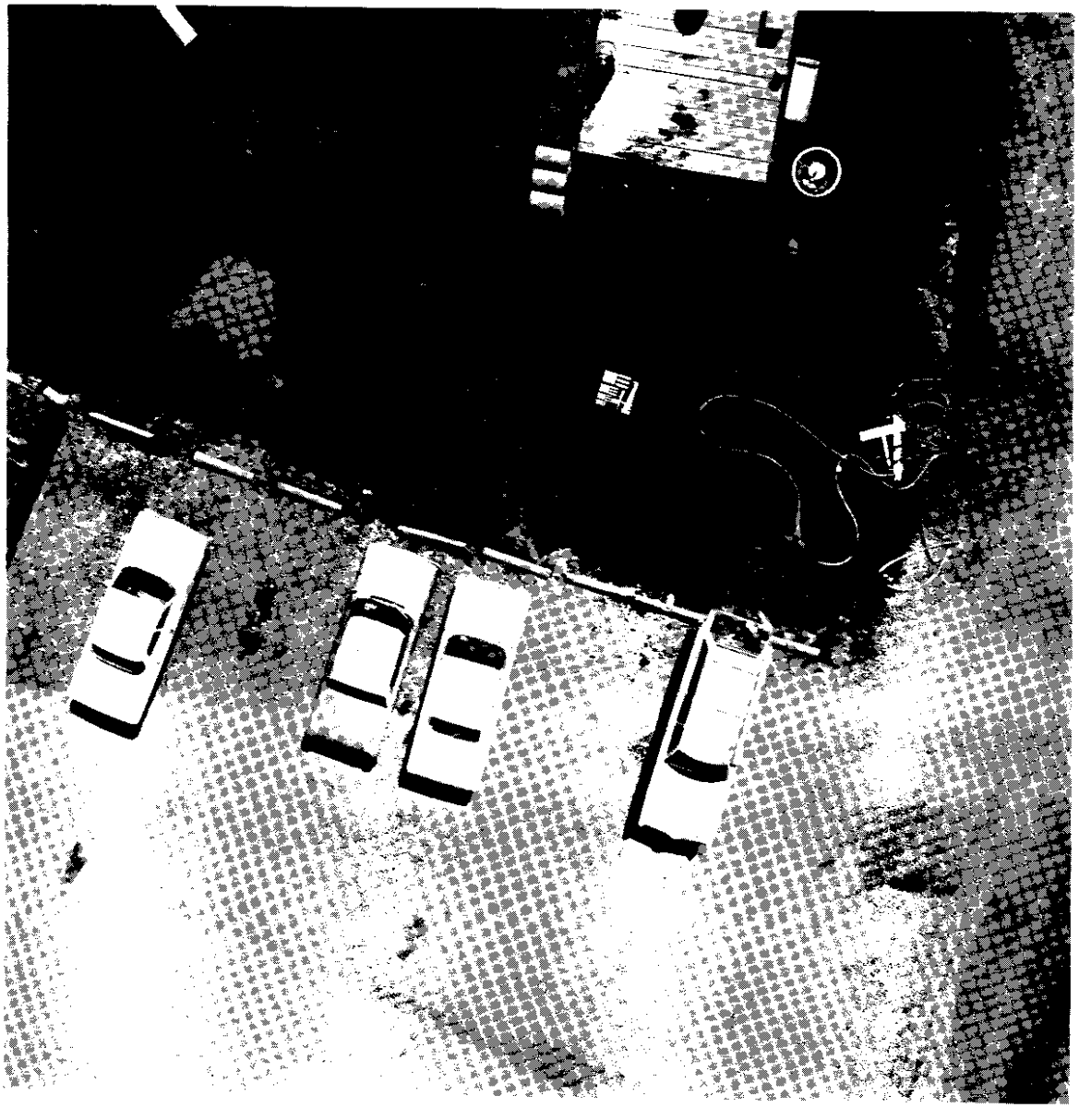

Figure 43.

2. Ground control photographs yielded similar resolution to photographs taken with the camera (on rubber pads) undergoing vibrations with the helicopter in a hovering position. The faster 1/700 second shutter speed gave the best resolution. Thus, the rubber pads were found to be suitable for isolating the vibrations caused by the hovering of the helicopter.
3. Under the vibration conditions induced by the helicopter flying at 30 m.p.h., the rubber pads again proved to be a suitable isolator. This is for a shutter speed of 1/400 second. It is also interesting to note that detrimental effects due to helicopter vibrations were not as bad as had been anticipated.
4. At a 300 foot flying height, the minimum shutter speed which did not cause an appreciable loss of resolution due to image motion was 1/400 second.

It is particularly interesting to note that the mean attainable resolution was only 8 lines/mm for flight conditions of: 300 foot flying height, 1/200 second shutter speed, and 30 m.p.h. helicopter velocity. The low flying height and high speed contribute to this low value of resolution. The image motion:

$$M = 1.467Vtf/H$$

due to these variables is calculated as 0.112 mm on the photograph. With the formula:

$$1/R^2 = 1/R_o^2 + D^2,$$

it was shown previously that a limiting dynamic resolution of 8 lines/mm theoretically should result from a static lens-film resolution of 22.5

lines/mm and a blur distance of 0.112 mm. This formula proved to be correct when compared to the measured 8 lines/mm, which was the actual attained mean dynamic resolution. Similar calculations, based on the photographs taken at 600 and 900 foot flying heights, also verified this formula. Thus, if the static film-lens resolution is known and the required dynamic resolution is specified, then the limiting blur distance may be calculated. This blur distance, "D", is equivalent to the linear motion distance, "M" (blur due to angular motions is negligible). Using the linear motion formula with the limiting value for "M", the variables of flying speed, "V", flying height, "H", and shutter speed, "t", may be manipulated to satisfy the formula. In summary, then, for flight design purposes the procedure would be to:

1. Specify a required resolution, "R", and knowing the static film-lens resolution, "R_o",
2. Calculate allowable blur distance, "D", from $1/R^2 = 1/R_o^2 + D^2$, and
3. Choose "V", "H", and "t" values so that $D = M \geq 1.467Vtf/H$.

Design charts can be drawn up for these test variables. These charts are shown in Figure 44. With reference to Figure 44, these charts are used as follows:

1. Enter top right scale with shutter speed, "t".
2. Draw a vertical line to intersect helicopter velocity curve, "V".
3. From intersection point draw a horizontal line to interesect "Y" axis.
4. Extend this horizontal line into top left scale to intersect flying height curve, "H".

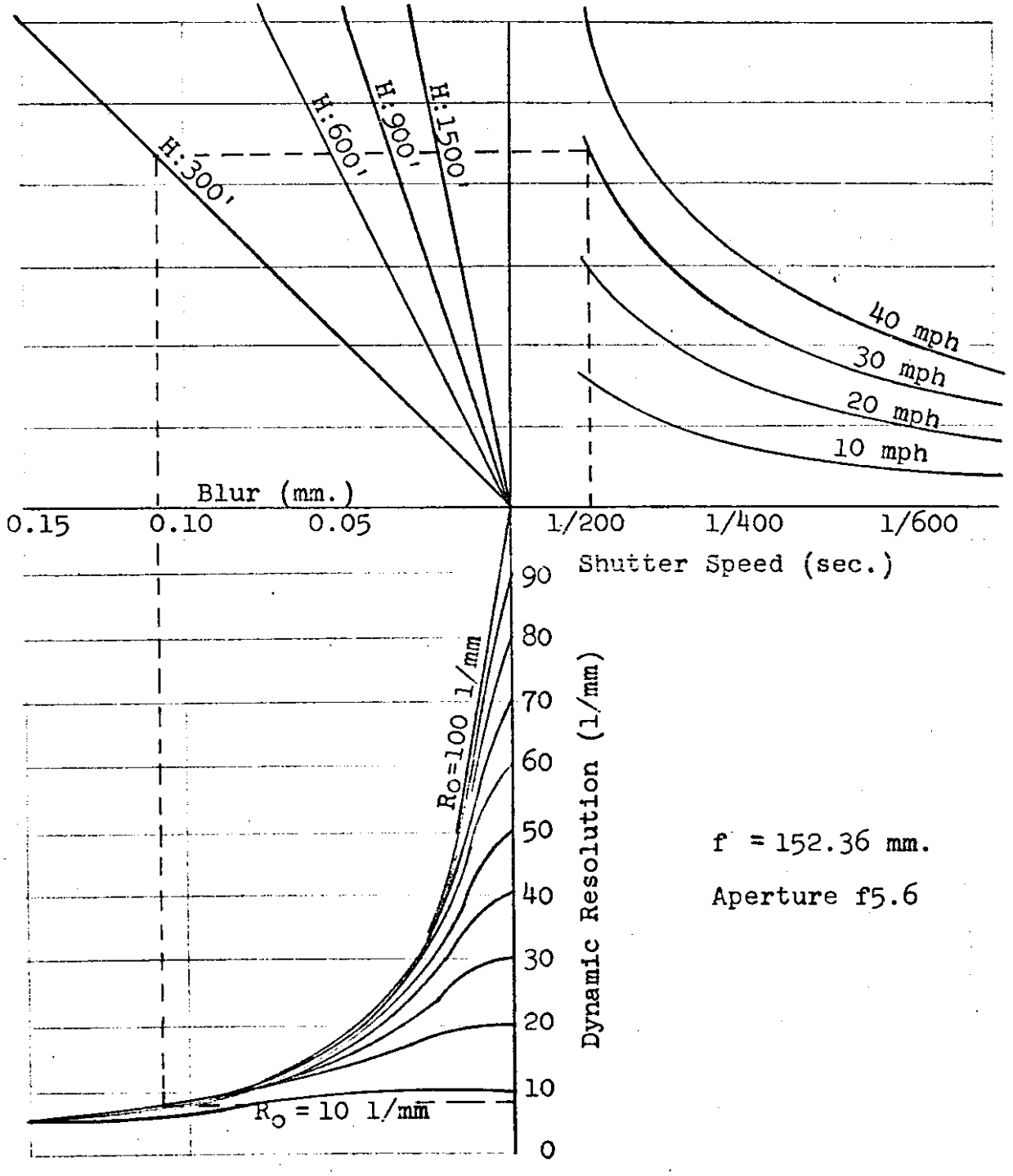

Figure 44. Design charts (f = 152.36 mm)

5. From intersection point draw a vertical line down to intersect blur axis (B = M). This is the value of image motion due to the previous values of shutter speed, velocity and flying height for a constant camera focal length of f = 152.36 mm.
6. Extend this vertical line into the bottom scale to intersect static film-lens curve, "R_o".
7. From intersection point draw a horizontal line to intersect dynamic resolution axis, "R".

The example depicted by the dotted line is for the following variables:

f = 152.36 mm

t = 1/200 second

V = 30 m.p.h.

H = 300 feet

R_o = 22.5 l/mm

The resulting dynamic resolution is shown to be 8 l/mm. The use of these charts can greatly simplify flight design calculations and aid in predicting the quality, or dynamic resolution, which will result when this helicopter system is used.

Further results of these flights are shown in Table 12. The resolution values were read by two observers off the resolution boards situated at the approximate centers of the photographs. A constant f5.6 aperture was used.

These results show again that vibration effects are not as large as anticipated and that the rubber pads are suitable isolators. As expected, the blur, or loss of resolution, increases with increasing helicopter velocity. Calculations using the dynamic resolution formula ($1/R^2 = 1/R_o^2 + D^2$)

Table 12. Calculations of Dynamic Resolution Formula.

Photos	$\overline{R_o}$	Blur	R_{theory}	R_T	$\overline{R_A}$	R_A
H 2-1, H 2-2	9.3					
2-3, 2-4		0.03726	8.8	7.5	6	5-7.5
2-5, 2-6		0.07452	7.6	7.5	6	5-7.5
2-7, 2-8		0.11179	6.4	5	2.5	0-2.5
2-9, 2-10	20					
2-11, 2-12		0.03726	16	15	18	15-20
2-13, 2-14		0.05589	13.4	12.5	11	10-12.5
2-15, 2-16		0.07452	11.1	10	11	10-12.5
2-17, 2-18	28.7					
2-19, 2-20		0.03194	21.3	20	19	17.5-20
2-21, 2-22		0.04259	18.3	17.5	16	12.5-17.5

$\overline{R_o}$ = mean static film-lens resolution (l/mm)

R_{theory} = theoretical dynamic resolution (l/mm)

R_T = theoretical dynamic resolution which can be read on resolution board (l/mm)

R_A = range of attained dynamic resolutions (l/mm)

$\overline{R_A}$ = mean attained dynamic resolution (l/mm)

are tabulated.

From these results the dynamic resolution formula is proven to be valid for low altitude, large scale photography. It should be noted that all these calculations have been based on resolutions as read from the bars lying transverse to the flight direction. These are the bars which are most susceptible to blur degradation. It was noted in all cases that greater resolution would be read off the bars lying in the longitudinal (flight) direction.

These flights have resulted in criteria for defining the limitations and use characteristics of the helicopter as an aerial platform. With the design charts shown in Figure 44, the quality of the resultant photographs may be predicted and flight variables may be designed for optimum conditions, depending on the use to which the photographs will be applied.

7.3 Variation in Orientation Elements

One of the major problems encountered while using the helicopter as a camera platform is to keep the parameters of flight within an acceptable range. This is particularly noticeable for photographs taken at low altitudes. The first flight produced a variation in flying height of as much as 50 feet at a 300 foot altitude. The rotational elements varied from 5 to 10 degrees. Consequently, these photographs cannot be used in conventional stereoplotters because their range is less than the above values.

The possibility of employing auxiliary equipment has been considered. However, the final conclusion was that this equipment will not provide the required results because the basic problem lies with pilot training.

The problem with the orientation elements in the second and third flights seem to have been acceptably corrected for these flights. Again,

this improvement is only attributable to a better piloting of the helicopter. The results from the analytical examination are shown in Table 13, along with the calculated camera station coordinates. The range of phi values is between 0 - 6 degrees and of omega between 0.5 - 4.5 degrees. Nearly all of these attitude parameters are adaptable to most instrumental systems. The kappa values, however, show a marked increase in disorientation, with the maximum value approaching 25 degrees. But even these values of kappa should not provide a great deal of concern for most instruments. This does point up the difficulty involved in attitude which is uniquely applicable to the helicopter system.

The evaluation of camera station values are noted here to further establish the need for some intervalometer adaptation. It appears that it is quite difficult for the pilot to determine when he is exactly above the correct exposure location, even in a hovering position. Calculated values for this parameter are shown in Table 14.

Further experimentation of various flights have shown that the large variation in orientation elements can be overcome by pilot skill. In order to maintain proper flying height, it is advisable to land (if possible at all) on the photographic site to zero the altimeter.

The photographs obtained with 60% overlap and in strip form show acceptable variation from the flight line (for example, 1.7° for six photographs).

7.4 Achievable Accuracy

It is often advantageous to use a high precision plotter as a comparator. At the University of Washington, data can be accomplished with either a Santoni IIC instrumentally or a Nistri Analytical Plotter/Civilian (AP/C) analytically. The latter was chosen for this project due to the extreme

Model Number	Resolution (l/mm)	Omega (degrees)	Phi (degrees)	Kappa (degrees)	Camera Station		
					X (feet)	Y (feet)	Z (feet)
1	16	1-20-58.5 1-14-35.1	2-08-22.0 1-27-20.7	17-05-15.6 18-57-01.6	354.629 529.728	601.028 637.288	445.869 460.268
2	10	2-47-29.3 1-46-28.1	0-08-09.8 2-49-06.7	20-00-15.2 21-21-22.6	375.526 546.348	563.599 607.737	453.113 452.761
3	10	2-23-34.2 1-55-30.0	3-43-15.3 3-15-44.8	21-26-18.8 21-36-30.3	400.789 567.182	564.449 587.822	456.982 446.688
4	2	0-27-24.4 2-53-21.8	2-54-00.2 1-02-04.3	24-52-34.3 17-10-06.4	401.391 551.269	566.533 602.591	461.384 464.137
5	16	2-49-47.2 2-44-43.1	2-06-08.8 0-37-24.0	23-23-47.4 6-05-48.3	361.328 528.684	538.989 626.303	461.274 455.324
6	11	1-36-18.6 1-28-49.6	3-05-29.6 3-24-25.8	18-42-35.8 22-24-51.0	395.611 559.911	573.933 604.613	457.435 464.905
7	9	0-42-16.5 1-44-58.8	3-30-43.6 3-40-15.5	17-56-59.0 22-26-00.0	390.692 552.417	576.810 616.181	470.438 472.854
8	11	1-45-12.3 1-06-09.7	3-48-06.6 2-55-41.8	17-18-16.1 19-38-48.3	385.511 542.138	579.499 617.776	462.801 462.851
9	20	0-15-49.3 2-22-06.9	3-28-27.9 0-29-52.0	20-50-40.1 11-05-32.0	399.283 519.259	556.608 618.707	471.191 478.611
10	17	1-57-07.3 4-24-51.6	5-33-02.0 6-14-24.5	24-44-59.2 16-50-09.2	382.371 551.277	581.871 623.639	479.010 481.295
11	17	1-27-49.5	3-40-54.0	15-37-04.8	548.672	622.042	470.615

Table 13. Analytical Results, Flight 3.

Coordinate	Photograph	Range (diff.)	Mean	Standard Deviation
X	1	46.76	382.71	16.23
	2	47.92	545.17	14.26
Y	1	62.04	570.33	16.60
	2	49.47	614.97	13.51
Z	1	33.14	461.95	9.61
	2	34.61	464.57	10.72

Table 14. Camera Station Coordinate Evaluation (in Feet).

values of the orientation elements resulting from helicopter instability.

Basically, the AP/C was used only for photo-coordinate measurement as a stereo-comparator.

There are two main plate coordinate systems per each photo carriage: (1) x,y and (2) x + TSx, y + TSy. The x,y coordinates are normally displayed on reader output, and represent the plain absolute machine. The second plate coordinate system is normally printed out on the teletype system, and represents photo-coordinates incremented by the total correction computed precisely on the final location of the reading marks.

Analytical methods were utilized to transfer plate coordinates to the ground for a number of reasons. As noted previously, the extreme values observed in the orientation parameters made instrumental methods inadequate (see Manual of Photogrammetry, 3rd Ed.). Also, analytical photogrammetry is quite efficient for data collecting, as at this point in the research we are primarily interested in highest achievable accuracies, rather than plotting capability. The analytical method utilized does present us with information on all parameters.

The basic procedure was to follow a standard analytical photogrammetry method of space resections and space intersections. Basically, this incorporates a mathematical relationship between points and lines in the photograph coordinate system and the object space coordinate system. A print-out of the program used for final transformation is shown in Appendix A. The program name is "FIXED" and was input into a CDC 6400 computer. The procedure is given as follows:

A basic assumption in analytical photogrammetry is that the observed image coordinates conform to a central projection. However, this is rarely the case, and corrections must be applied. The AP/C has the capability of assuming these corrections before coordinate print-out, utilizing a real-time program operation.

Model-point corrections are made for atmospheric refraction and earth curvature. By placing the approximate scale into the computer, these corrections are automatically made. Photo-point corrections are made for lens distortion and film shrinkage. (For the complete write-up on correction equations utilized, see Bendix Corporation Report No. 2433, dated 10 April, 1964).

The first step is to read the values of fiducial marks and control points. These plate coordinate values are given with respect to the instrumental coordinate axes, and therefore must be reduced to the origin at the principal point of each photograph.

Four points in the ground network were picked as control, their locations based on the best overall adjustment of the entire network. This, then, made a least squares solution necessary, and residual deformations were noted (see Figure 45).

$$x_c = \frac{x'_4 + x'_2}{2}$$

$$y_c = \frac{y'_4 + y'_2}{2}$$

$$\delta_\alpha c = \frac{y''_1 - y''_2}{x'_1 - x'_2}\rho^c$$

$$\rho^c = 6366.2$$

$$X_P = \overline{X} - X_c - (\overline{Y} - Y_c)\frac{\delta_\alpha c}{\rho^c}$$

$$Y_P = \overline{Y} - Y_c + (\overline{X} - X_c)\frac{\delta_\alpha c}{\rho^c}$$

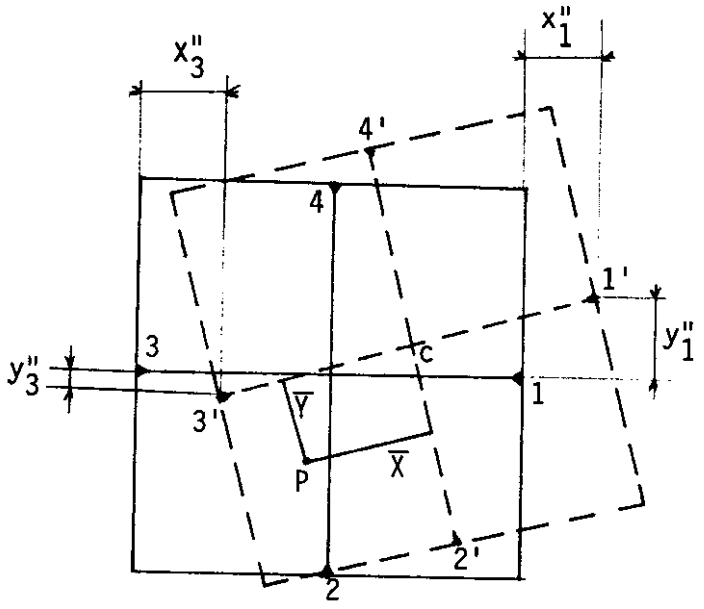

Figure 45. Coordinate adjustment.

Space resection is the problem of determining the exposure station of a photograph from measurements of the images of several points. From a geometrical consideration, three control points are necessary for a unique solution.

The only data to be entered are approximate principle point locations of each photograph, and the calibrated camera focal length. Since a good first estimation corresponds to fewer iterations, a graphic solution was applied for the approximation.

The following format (Hou, 1971) is one of numerous possibilities, and picked for ease of initial input. It is based on the collinearity equations:

$$x = \left[\frac{(X - X_o)\, m_{11} + (Y - Y_o)\, m_{12} + (Z - Z_o)\, m_{13}}{(X - X_o)\, m_{31} + (Y - Y_o)\, m_{32} + (Z - Z_o)\, m_{33}}\right]C \qquad \text{.....7.1}$$

$$y = \left[\frac{(X - X_o)\, m_{21} + (Y - Y_o)\, m_{22} + (Z - Z_o)\, m_{23}}{(X - X_o)\, m_{31} + (Y - Y_o)\, m_{32} + (Z - Z_o)\, m_{33}}\right]C$$

where x and y are the image coordinates of the control point whose space coordinates are X, Y and Z. X_o, Y_o and Z_o are the initial estimations of the camera station, and "C" is the principal distance of the camera. The "m" values are elements of the rotational "M" orthogonal matrix, which consists of direction cosines or orientation elements of the unknown camera station.

Because four control points were used, a least squares adjustment is necessary, and the observation equations are:

$$V_x = F'_x + dF'_x , \qquad V_y = F'_y + dF'_y \qquad \text{.....7.2}$$

where the F' values are the initial estimates X_o, Y_o and Z_o.
Therefore:

$$dF'_x = \frac{\partial F'_x}{\partial X_o}\Delta X_o + \frac{\partial F'_x}{\partial Y_o}\Delta Y_o + \frac{\partial F'_x}{\partial Z_o}\Delta Z_o + \frac{\partial F'_x}{\partial \omega}\Delta\omega + \frac{\partial F'_x}{\partial \phi}\Delta\phi + \frac{\partial F'_x}{\partial \kappa}\Delta\kappa \qquad \text{.....7.3}$$

A similar equation can be formed for dF'_y. The Δ values, then, are the corrections to the initial estimates.

From the observation equations, the normal equations are formulated and the Δ values computed. By reiteration, this process is continued until the Δ values approach zero.

The final step is to determine point coordinates from the previously calculated camera station coordinates by space intersection. This is a simple observation method problem. Since the actual ground values of all points are known, they can be compared to the computed values to determine the accuracy of this approach.

Instrumental errors and observer pointing errors have been regarded as constant, and therefore provide a simple shift in the accuracy curve. We have found that the standard deviation of pointing is approximately ± 4 microns for our observers. At a flying height of 300 feet, this amounts to a ground residual of 0.008 feet. Instrumental errors are incalculable. However, by using a first order instrument, these errors should remain relatively small, and therefore this method produces the best accuracy possible.

We have also found a deviation of accuracy as points move from the principal point of a photograph. As shown in Figure 46, this curve simulates a parabola. The residual values are taken as the vector residual of the X, Y, and Z coordinates. This indicates a need for individual adjustment of each point in each model. However, if average residual values are used for each model, then a constant position will be maintained for every individual model, as all models are theoretically to be in the same position. This is the way the flights have been designed, and therefore average residual seems to be the best overall indicator.

The other obvious alternative is to use standard deviation values for accuracy. But due to the large rotational orientation elements involved, and also the previously mentioned position residual curve, this would indicate false values assigned to each point.

By use of the analytical approach for evaluation, X and Y coordinates should maintain some residual similarity. The Z coordinates, however, have no observational basis in an analytical approach and become completely mathematical in nature. For this reason, elevation should be the foremost problem encountered. When plotting results, therefore, separate graphs will be made for X and Y coordinates and for Z coordinates.

Position residual =

$$\sqrt{(\Delta X)^2 + (\Delta Y)^2 + (\Delta Z)^2}$$

(0.001 feet)

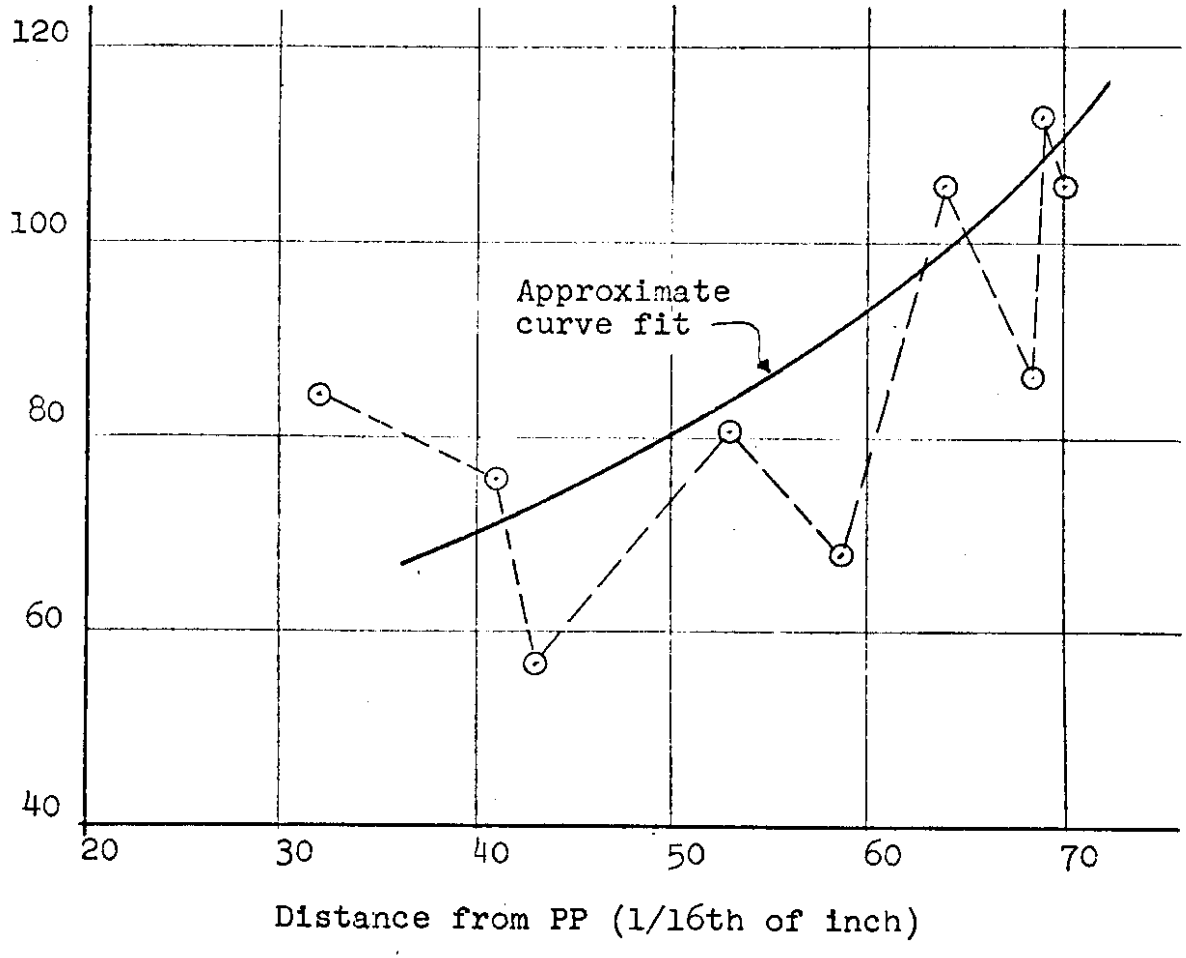

Figure 46. Accuracy variance for a single photograph

Very little has been written on specific aspects of resolution, particularly of dynamic resolution and accuracy, although it is generally accepted that the loss of resolution decreases the achievable accuracy.

It is well recognized that innumerable variables are involved in determining the degree of obtainable accuracy: the quality of the photograph, the kind of plotter, the skill of the plotter operator, etc. As a result, there was no intention to define an exact relationship between the dynamic resolution and the achievable accuracy, because such a relation would represent very little value to the practicing photogrammetrist due to its complexity. Nonetheless, it was felt that an approximate relation would be desirable to enable the photogrammetrist to design parameters for helicopter photography upon specified residual errors.

The data collected for this purpose was obtained by the analytical photogrammetric method, as previously described, and the semi-analytical method with the Wild A-7 autograph of the Washington State Highway Department. The data was compiled from about 60 models, each containing nearly 20 control points.

The results from the Wild or Zeiss cameras indicate that the dynamic resolution has little effect beyond 20 l/mm. At a higher resolution, the major influencing factors are other parameters, which will be discussed later.

The relationship between dynamic resolution and the achievable accuracy can be expressed by the following equation:

$$\text{Achievable accuracy} = C_0 + C_1R + C_2R^2 + C_3R^3 \quad \ldots\ldots\ldots\ldots\ldots\ldots 7.4$$

$C_0 \cdots C_3$ are constant, their numerical values determined by experimental polynomial computation for any photogrammetric organization, and R is the dynamic resolution.

Curve-fitting was done by a FORTRAN program written for this purpose (name CURFIT). It incorporates a least-squares polynomial solution. Row interchanges were used to reduce error possibilities. The program is indicated in Appendix . The only inputs necessary are number of points, degree of curve desired, and two-dimensional coordinates of each point. For the X and Y values, the final equation is:

$$\text{Accuracy} = 0.00000387R^3 - 0.000116R^2 - 0.000864R + 0.0685 \quad \ldots\ldots 7.5$$

with the standard error of estimate equaling ± 0.00443 feet. For the Z values, the equation is:

$$\text{Accuracy} = 0.00000280R^3 - 0.000106R^2 - 0.00130R + 0.123 \quad \ldots\ldots\ldots 7.6$$

with the standard error of estimate equaling ± 0.0155 feet.

Qualitative analysis notes the largest errors occurring for shutter speeds of 1/200. This is probably due to the amount of blur associated with this slow speed. Although the highest resolution value obtained was hovering at a shutter speed of 1/700, this also is on a positive-slope portion of the curve. The graphic representations of the results are shown in Figures 47 and 48

The most stable portion of both curves is for a shutter speed of 1/400, and no real appreciable differences due to variable velocities. In the X,Y plot, this accuracy amounts to 1:7500, and for the Z plot it is 1:3500. Better accuracies had been hoped for. However, the analysis showed that the major contribution was inaccuracies of ground control, which therefore had to be remeasured as was explained earlier.

Graphs of the results of the flights and measured control points are shown in Figures 49 and 50. The ordinate values indicate the average residual in feet, and the abscissa indicates resolution in line-pairs per

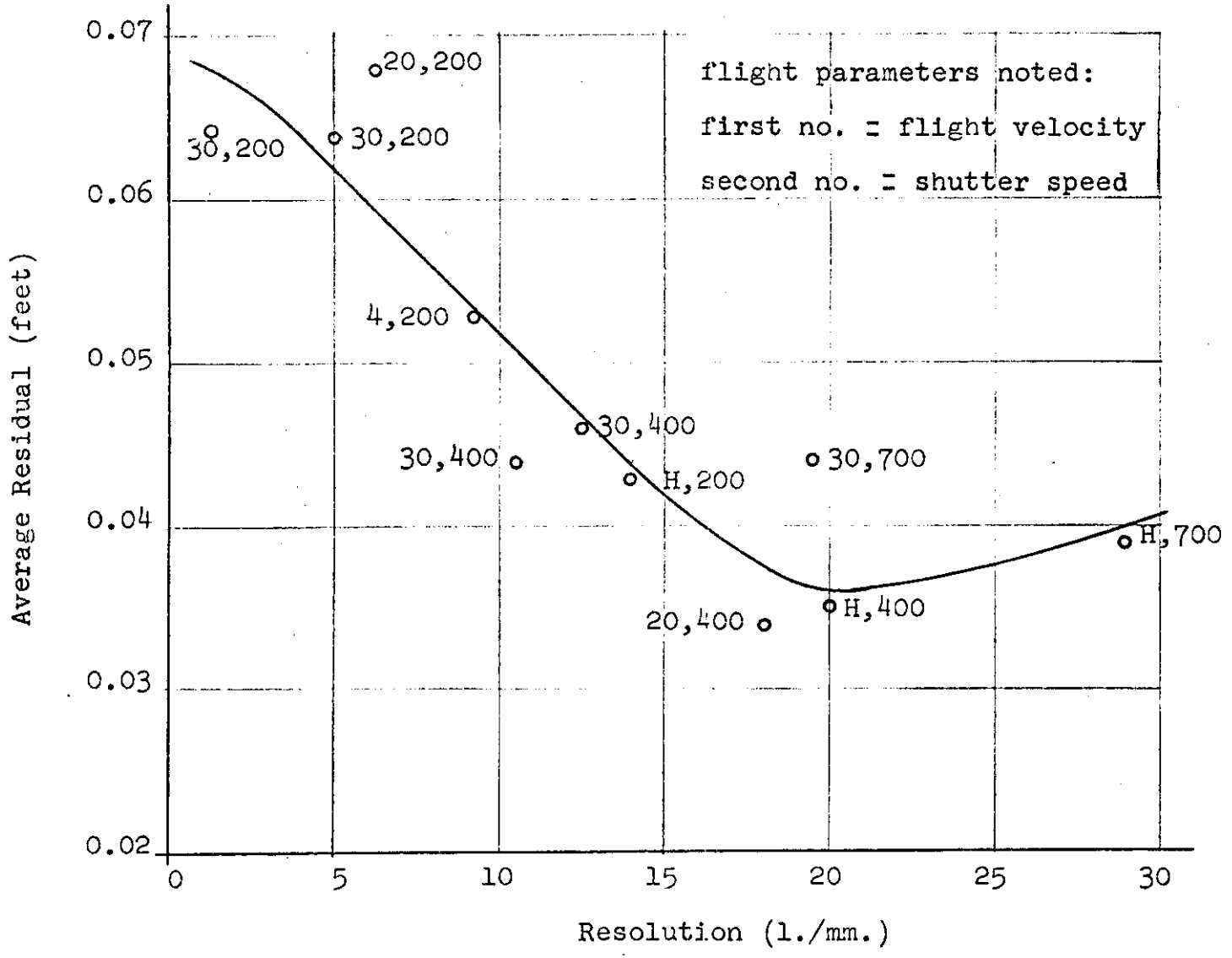

Figure 47. XY coordinate accuracy results, Flight 2.

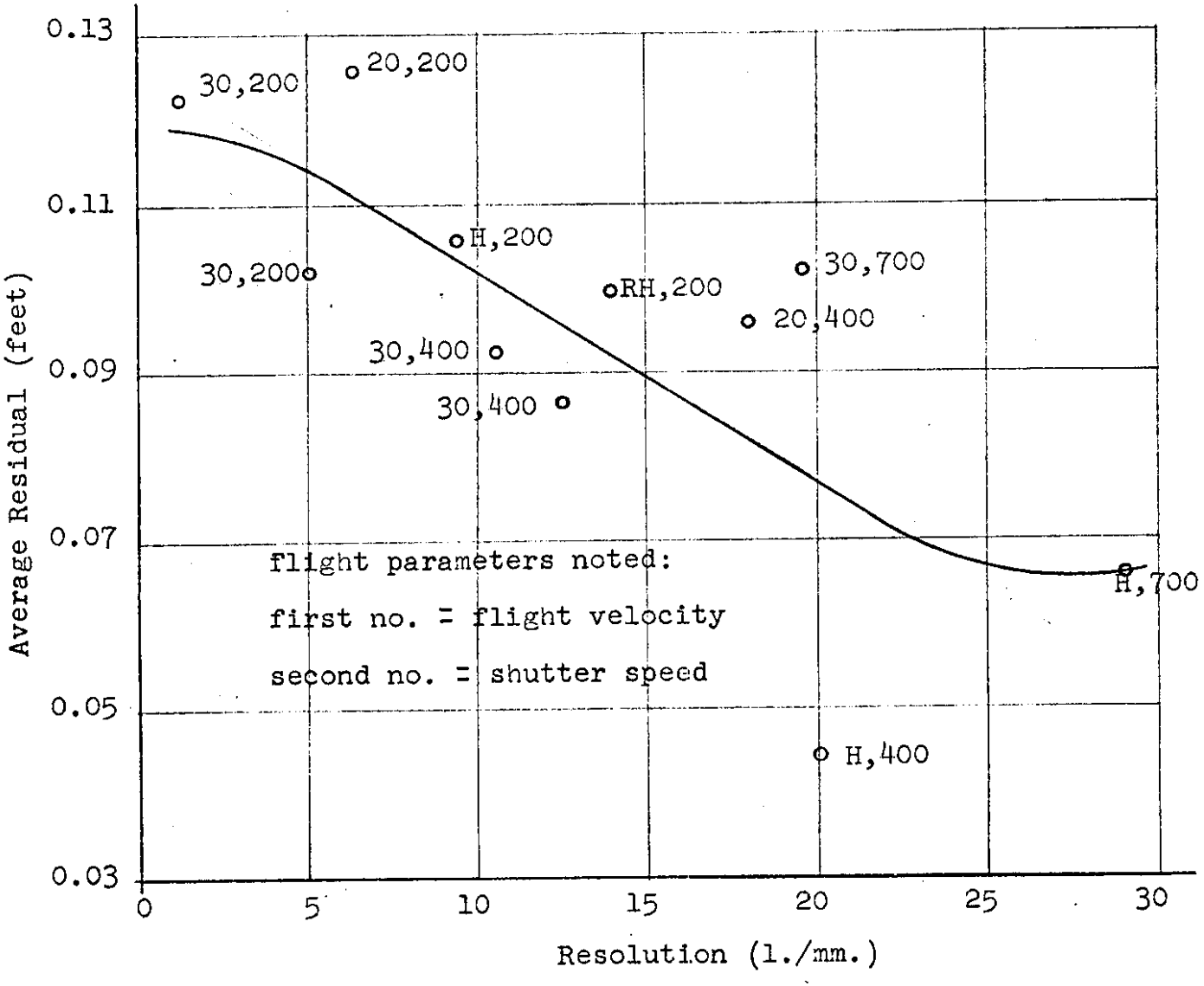

Figure 48. Z coordinate accuracy results, Flight 2.

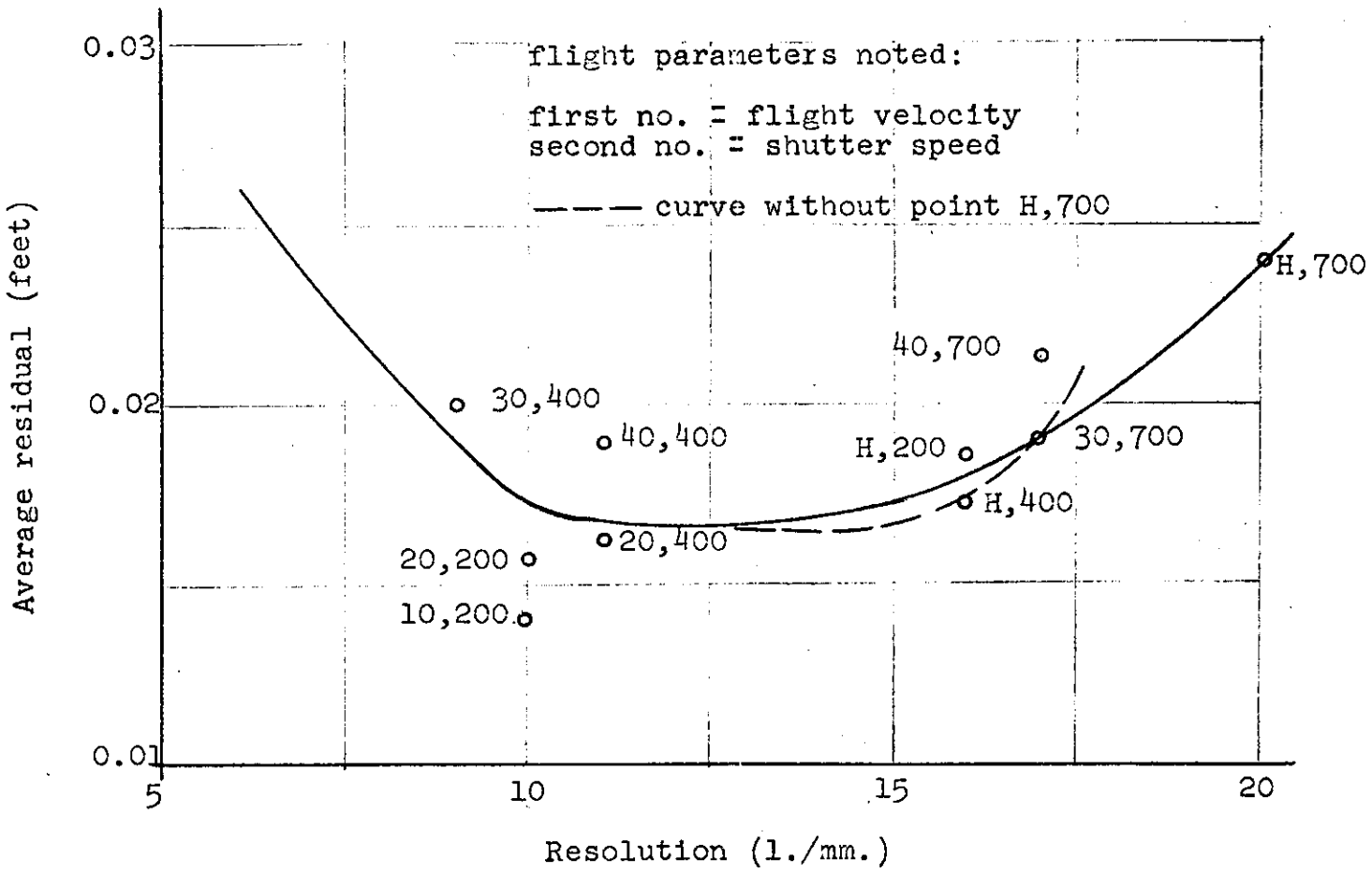

Figure 49. X,Y coordinate accuracy results.

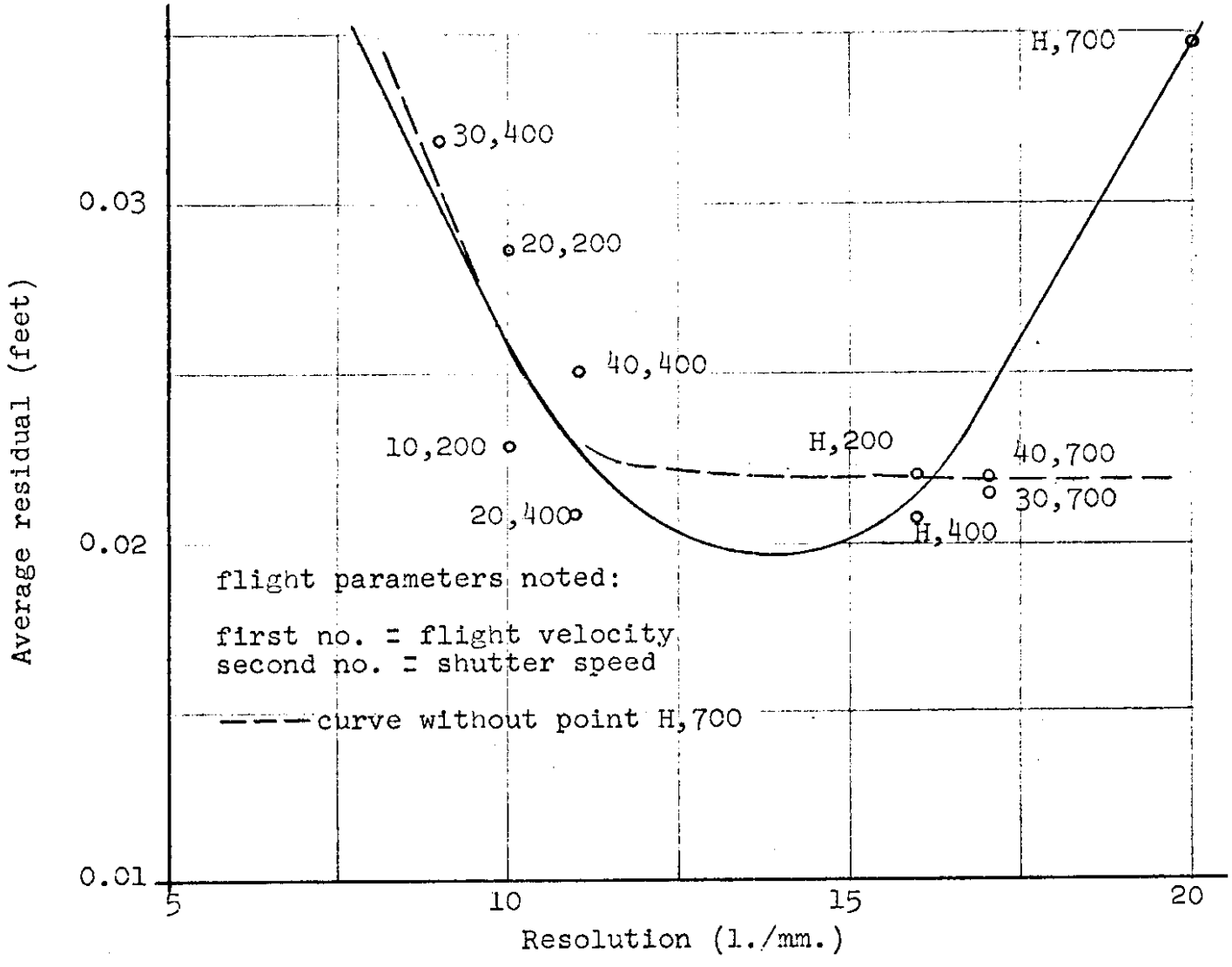

Figure 50. Z coordinate accuracy results.

millimeter. Figure 49 is the X and Y residual average, and Figure 50 is the Z residual average. The curve-fitted equation for the X and Y residual plot is:

$$\text{Accuracy} = 0.00000360R^3 + 0.000303R^2 - 0.00591R + 0.050 \quad \ldots\ldots\ldots 7.7$$

with a standard error of estimate equaling $\pm$0.00180 feet. For the Z values, the equation is:

$$\text{Accuracy} = 0.00000586R^3 + 0.000682R^2 - 0.0155R + 0.119 \quad \ldots\ldots\ldots 7.8$$

with the standard error of estimate equaling $\pm$0.00191 feet. When comparing these values with the previous two sets of values, note that the curve-fit of the third provides a much closer approximation.

Further, the stable portions (about the minimum) in each curve again is around the 1/400 second shutter speed, but with some encroachment by the other shutter speeds. It would seem that this encroachment can be primarily attributable to better target design and control point accuracy, which then becomes:

$$\text{Accuracy} = -0.0000354R^3 + 0.00148R^2 - 0.0199R + 0.104 \quad \ldots\ldots\ldots 7.9$$

with a standard error of estimate equaling $\pm$0.00192. For the Z values, the equation becomes:

$$\text{Accuracy} = -0.000114R^3 + 0.00467R^2 - 0.0632R + 0.304 \quad \ldots\ldots\ldots 7.10$$

with the standard error of estimate equaling $\pm$0.00160. The above curves are shown with dashed lines in Figures 49 and 50. Note that, particularly in Figure 50, the curve assumes a constant slope after a minimum resolution of 11 l/mm, and limits may then possibly be placed at this point.

Initial instrumental evaluation was also attempted. The instrument utilized was the Wild Model A-7, and the point coordinates transformed

using the "Schut" adjustment. The photogrammetric accuracy for X and Y coordinate residuals amounts to 1:16900, and for Z residuals it is 1:15700. These values correspond quite well to the analytical accuracies noted previously.

8.0 APPLICATION OF MODULATION TRANSFER FUNCTION

The principle and the advantage of the use of Modulation Transfer Function (MTF) were discussed in Section 2.3. It was pointed out that if the individual parameters are to be determined in a complex function, the use of MTF is more advantageous than the resolution. The use of the MTF in aerial survey is limited due to the requirement of a sine-wave target.

In this research, square-wave response was used as a preliminary investigation. If desired, the square-wave response can be converted into sine-wave response by the following equation (Scott and Schack, 1963):

$$M_{(k)} = \frac{\pi}{4} \overline{M}_{(u)} + \frac{M(3k)}{3} - \frac{M(5k)}{5} + \cdots \quad \text{.....8.1}$$

where k is the spatial frequency, M is the sine-wave modulation and $\overline{M}$ is the square-wave modulation.

The procedure can further be simplified by substituting the modulation with Density Difference (DD). This substitution is permitted if the DD is between 0.04 and 0.7. (Proceedings of I.S.P., 1972)

The use of the MTF in this research was necessitated by the fact that the residual errors are not an expected exponential function of the resolution but rather, parabolic function (see Figures 49 and 50). These phenomena indicate that the main influence in the 1/700 sec. exposure region is not the resolution but some other parameter.

8.1 Relations Between Pointing Accuracy, Residual Error and Exposure Level

The following material has been obtained in the Joyce Loebl high-resolution microdensitometer at the University of Washington by scanning more than one hundred photographs. This large amount of data is condensed and will be presented in the form of graphs, in order to draw uniform and meaningful conclusions. As was emphasized earlier, the advantage of the MTF is that the effect of the large number of parameters can be individually analyzed. As a consequence, a rather large number of relations and inter-relations of parameters have been evaluated during the course of this project. Here, however, only the most pertinent will be presented.

One such important relation is presented in Figure 51, where the pointing errors and the residual errors are analyzed. There are three different lines presented according to the various exposure levels at which the photographs were obtained. Thus:

A corresponds to $f_{\#}$ = 5.6 exposure time 1/200 sec.,

B corresponds to $f_{\#}$ = 5.6 exposure time 1/400 sec., and

C corresponds to $f_{\#}$ = 5.6 exposure time 1/700 sec.

It can be seen from Figure 51 that a linear relation exists between the residual and pointing errors. The major influence is indicated by the exposure level. The linear image motion, as noted in the figure by LIM = 40 μm and LIM = 0 μm, has no influence on the residual error. The linear image motion has been computed at the negative scale. Figure 51 gives an explanation for Figure 50, where the accuracy decreases at 1/700 sec. shutter speed, contrary to the expected result. This graph shows that while the major influencing factor on the achievable accuracy is the resolution at normal exposure, which corresponds to the A and B exposure levels, the major influencing

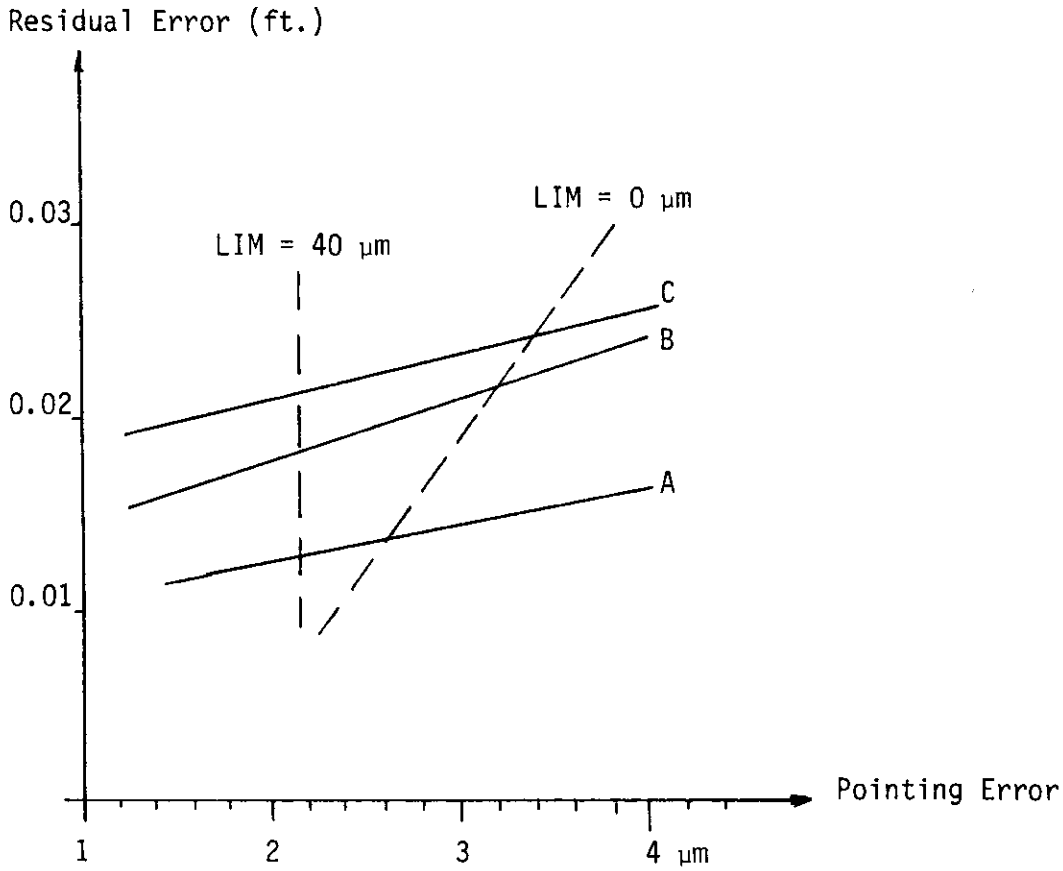

Figure 51. Relation between residual error and pointing error of function of exposure level.

factor is the exposure level if it is changed from normal, such as exposure level C.

8.2 The Influence of Exposure Level

It has been shown in the previous section that the exposure level is one of the prime influencing parameters. Consequently, it was important to investigate and evaluate this parameter. The results of this investigation are summarized in Figures 52, 53 and 54.

Figure 52 represents the relationship between the pointing error and the exposure level. It can be seen that the minimum pointing error occurs at $f_{\#}$ = 5.6 and 1/200 sec. exposure time. The pointing error at this level is found to be 2.1 microns. It must be emphasized strongly that the observations were made on an AP/C plotter, which has a minimum reading of 2 microns. Thus the above-mentioned accuracy is the best limit possible within the system.

A similar relationship can be found between residual error and exposure level in Figure 53. The influence here is much more pronounced, as can also be concluded from Figures 49 and 50, where the residual error in relation to the resolution is examined. It can be concluded that at a normal exposure, the major influence on the achievable accuracy is done by the resolution. However, this influence is shifted to the exposure level when the normal exposure is not maintained.

The relation between the density difference and the exposure level is exhibited in Figure 54. The relation hue is an exponential function, thus expressing the already established fact that the exposure level is critical. The exposure level overpowers any other variable. Thus, it can be concluded that no possibility exists to obtain the maximum accuracy unless the proper exposure is obtained.

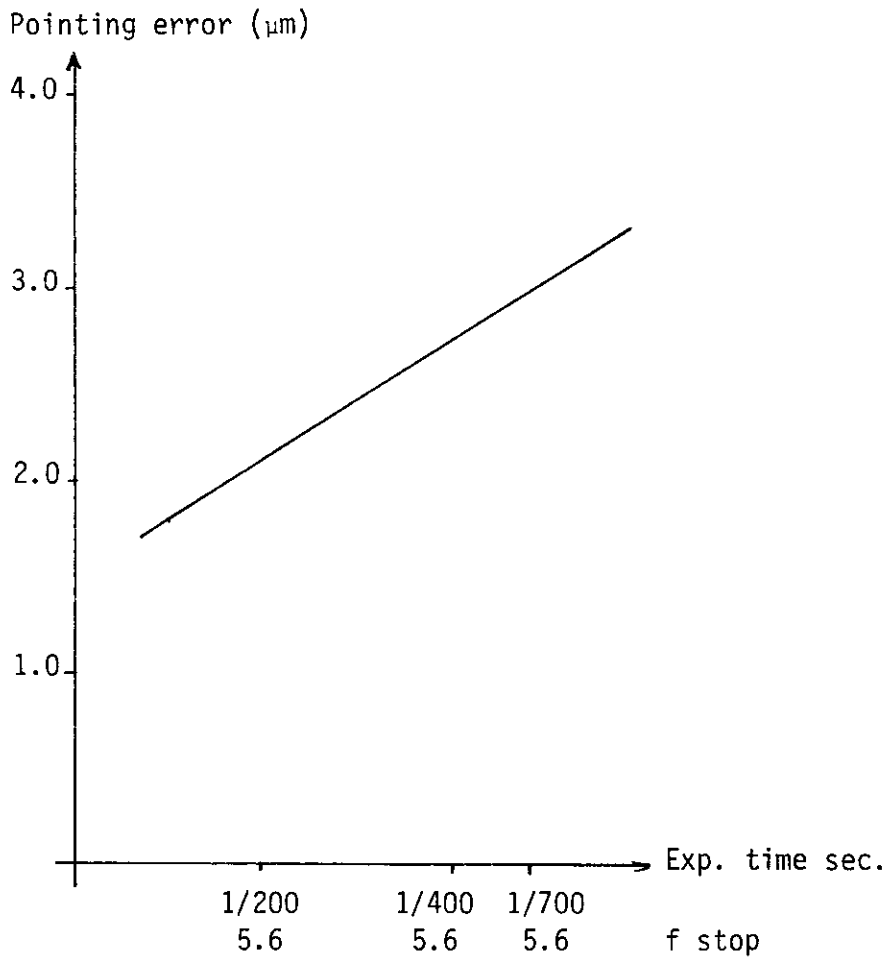

Figure 52. Relation between exposure level and pointing error.

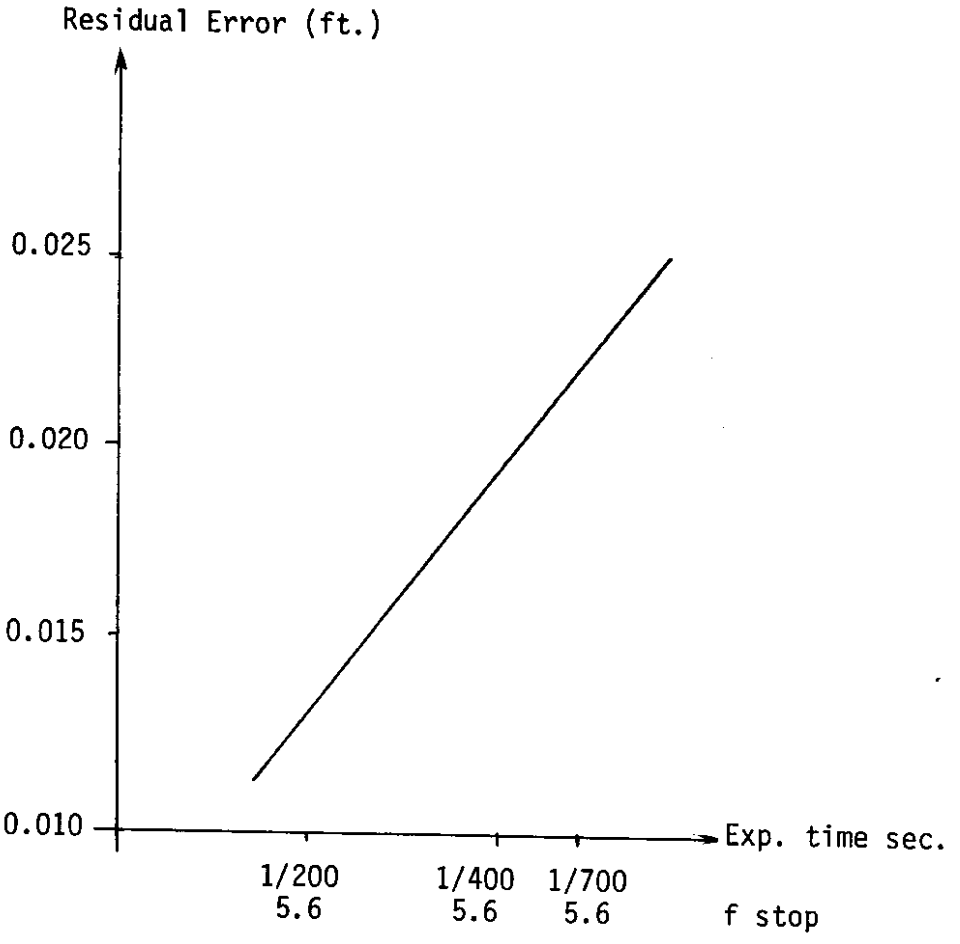

Figure 53. Relation between residual error and exposure level.

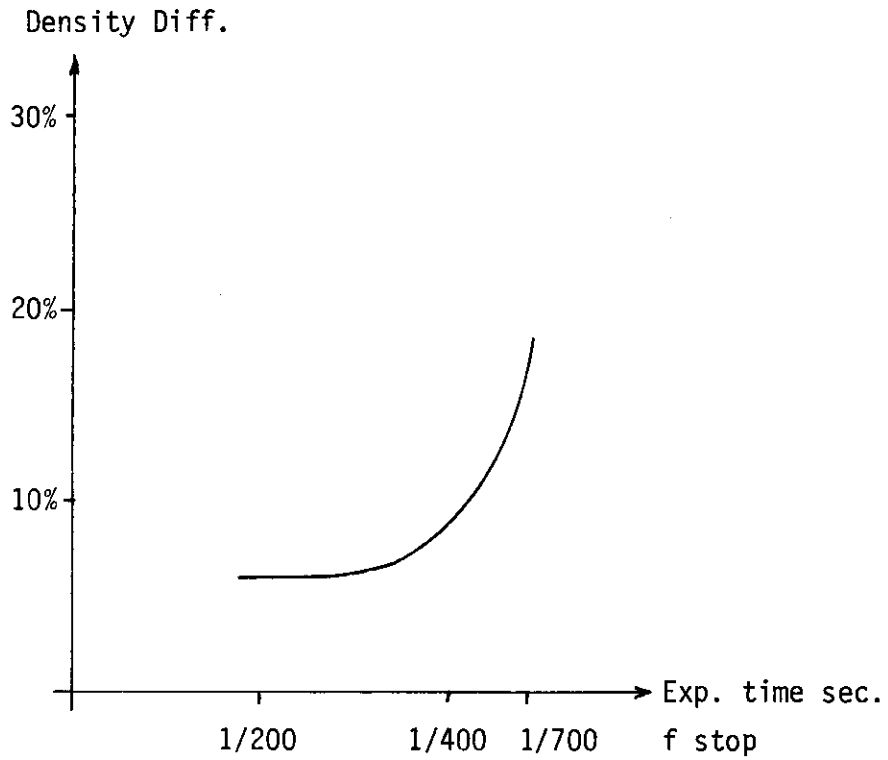

Figure 54. Relation between density difference and exposure level.

8.3 The Effect of the Linear Image Motion

It was shown earlier that the image motion is a major influencing factor on the resolution, and as such, on the achievable accuracy. For this reason the MTF has also been used to evaluate this influence.

A basic relation is shown between Density Difference and Linear Image Motion in Figure 55. It is easily recognizable from this figure that the Density Difference, and with it the contrast, is decreasing with the increase of Linear Image Motion. The Density Difference is less than 10% beyond 60 μm of image motion, which is an indication that the image motion has no major influence under 50 - 60 μmicrons.

A similar conclusion can be drawn from Figure 56, where the relation between pointing error and Linear Image Motion is illustrated. This figure indicates that there is no effect on the achievable accuracy in pointing if the Linear Image Motion does not exceed 40 μmicrons. Very rapid deterioration in accuracy results in cases where the image motion is more than 80 μmicrons.

9.0 Testing the Fixed-Wing Aircraft

9.1 Verification of the Result

The testing of the fixed-wing aircraft was designed so that its purpose was to verify the results and not to introduce new experimentation. There have been two flights with fixed-wing aircraft, and from the data gathered the following results have been obtained.

It has been found that the major influencing factor in fixed-wing aircraft is the Linear Image Motion. One of the flights was done at 1200 ft. (above the ground) elevation and 70 mph. This flight has proved that the Kodak High Definition 3414 aerial film cannot be used even where the terrain

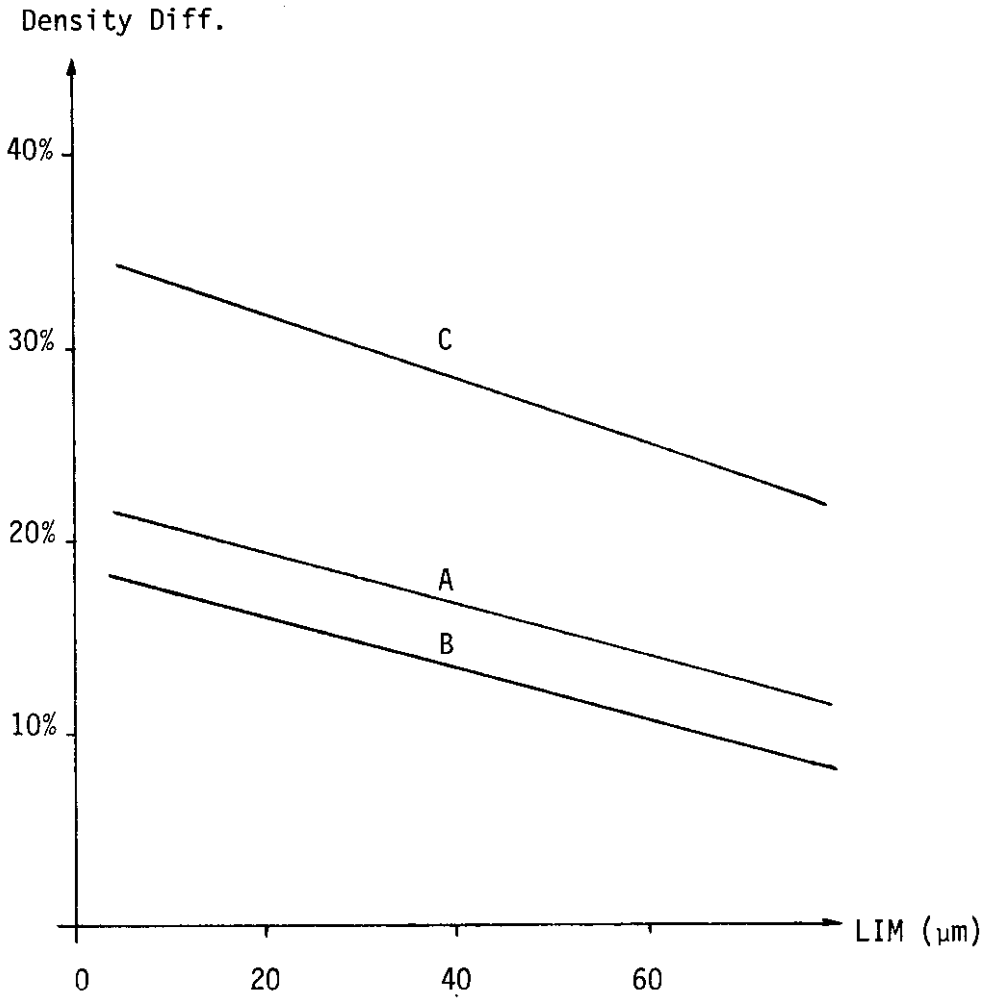

Figure 55. Relation between density difference and linear image motion.

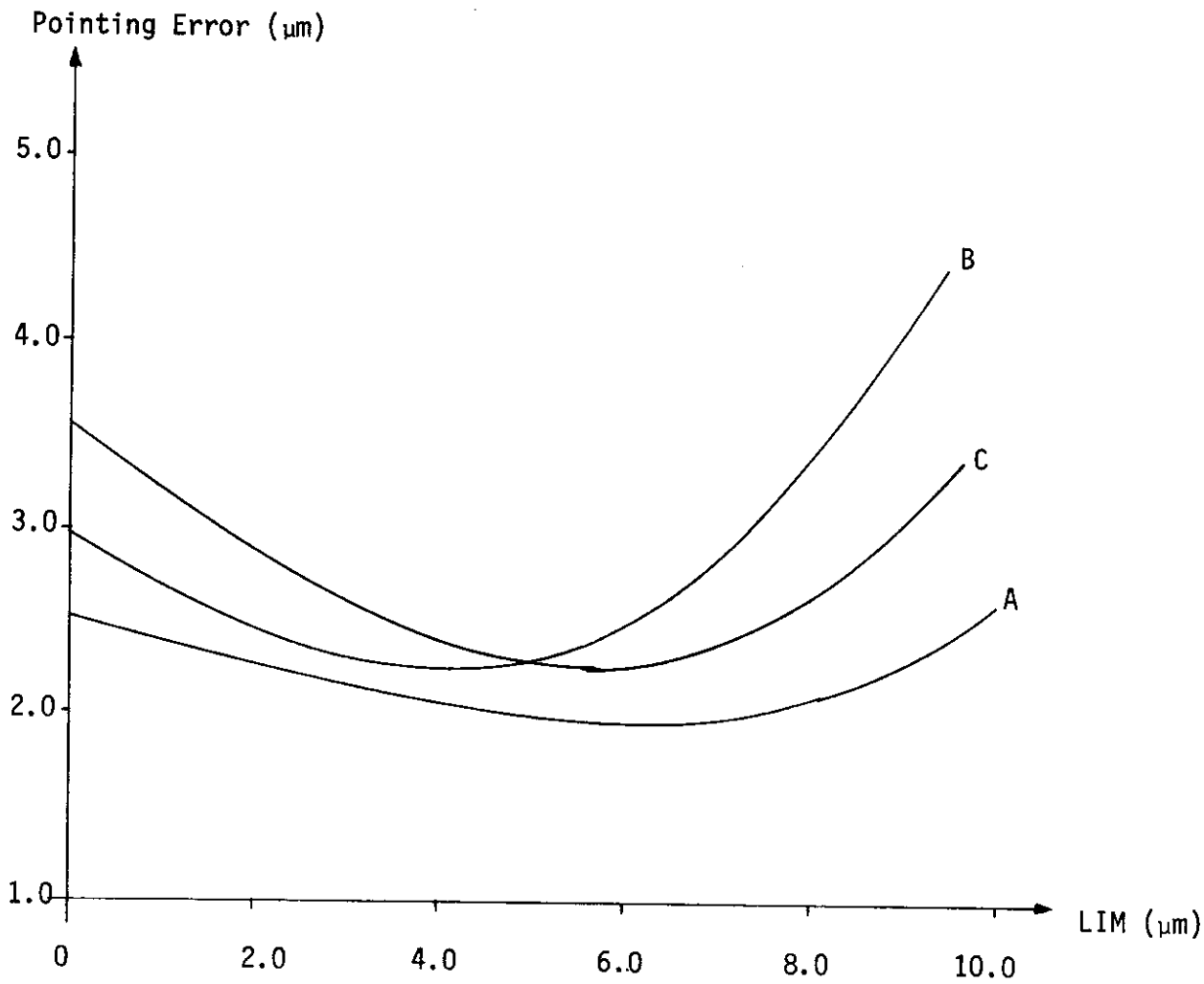

Figure 56. Relation between pointing error and linear image motion.

has optimum illumination. It appears, however, that the Kodak Panatomic-X aerial film on 0.10 mm estar base should be used for high altitude photography in order to obtain a maximum accuracy.

The experimentation with fixed-wing aircraft has further underlined the opinion that the helicopter as a camera platform is complementary and not competitive to the fixed-wing aircraft. The relationship between the two forms of camera platform is defined by the speed of the craft and the flying altitude; i.e., the linear image motion should not exceed 40 microns.

For the fixed-wing aircraft a similar design chart can be used as presented in Figure 44 for the helicopter. The validity of the chart has been examined and found to be applicable with properly modified values.

In summary, the two kinds of camera platform, properly utilized, can solve all of the photographic problems (with the exception of terrestrial) existing in the operation of the Department of Highways.

10.0 REFERENCES

Alter, H., "New Photo Installation Especially on New High Performance Aircraft," Photogrammetric Engineering, Vol. 22, No. 4, 1956.

Avery, G., "Helicopter Stereophotography of Forest Plots," Photogrammetric Engineering, Vol. 24, No. 4, 1956.

Bendix Corporation, AP-C Control Computer Theory and Maintenance Manual, Southfield, Michigan, April, 1965.

Brock, G. C., "Microimage Quality," Photographic Considerations for Aerospace, Itek Corporation, Lexington, Massachusetts, 1966.

Brown, H., "Vibration of Air Survey Cameras," The Canadian Surveyor, Vol. 14, No. 10, 1959.

Campbell, C. E., "The Optimization of Photographic Systems," Photogrammetric Engineering, Vol. 28, No. 3, 1962.

Carman, P. D. and H. Brown, "Resolution of Four Films in a Survey Camera," The Canadian Surveyor, Vol. 24, No. 5, 1970.

Casper, R., "Resolution of Vibration Isolated Cameras," Photogrammetric Engineering, Vol. 30, No. 4, 1964.

Cheffins, O. W., "Accuracy of Heighting from Vertical Photography Obtained by Helicopter," The Photogrammetric Record, Vol. 6, No. 34, 1969.

Colcord, J. E., "Considerations in Pre-marking," Papers from the 35th Annual Meeting, American Society of Photogrammetry, March 9 - 14, 1969.

Colwell, R. N., "The Taking of Helicopter Photography for Use in Photogrammetric Research and Training," Photogrammetric Engineering, Vol. 22, No. 4, 1956.

Doyle, I., "Problems in the Integration of Stabilized Mounts into Photo Systems," Photogrammetric Engineering, Vol. 22, No. 4, 1956.

Gubisch, R. W., "Optical Performance of the Human Eye," Journal of the Optical Society of America, Vol. 57, No. 3, 1967.

Hall, J. K., Helicopter Photography, University of Washington, 1971.

Hallert, B., Photogrammetry, McGraw-Hill Book Company, Inc., New York, 1960.

Hou, C.-Y., "Image Blur and Film Shrinkage of Aerial Photographs in the Photogrammetric Process," Proceedings of the 38th Annual Meeting, American Society of Photogrammetry, 1972.

Hou, C.-Y. and S. A. Veress, "Determination of Surface Area and Volume of a Specimen by Photogrammetry," Symposium on Close-Range Photogrammetry, American Society of Photogrammetry, 1971.

Jackson, K. B., "Factors Affecting the Interpretability of Air Photos," The Canadian Surveyor, Vol. 14, No. 10, 1959.

James, T. H. (Ed.), The Theory of the Photographic Process, The Macmillan Company, New York, 1966.

Jensen, N., Optical and Photographic Reconnaissance Systems, John Wiley and Sons, Inc., New York, 1968.

Jones, R. and W. G. Flannelly, "Application of the Dynamic Antiresonant Vibration Isolator to Helicopter Vibration Control," The Shock and Vibration Bulletin, Bulletin 37, Part 6, 1968.

Karara, H. M., "Planning and Design of Aerotriangulation Projects," Journal of the Surveying and Mapping Division, Proceedings of the American Society of Civil Engineers, July, 1964.

Kawachi, D. A., "Image Motion Due to Camera Rotation," Photogrammetric Engineering, Vol. 31, No. 11, 1965.

Kelsey, R. A., "Resolution Experiments in Contact Printing Through the Film Base," Photogrammetric Engineering, Vol. 21, No. 3, 1955.

Lyons, E. H., "Preliminary Studies of Two Camera, Low Elevation Stereophotography from Helicopters," Photogrammetric Engineering, Vol. 28, No. 1, 1961.

Lyons, E. H., "Recent Developments in 70 mm. Stereophotography from Helicopters," Photogrammetric Engineering, Vol. 30, No. 5, 1964.

Manual of Photogrammetry, American Society of Photogrammetry, Falls Church, Virginia, Third Edition, 1966.

McDonald, R. K., "Optus and Information Theory," Physics Today, Vol. 14, No. 7, New York, July, 1961.

O'Connor, D. C., "Visual Factors Affecting the Precision of Coordinate Measurements in Aerotriangulation," U.S. Army Engineer, GIMRADA Research Note No. 21, Fort Belvoir, Virginia, 1967.

Pallme, E. H., "Camera Mounting for Photogrammetric Purposes," Photogrammetric Engineering, Vol. 22, No. 5, 1956.

Perrin, F. H. and J. H. Altman, "Studies in the Resolving Power of Photographic Emulsions. VI. The Effect of the Type of Pattern and the Luminance Ratio in the Test Object," Journal of the Optical Society of America, Vol. 43, No. 10, 1953.

Robison, F. B. and L. I. Withem, "Helicopter Photography and Mapping," Photogrammetric Engineering, Vol. 33, No. 10, 1967.

Rosenberg, P., "Resolution, Detectability and Recognizability," Photogrammetric Engineering, Vol. 37, No. 12, 1971.

Scott, W. H., "Helicopter Photography," Photogrammetric Engineering, Vol. 34, No. 9, 1968.

Trinder, J. C., "Pointing Accuracies to Blurred Signals," Photogrammetric Engineering, Vol. 37, No. 2, 1971.

Trott, T., "The Effects of Motion on Resolution," Photogrammetric Engineering, Vol. 26, No. 5, 1960.

Van Santen, G. W., Introduction to a Study of Mechanical Vibration, Philip's Technical Library, Eindhoven, Holland, 1953.

Washer, F. E. and I. C. Gardner, Method for Determining the Resolving Power of Photographic Lenses, National Bureau of Standards Circular 533, May 20, 1953.

Wiley, C. R., Advanced Engineering Mathematics, McGraw-Hill Book Company, Toronto, Canada, 1966.

Wilson, L. T., "Resilient Cushioning Materials," Shock and Vibration Bulletin, Part 2, 1957.

Yost, E. F., "Resolution and Sinewave Response as Measures of Photo-Optical Quality," Photogrammetric Engineering, Vol. 26, No. 3, 1960.

Zweig, H. J., G. C. Higgins and D. L. McAdam, "On the Information-Detecting Capacity of Photographic Emulsions," Journal of the Optical Society of America, Vol. 43, No. 12, 1958.

APPENDIX I

COMPUTER FLOW CHARTS

1. RESOLUTION CALCULATIONS
2. STANDARD ERROR OF POINTING

Flow Chart

Resolution Calculations

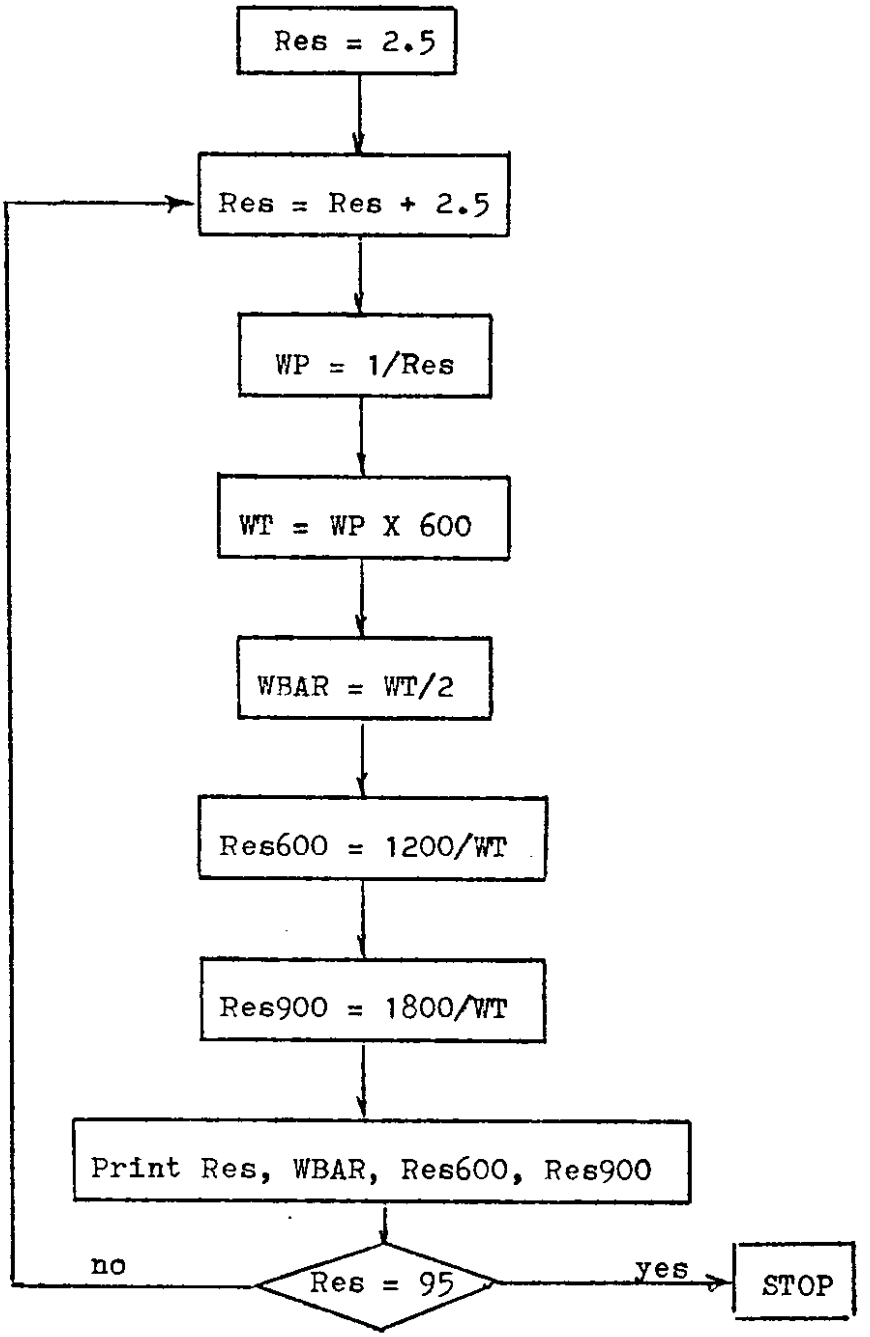

WP = width on photo for a space and a bar (mm.)
WT = WP on target board (mm.)
WBAR = width of bar on target board (mm.)
Res X = equivalent resolution at "X" feet (l./mm.)

Flow Chart

Standard Error of Pointing

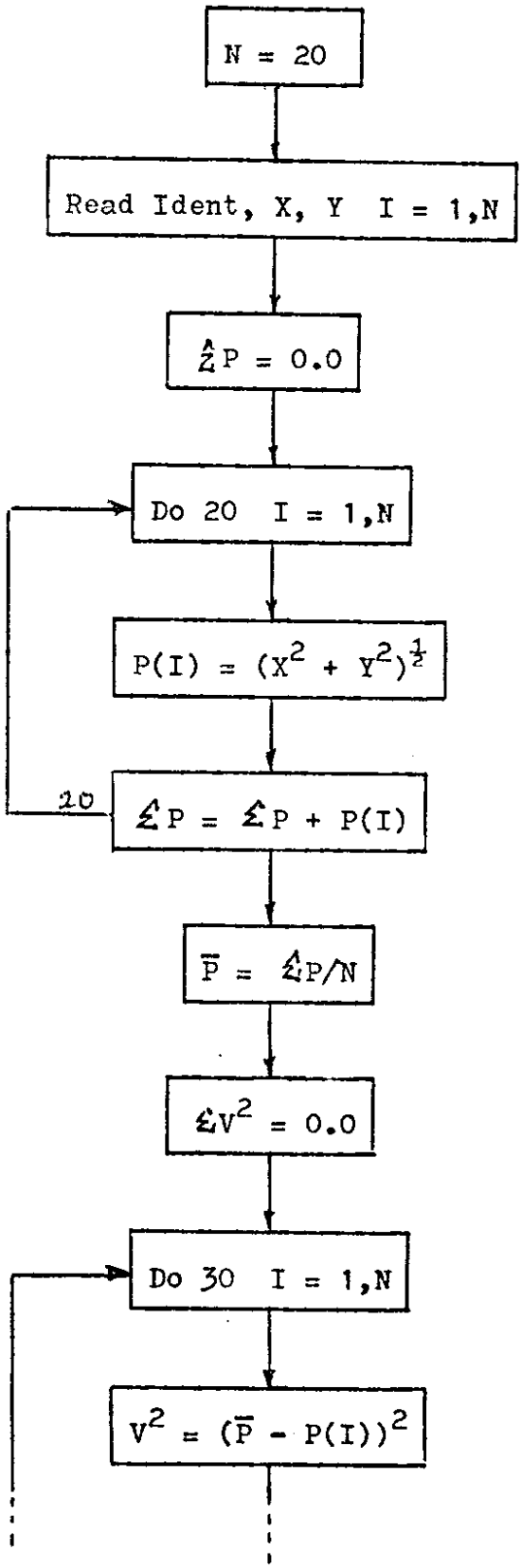

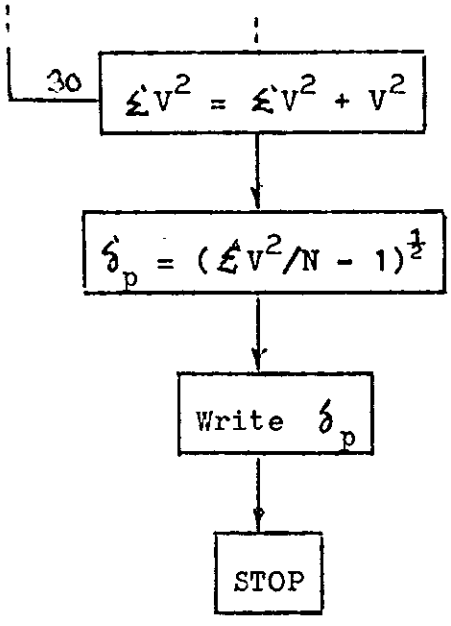

N = number of observations
X, Y = AP/C plate positional coordinates
$\underline{P}$ = position coordinate
$\overline{P}$ = mean position coordinate
V = difference between mean position coordinate and each position coordinate
δ_p = standard error of pointing or position

APPENDIX II

Program FIXED: Analytical photogrammetric adjustment routine

Input data deck for FIXED program:

model name (1–20)	

f (1–10)		Principal distance

X_oL (1–10)	Y_oL (11–20)	Z_oL (21–30)		Approximate values of left perspective center

X_oR (1–10)	Y_oR (11–20)	Z_oR (21–30)		Approximate values of right perspective center

wL (1–10)	øL (11–20)	kL (21–30)		Approximate values of left photo

wR (1–10)	øR (11–20)	kR (21–30)		Approximate values of right photo

No. of fiducial marks

1 (1–10)	X1 (11–20)	Y1 (21–30)	x1 (31–40)	y1 (41–50)	
2	X2	Y2	x2	y2	For left photo
3	X3	Y3	x3	y3	
4 (1–10)	X4	Y4	x4	y4	

Calibrated data — Observed photo coordinates of fiducials

11111 (51–70)	End mark

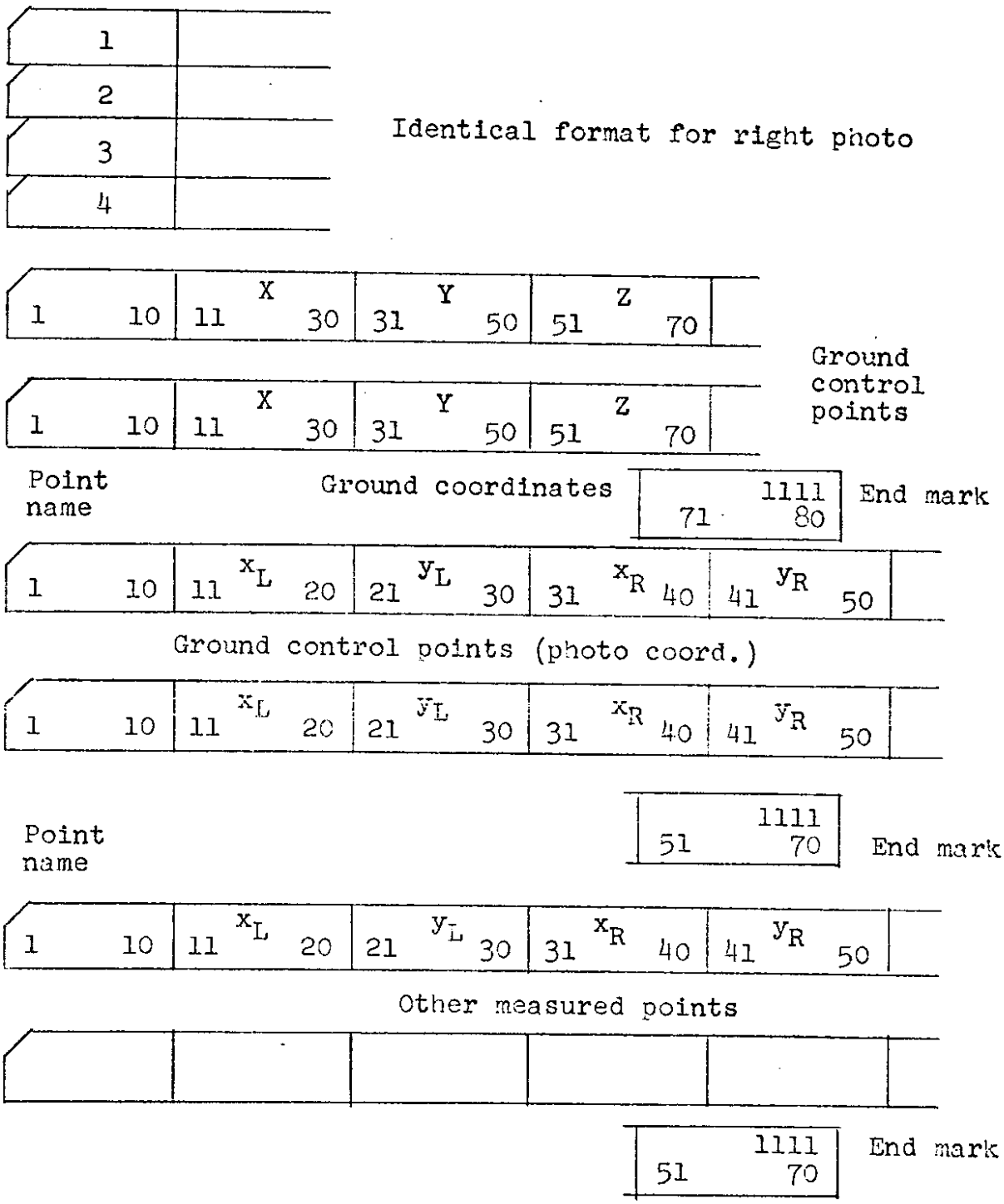
1
2
3
4
Identical format for right photo
1 10
X
11 30
Y
31 50
Z
51 70
Ground control points
Point name
Ground coordinates
1111
71 80
End mark
x_L
y_L
x_R
y_R
Ground control points (photo coord.)
Other measured points

```
      PROGRAM FIXED(INPUT,OUTPUT,TAPE5=INPUT,TAPE6=OUTPUT)
      DIMENSION HELL(200), XG(100),YG(100),ZG(100),PCTL1(100
     *                                              ),PCTL2(100)
     $          ,YPC1(100),XPC2(100),YPC2(100),PASSP1(100),P
     *                                              ASSP2(100)
      DIMENSION YPASS1(100),XPASS2(100),YPASS2(100),C1(15,3)
     *                                              ,C2(15,3),
     $          E2(2,9),BANSR(4), FDM(10,6),AFID(10),BFID(10
     *                                              ),E1(2,9)
      DIMENSION XPASS1(100),XPC1(100),HE(200),ANS(20),ANSWER
     *                                              (20),
     $          ANS1(20),BANSL(4),GCTL1(100),GCTL2(100),EP(1
     *                                              00,9)
      COMMON /BLKA/COEF(400,20)/BLKC/IPAGE
      COMMON /BLKE/AMODEL,BMODEL,CMODEL,DMODEL
      REAL KAPPA1,KAPPA2
    1 FORMAT(1H1,2X*PAGE*I3,80X,4A10/)
    2 FORMAT(1H0)
    3 FORMAT(4A10)
    4 FORMAT(A6,A4,3F20.5,I10)
    5 FORMAT(3F10.1)
    6 FORMAT(1H0,3X*(3) ITERATIVE SOLUTION TO SPACE RESECTIO
     *                                              N PROBLEM*)
    7 FORMAT(1H0,3X*MODEL NAME = *4A10,5X*F = *F10.3/)
    8 FORMAT(A6,A4,4F10.3,I20)
    9 FORMAT(1H0,2X,4H***(,1X*ITERATION *I2,1X,4H)***/)
   10 FORMAT(1H1,16HINPUT DATA ERROR,2I10)
   11 FORMAT(1H0, 7X,10HX1,Y1,Z1 =,3F15.3,10X,10HX2,Y2,Z2 =,
     *                                              3F15.3)
   12 FORMAT(1H0,9X*(OMEGA 1)*13X*(PHI 1)*11X*(KAPPA 1)*20X*
     *                                              (OMEGA 2)*
     $13X*(PHI 2)*11X*(KAPPA 2)*)
   13 FORMAT(1H0, 4X,I5,2H -,I3,2H -,F5.1,I8,2H -,I3,2H -,F5
     *                                              .1,I8,2H -,
     $I3,2H -,F5.1,I17,2H -,I3,2H -,F5.1,I8,2H -,I3,2H -,F5.
     *                                              1,I8,2H -,
     $I3,2H -,F5.1)
   14 FORMAT(1H0,17X,37HSPACE RESECTION/INTERSECTION SOLUTIO
     *                                              N/)
   15 FORMAT(1H0,3X*(C) DETERMINATION OF CAMERA STATIONS AND
     *                                               ORIENTATION
     $ PARAMETERS*/)
   16 FORMAT(1H0,8X*(X) =*F15.3,7X*(Y) =*F15.3,7X*(Z) =*F15.
     *                                              3///)
   17 FORMAT(32X,7H(OMEGA),14X,5H(PHI),14X,7H(KAPPA)//)
   18 FORMAT(9X,9H(RADIANS),F23.9,2F20.9//)
   19 FORMAT(9X,9H(DEGREES),I13,2H -,I3,2H -,F5.1,I8,2H -,I3
     *                                              ,2H -,F5.1,
     $I8,2H -,I3,2H -,F5.1//)
   20 FORMAT(9X,7H(GRADS),F25.9,2F20.9//)
```

```
21  FORMAT(9X*(SIN)*F27.9,2F20.9///9X*(COS)*F27.9,2F20.9//
   *                                                  /9X*(TAN)*
   $F27.9,2F20.9///)
22  FORMAT(1H0,8X*(ORIENTATION MATRIX)*//)
23  FORMAT(A6,A4,4F10.5,I20)
24  FORMAT(1H0,36X*(LEFT PHOTO)*45X*(RIGHT PHOTO)*)
25  FORMAT(1HC,5X*(2) TRANSFORMATION OF CONTROL POINT COOR
   *                                                  DINATES*/)
26  FORMAT(1H ,7X*CORRECTION VALUES*///8X*DX1,DY1,DZ1 =*F1
   *                                                  3.4,2F16.4,
   $10X*DX2,DY2,DZ2 =*F12.4,2F15.4/)
27  FORMAT(1H0,3X*MODEL NAME = *4A10/)
28  FORMAT(1H0,3X*(A) REDUCTION OF OBSERVED IMAGE COORDINA
   *                                                  TES TO PRINC
   $IPAL-POINT ORIGIN*/)
29  FORMAT(1H0,5X*(1) TRANSFORMATION OF FIDUCIAL MARK COOR
   *                                                  DINATES*/)
30  FORMAT(1H0,5X*(LEFT PHOTO)*)
31  FORMAT(1H0,5X*(RIGHT PHOTO)*)
32  FORMAT(1H0,24X*(MEASURED)*22X*(GIVEN)*22X*(TRANSFORMED
   *                                                  )*18X*(RESID
   $UALS)*)
33  FORMAT(1H0,7X*(NAME)*8X*(X)*10X*(Y)*15X*(X)*10X*(Y)*15
   *                                                  X*(X)*10X*(Y
   $)*15X*(VX)*8X*(VY)*/)
34  FORMAT(1H0,5X,A6,A4,F11.3,F13.3,F10.3,F13.3,F10.3,F13.
   *                                                  3,F17.3,
   $F12.3)
35  FORMAT(1H0,27X*STANDARD DEVIATION  = *F9.3)
36  FORMAT(1H0,25X*(MEASURED)*15X*(TRANSFORMED)*19X*(MEASU
   *                                                  RED)*15X*(TR
   $ANSFORMED)*)
37  FORMAT(1H0,8X*(NAME)*9X*(X)*8X*(Y)*12X*(X)*8X*(Y)*17X*
   *                                                  (X)*8X*(Y)*
   $12X*(X)*8X*(Y)*/)
38  FORMAT(1H0,6X,A6,A4,F12.3,F11.3,F15.3,F11.3,F20.3,F11.
   *                                                  3,F15.3,
   $F11.3)
39  FORMAT(1H0,5X*(3) TRANSFORMATION OF PASS POINT COORDIN
   *                                                  ATES*/)
40  FORMAT(1H0,5X*(3) TRANSFORMATION OF PASS POINT COORDIN
   *                                                  ATES-----CON
   $TINUED*/)
41  FORMAT(1H0,3X*(D) SPACE INTERSECTION SOLUTION*/)
42  FORMAT(1H0,5X*(1) OBJECT-SPACE COORDINATES OF PASS POI
   *                                                  NTS-----CONT
   $INUED*)
43  FORMAT(1H0,5X*(1) OBJECT-SPACE COORDINATES OF PASS POI
   *                                                  NTS*)
```

```
44  FORMAT(1H0,7X*(NAME)*15X*(X)*20X*(Y)*20X*(Z)*13X*(LEFT
     *                                          VECTOR)*3X
     $*(RIGHT VECTOR)*/)
45  FORMAT(1H0,5X,A6,A4,F18.3,2F23.3)
46  FORMAT(1H0,89X*(DISCREPANCY BETWEEN INTERSECTED*/91X*P
     *                                          OINT AND OBJ
     $ECT-SPACE VECTORS)*)
47  FORMAT(1H0,5X*(2) ACCURACY CHECKING*)
48  FORMAT(1H0,5X*(2) ACCURACY CHECKING-----CONTINUED*)
49  FORMAT(1H ,8X*(GIVEN)*F18.3,2F23.3/)
50  FORMAT(1H ,F40.3,F23.3,F23.3,F13.3,F16.3)
51  FORMAT(1H0,7X*(NAME)*15X*(X)*5X*(DX)*11X*(Y)*5X*(DY)*1
     *                                          1X*(Z)*5X*(D
     $Z)*4X*(LEFT VECTOR)*3X*(RIGHT VECTOR)*/)
52  FORMAT(1H0,5X*(2) TRANSFORMATION OF CONTROL POINT COOR
     *                                          DINATES-----
     $CONTINUED*/)
53  FORMAT(8X*F-CORRECTION = *F11.6)
54  FORMAT(1H0,46X*(STANDARD DEVIATION)*//27X*<DX> =*F8.3,
     *                                          9X*<DY> =*,
     $F8.3,9X*<DZ> =*F8.3)
55  FORMAT(4X*CONVERGED CONVERGED CONVERGED CONVERGED CONV
     *                                          ERGED CONVER
     $GED CONVERGED CONVERGED CONVERGED CONVERGED CONVERGED
     *                                          CONVERGED CO
     $NVERGED*)
56  FORMAT(1H ,25X*+-*54X*-+*)
57  FORMAT(1H ,25X*I*56X*I*)
58  FORMAT(1H ,25X*I*F13.9,2F20.9,3X*I*)
59  FORMAT(1H0,5X,A6,A4,F18.3,2F23.3,F20.3,F16.3/)
60  FORMAT(1H0,7X*DW1,DP1,DK1 =*F13.6* RAD.*F11.6* RAD.*F1
     *                                          1.6* RAD.*
     $5X*DW2,DP2,DK2 =*F12.6* RAD.*F10.6* RAD.*F10.6* RAD.*/
     *                                          /)
61  FORMAT(1H0,9X*TOTAL NUMBER OF CONTROL POINTS = *I3)
62  FORMAT(1H0,9X*TOTAL NUMBER OF PASS POINTS = *I3)
63  FORMAT(4X*END OF PASS  END OF PASS  END OF PASS  END O
     *                                          F PASS  END
     $OF PASS  END OF PASS  END OF PASS  END OF PASS  END OF
     *                                           PASS  END O
     $F PASS*)
64  FORMAT(1H0,5X*(STANDARD DEVIATION)*24X*<DISCREPANCY>*1
     *                                          0X*<X-COMPON
     $ENT>*3X*<Y-COMPONENT>*3X*<Z-COMPONENT>*)
65  FORMAT(1H0,9X*(RESIDUAL PASS-POINT DISCREPANCIES : DIS
     *                                          CREPANCY COM
     $PONENTS IN OBJECT-SPACE COORDINATE SYSTEM)*)
66  FORMAT(1H0,12X*(NAME)*31X*(DISCREPANCY)*10X*(X-COMPONE
     *                                          NT)*3X*(Y-CO
     $MPONENT)*3X*(Z-COMPONENT)*/)
```

```
 67   FORMAT(1HC,10X,A6,A4,10X*(LEFT VECTOR)*F16.3,6X,3F16.3
     *                                        /31X*(RIGHT
     $ VECTOR)*F15.3,6X,3F16.3/)
 68   FORMAT(1HC,30X*(LEFT VECTOR)*F16.3,6X,3F15.3//31X*(RIG
     *                                        HT VECTOR)*
     $F15.3,6X,3F16.3)
 69   FORMAT(1HC,9X*(MATHEMATICAL-MODEL DEFORMATIONS RELATIV
     *                                        E TO GROUND
     $CONTROL POINTS : (DX),(DY),(DZ) )*)
 70   FORMAT(1HC,9X*(DISCREPANCIES OF INTERSECTED GROUND CON
     *                                        TROL POINTS
     $: DISCREPANCY COMPONENTS IN OBJECT-SPACE COORDINATE SY
     *                                        STEM)*)
 71   FORMAT(1HC,9X*(RESIDUAL PASS-POINT DISCREPANCIES : DIS
     *                                        CREPANCY COM
     $PONENTS IN OBJECT-SPACE COORDINATE SYSTEM)-----CONTINU
     *                                        ED*)
 72   FORMAT(1HC,9X*(DISCREPANCIES OF INTERSECTED GROUND CON
     *                                        TROL POINTS
     $: DISCREPANCY COMPONENTS IN OBJECT-SPACE COORDINATE SY
     *                                        STEM)*/55X,
     $59X*-----CONTINUED*)
 73   FORMAT(1HC,9X*(MATHEMATICAL-MODEL DEFORMATIONS RELATIV
     *                                        E TO GROUND
     $CONTROL POINTS : (DX),(DY),(DZ) )-----CONTINUED*)
      DO 500 NDATA=1,20
      IPAGE=1
      READ(5,3) AMODEL,BMODEL,CMODEL,DMODEL
      IF(EOF,5) 1000,99
 99   READ(5,5) FL
      READ(5,5) XCL,YCL,ZCL
      READ(5,5) XCR,YCR,ZCR
      READ(5,5) OMEGA1,PHI1,KAPPA1
      READ(5,5) OMEGA2,PHI2,KAPPA2
      WRITE(6,1) IPAGE,AMODEL,BMODEL,CMODEL,DMODEL
      WRITE(6,14)
      WRITE(6,7)  AMODEL,BMODEL,CMODEL,DMODEL,FL
      WRITE(6,28)
      WRITE(6,2)
      WRITE(6,29)
      WRITE(6,30)
      DO 350 I=1,10
      READ(5,23) AFID(I),BFID(I),(FDM(I,J),J=1,4),IEND
      IF(IEND.GT.0) GO TO 351
350   CONTINUE
351   IFID=I-1
      IGO = 1
      CALL HELCO(FDM,IFID,HELL,BANSL,STDVL)
300   WRITE(6,32)
      WRITE(6,33)
```

```
      DO 301 I=1,IFID
      L=I*2-1
      WRITE(6,34)  AFID(I),BFID(I),FDM(I,3),FDM(I,4),FDM(I,1)
     *                                        ,FDM(I,2),
     $HELL(L),HELL(L+1),HELL(L+8),HELL(L+9)
  301 CONTINUE
      WRITE(6,2)
      WRITE(6,35)  STOVL
      WRITE(6,2)
      GO TO (302,303),IGO
  302 DO 304 I=1,10
      READ(5,23) AFID(I),BFID(I),(FDM(I,J),J=1,4),IEND
      IF(IEND) 304,304,305
  304 CONTINUE
  305 IFID=I-1
      IGO = 2
      CALL HELCO(FDM,IFID,HELL,BANSR,STOVL)
      WRITE(6,2)
      WRITE(6,31)
      GO TO 300
  303 IPAGE=IPAGE+1
      DO 100 I=1,100
      READ(5,4) GCTL1(I),GCTL2(I),XG(I),YG(I),ZG(I),IEND
      IF(IEND) 100,100,101
  100 CONTINUE
  101 IGCTL=I-1
      DO 102 I=1,100
      READ(5,8) PCTL1(I),PCTL2(I),XPC1(I),YPC1(I),XPC2(I),YP
     *                                        C2(I),IEND
      IF(IEND) 102,102,103
  102 CONTINUE
  103 IPCTL=I-1
      IF(IGCTL.EQ.IPCTL) GO TO 104
      WRITE(6,10) IGCTL,IPCTL
      GO TO 1000
  104 DO 105 I=1,200
      READ(5,8) PASSP1(I),PASSP2(I),XPASS1(I),YPASS1(I),XPAS
     *                                        S2(I),
     $YPASS2(I),IEND
      IF(IEND) 105,105,106
  105 CONTINUE
  106 IPASS=I-1
      CALL PAGE(3,3,P)
      WRITE(6,25)
      WRITE(6,61) IPCTL
      WRITE(6,24)
      WRITE(6,36)
      WRITE(6,37)
      DO 109 I=1,IPCTL
      CALL HELMT(BANSL,XPC1(I),YPC1(I),HX,HY)
```

```
      AB1=XPC1(I)
      AB2=YPC1(I)
      XPC1(I)=HX
      YPC1(I)=HY
      CALL HELMT(BANSR,XPC2(I),YPC2(I),HX,HY)
      CALL PAGE(I,23,P)
      IF(P) 109,108,107
  107 WRITE(6,52)
      WRITE(6,24)
      WRITE(6,36)
      WRITE(6,37)
  108 WRITE(6,38) PCTL1(I),PCTL2(I),AB1,AB2,XPC1(I),YPC1(I),
     *                                          XPC2(I),
     $YPC2(I),HX,HY
      XPC2(I)=HX
      YPC2(I)=HY
  109 CONTINUE
      CALL PAGE(3,3,P)
      WRITE(6,39)
      WRITE(6,62) IPASS
      WRITE(6,24)
      WRITE(6,36)
      WRITE(6,37)
      DO 112 I=1,IPASS
      CALL HELMT(BANSL,XPASS1(I),YPASS1(I),HX,HY)
      AB1=XPASS1(I)
      AB2=YPASS1(I)
      XPASS1(I)=HX
      YPASS1(I)=HY
      CALL HELMT(BANSR,XPASS2(I),YPASS2(I),HX,HY)
      CALL PAGE(I,23,P)
      IF(P) 112,111,110
  110 WRITE(6,40)
      WRITE(6,24)
      WRITE(6,36)
      WRITE(6,37)
  111 WRITE(6,38) PASSP1(I),PASSP2(I),AB1,AB2,XPASS1(I),YPAS
     *                                          S1(I),
     $XPASS2(I),YPASS2(I),HX,HY
      XPASS2(I)=HX
      YPASS2(I)=HY
  112 CONTINUE
      CALL PAGE(3,3,P)
      WRITE(6,14)
      WRITE(6,7)  AMODEL,BMODEL,CMODEL,DMODEL,FL
      WRITE(6,6)
      CALL PAGE(3,3,P)
      ITER=1
  199 WRITE(6,2)
      WRITE(6,9) ITER
```

```
      WRITE(6,11)  XCL,YCL,ZCL,XCR,YCR,ZCR
      WRITE(6,2)
      CALL  DMS(OMEGA1,I1,J1,01)
      CALL  DMS(OMEGA2,I4,J4,04)
      CALL  DMS(PHI1,I2,J2,02)
      CALL  DMS(PHI2,I5,J5,05)
      CALL  DMS(KAPPA1,I3,J3,03)
      CALL  DMS(KAPPA2,I6,J6,05)
      WRITE(6,12)
      WRITE(6,13)  I1,J1,01,I2,J2,02,I3,J3,03,I4,J4,04,I5,J5,
     *                                                 05,I6,J6,06
      WRITE(6,2)
C     ZEROING
      N=IGCTL *4
      DO 200 I=1,N
      DO 200 J=1,14
  200 COEF(I,J)=0.0
      CALL  GRUBER(OMEGA1,PHI1,KAPPA1,C1)
      CALL  GRUBER(OMEGA2,PHI2,KAPPA2,C2)
      DO 202 I=1,IGCTL
      U1=XG(I)-XCL
      U2=XG(I)-XCR
      V1=YG(I)-YCL
      V2=YG(I)-YCR
      W1=ZG(I)-ZCL
      W2=ZG(I)-ZCR
      CALL  COEFF(U1,V1,W1,XPC1(I),YPC1(I),FL,C1,E1)
      CALL  COEFF(U2,V2,W2,XPC2(I),YPC2(I),FL,C2,E2)
      J=I*4-3
      DO 202 L=1,6
      COEF(J,L)=E1(1,L+1)
      COEF(J+1,L)=E1(2,L+1)
      COEF(J+2,L+6)=E2(1,L+1)
      COEF(J+3,L+6)=E2(2,L+1)
      COEF(J,13)=E1(1,8)
      COEF(J+1,13)=E1(2,8)
      COEF(J+2,13)=E2(1,8)
  202 COEF(J+3,13)=E2(2,8)
      NU=12
      CALL  NORMAL(NU,N,ANSWER)
      DO 203 I=1,13
      ANS(I)=ANSWER(I)
  203 CONTINUE
      WRITE(6,26)  ANS(4),ANS(5),ANS(6),ANS(10),ANS(11),ANS(1
     *                                                    2)
      WRITE(6,60)  ANS(1),ANS(2),ANS(3),ANS(7),ANS(8),ANS(9)
      WRITE(6,2)
      WRITE(6,2)
      OMEGA1=OMEGA1+ANSWER(1)
      PHI1=PHI1+ANSWER(2)
```

```
      KAPPA1=KAPPA1+ANSWER(3)
      XCL=XCL+ANSWER(4)
      YCL=YCL+ANSWER(5)
      ZCL=ZCL+ANSWER(6)
      OMEGA2=OMEGA2+ANSWER(7)
      PHI2=PHI2+ANSWER(8)
      KAPPA2=KAPPA2+ANSWER(9)
      XCR=XCR+ANSWER(10)
      YCR=YCR+ANSWER(11)
      ZCR=ZCR+ANSWER(12)
      CALL PAGE(ITER,2,P)
C     TEST FOR CONVERGENCY
      ITER=ITER+1
      DO 207 I=1,3
      IF( ABS(ANSWER(I))   .GT.  0.000001) GO TO 199
      IF( ABS(ANSWER(I+3)) .GT. 0.000001) GO TO 199
      IF( ABS(ANSWER(I+6)) .GT.  0.0001)   GO TO 199
      IF( ABS(ANSWER(I+9)) .GT.  0.001)    GO TO 199
  207 CONTINUE
      WRITE(6,2)
      WRITE(6,2)
      DO 204 ILK=1,6
      WRITE(6,2)
  204 WRITE(6,55)
      CALL PAGE(3,3,P)
      WRITE(6,14)
      WRITE(6,7) AMODEL,BMODEL,CMODEL,DMODEL,FL
      WRITE(6,2)
      WRITE(6,15)
      WRITE(6,30)
      WRITE(6,2)
      CALL GRUBER(OMEGA1,PHI1,KAPPA1,C1)
      CALL DMS(OMEGA1,IDG1,MT1,SC1)
      CALL DMS(PHI1,IDG2,MT2,SC2)
      CALL DMS(KAPPA1,IDG3,MT3,SC3)
      CALL GRAD(OMEGA1,GRD1)
      CALL GRAD(PHI1,GRD2)
      CALL GRAD(KAPPA1,GRD3)
      WRITE(6,16)  XCL,YCL,ZCL
      WRITE(6,17)
      WRITE(6,19)  IDG1,MT1,SC1,IDG2,MT2,SC2,IDG3,MT3,SC3
      WRITE(6,18)  OMEGA1,PHI1,KAPPA1
      WRITE(6,20)  GRD1,GRD2,GRD3
      WRITE(6,21)  C1(2,1),C1(2,2),C1(2,3),C1(3,1),C1(3,2),C1
     *                                                 (3,3),
     $C1(1,1),C1(1,2),C1(1,3)
      WRITE(6,22)
      WRITE(6,2)
      WRITE(6,56)
      DO 208 I=4,5
```

```
      WRITE(6,58) C1(I,1),C1(I,2),C1(I,3)
      WRITE(6,57)
208   CONTINUE
      WRITE(6,58) C1(6,1),C1(6,2),C1(6,3)
      WRITE(6,56)
      CALL PAGE(3,3,P)
      WRITE(6,2)
      WRITE(6,15)
      WRITE(6,2)
      WRITE(6,31)
      WRITE(6,2)
      CALL GRUBER(OMEGA2,PHI2,KAPPA2,C2)
      CALL DMS(OMEGA2,IDG1,MT1,SC1)
      CALL DMS(PHI2,IDG2,MT2,SC2)
      CALL DMS(KAPPA2,IDG3,MT3,SC3)
      CALL GRAD(OMEGA2,GRD1)
      CALL GRAD(PHI2,GRD2)
      CALL GRAD(KAPPA2,GRD3)
      WRITE(6,16) XCR,YCR,ZCR
      WRITE(6,17)
      WRITE(6,19) IDG1,MT1,SC1,IDG2,MT2,SC2,IDG3,MT3,SC3
      WRITE(6,18) OMEGA2,PHI2,KAPPA2
      WRITE(6,20) GRD1,GRD2,GRD3
      WRITE(6,21) C2(2,1),C2(2,2),C2(2,3),C2(3,1),C2(3,2),C2
     *                                              (3,3),
     $C2(1,1),C2(1,2),C2(1,3)
      WRITE(6,22)
      WRITE(6,2)
      WRITE(6,2)
      WRITE(6,56)
      DO 209 I=4,5
      WRITE(6,58) C2(I,1),C2(I,2),C2(I,3)
      WRITE(6,57)
209   CONTINUE
      WRITE(6,58) C2(6,1),C2(6,2),C2(6,3)
      WRITE(6,56)
      CALL PAGE(3,3,P)
      WRITE(6,14)
      WRITE(6,7) AMODEL,BMODEL,CMODEL,DMODEL,FL
      WRITE(6,2)
      WRITE(6,41)
      CALL PAGE(3,3,P)
      WRITE(6,43)
      WRITE(6,62) IPASS
      WRITE(6,46)
      WRITE(6,44)
      NU=3
      JK=6
      IGO=1
      STOVX=0.0
```

```
      STDVY=0.0
      STDVZ=0.0
      VECTL=0.0
      VECTR=0.0
      GHA=0.0
      GHB=0.0
      GHC=0.0
      GHD=0.0
      GHE=0.0
      GHF=0.0
402   DO 400 J=1, IPASS
      CALL DCVECT(C1,FL,XPASS1(J),YPASS1(J),XSL,YSL,ZSL)
      CALL DCVECT(C2,FL,XPASS2(J),YPASS2(J),XSR,YSR,ZSR)
      COEF(1,1)=YSL
      COEF(1,2)=XSL*(-1.0)
      COEF(1,3)=0.0
      COEF(1,4)=YSL*XCL-XSL*YCL
      COEF(2,1)=YSR
      COEF(2,2)=XSR*(-1.0)
      COEF(2,3)=0.0
      COEF(2,4)=YSR*XCR-XSR*YCR
      COEF(3,1)=0.0
      COEF(3,2)=ZSL
      COEF(3,3)=YSL*(-1.0)
      COEF(3,4)=ZSL*YCL-YSL*ZCL
      COEF(4,1)=0.0
      COEF(4,2)=ZSR
      COEF(4,3)=YSR*(-1.0)
      COEF(4,4)=ZSR*YCR-YSR*ZCR
      COEF(5,1)=ZSL
      COEF(5,2)=0.0
      COEF(5,3)=XSL*(-1.0)
      COEF(5,4)=ZSL*XCL-XSL*ZCL
      COEF(6,1)=ZSR
      COEF(6,2)=0.0
      COEF(6,3)=XSR*(-1.0)
      COEF(6,4)=ZSR*XCR-XSR*ZCR
      CALL NORMAL(NU,JK,ANSWER)
      SA=ANSWER(1)-XCL
      SB=ANSWER(2)-YCL
      SC=ANSWER(3)-ZCL
      SD=ANSWER(1)-XCR
      SE=ANSWER(2)-YCR
      SF=ANSWER(3)-ZCR
      AM1=(SA*XSL+SB*YSL+SC*ZSL)/(XSL**2+YSL**2+ZSL**2)
      AM2=(SD*XSR+SE*YSR+SF*ZSR)/(XSR**2+YSR**2+ZSR**2)
      XHH=XCL+AM1*XSL-ANSWER(1)
      YHH=YCL+AM1*YSL-ANSWER(2)
      ZHH=ZCL+AM1*ZSL-ANSWER(3)
      XXH=XCR+AM2*XSR-ANSWER(1)
```

```
      YYH=YCR+AM2*YSR-ANSWER(2)
      ZZH=ZCR+AM2*ZSR-ANSWER(3)
      PSS=(SA*XSL+SB*YSL+SC*ZSL)**2
      QSS=(SD*XSR+SE*YSR+SF*ZSR)**2
      SS=SA**2+SB**2+SC**2-PSS/(XSL**2+YSL**2+ZSL**2)
      ST=SD**2+SE**2+SF**2-QSS/(XSR**2+YSR**2+ZSR**2)
      SSQ=SQRT(ABS(SS))
      STQ=SQRT(ABS(ST))*(-1.0)
      VECTL=VECTL+ABS(SS)
      VECTR=VECTR+ABS(ST)
      GHA=GHA+XHH**2
      GHB=GHB+YHH**2
      GHC=GHC+ZHH**2
      GHD=GHD+XXH**2
      GHE=GHE+YYH**2
      GHF=GHF+ZZH**2
      EP(J,1)=SSQ
      EP(J,2)=XHH*(-1.0)
      EP(J,3)=YHH*(-1.0)
      EP(J,4)=ZHH*(-1.0)
      EP(J,5)=STQ
      EP(J,6)=XXH*(-1.0)
      EP(J,7)=YYH*(-1.0)
      EP(J,8)=ZZH*(-1.0)
      IF(IGO-1) 400,406,405
405   VX=ANSWER(1)-XG(J)
      VY=ANSWER(2)-YG(J)
      VZ=ANSWER(3)-ZG(J)
      CALL PAGE(J,9,P)
      IF(P) 400,407,408
408   WRITE(6,48)
      WRITE(6,73)
      WRITE(6,46)
      WRITE(6,51)
407   WRITE(6,45) PASSP1(J),PASSP2(J),(ANSWER(L),L=1,3)
      WRITE(6,50) VX,VY,VZ,SSQ,STQ
      WRITE(6,49) XG(J),YG(J),ZG(J)
      STDVX=STDVX+VX**2
      STDVY=STDVY+VY**2
      STDVZ=STDVZ+VZ**2
      GO TO 400
406   CALL PAGE(J,16,P)
      IF(P) 400,409,410
410   WRITE(6,42)
      WRITE(6,46)
      WRITE(6,44)
409   WRITE(6,59) PASSP1(J),PASSP2(J),(ANSWER(L),L=1,3),SSQ,
     *                                                   STQ
400   CONTINUE
      IF(IGO-1) 428,427,428
```

```
428   STDVX=SQRT(STDVX/FLOAT(IPCTL))
      STDVY=SQRT(STDVY/FLOAT(IPCTL))
      STDVZ=SQRT(STDVZ/FLOAT(IPCTL))
      WRITE(6,2)
      WRITE(6,54)  STDVX,STDVY,STDVZ
427   VECTL=SQRT(VECTL/FLOAT(IPASS))
      VECTR=SQRT(VECTR/FLOAT(IPASS))*(-1.0)
      GHA=SQRT(GHA/FLOAT(IPASS))
      GHB=SQRT(GHB/FLOAT(IPASS))
      GHC=SQRT(GHC/FLOAT(IPASS))
      GHD=SQRT(GHD/FLOAT(IPASS))*(-1.0)
      GHE=SQRT(GHE/FLOAT(IPASS))*(-1.0)
      GHF=SQRT(GHF/FLOAT(IPASS))*(-1.0)
      CALL PAGE(3,3,P)
      WRITE(6,2)
      IF(IGO-1) 435,435,436
435   WRITE(6,47)
      GO TO 437
436   WRITE(6,48)
437   IF(IGO-1) 423,423,424
423   WRITE(6,65)
      WRITE(6,62)  IPASS
      GO TO 425
424   WRITE(6,70)
      WRITE(6,61)   IPCTL
425   WRITE(6,2)
      WRITE(6,64)
      WRITE(6,58)  VECTL,GHA,GHB,GHC,VECTR,GHD,GHE,GHF
      WRITE(6,2)
      WRITE(6,2)
      WRITE(6,66)
      IPG=3
      DO 450 J=1,IPASS
      CALL PAGE(IPG,9,P)
      IF(P) 420,420,421
421   WRITE(6,48)
      IF(IGO-1) 430,430,431
430   WRITE(6,71)
      GO TO 432
431   WRITE(6,72)
432   WRITE(6,2)
      WRITE(6,66)
420   WRITE(6,67)  PASSP1(J),PASSP2(J),(EP(J,I),I=1,8)
      IPG=IPG+1
450   CONTINUE
      GO TO (411,413),IGO
411   DO 412 I=1,IPCTL
      XPASS1(I)=XPC1(I)
      XPASS2(I)=XPC2(I)
      YPASS1(I)=YPC1(I)
```

```
      YPASS2(I)=YPC2(I)
      PASSP1(I)=PCTL1(I)
  412 PASSP2(I)=PCTL2(I)
      CALL PAGE(3,3,P)
      WRITE(6,2)
      WRITE(6,48)
      WRITE(6,69)
      WRITE(6,61) IPCTL
      WRITE(6,46)
      WRITE(6,51)
      LPASS=IPASS
      IPASS=IPCTL
      VECTL=0.0
      VECTR=0.0
      GHA=0.0
      GHB=0.0
      GHC=0.0
      GHD=0.0
      GHE=0.0
      GHF=0.0
      IGO=2
      GO TO 402
  413 CALL PAGE(3,3,P)
      DO 498 I=1,3
  498 WRITE(6,2)
      DO 499 I=1,15
      WRITE(6,2)
  499 WRITE(6,63)
  500 CONTINUE
 1000 STOP
      END
```

```
      SUBROUTINE HELCO(FOM,IFIO,HEL,BANS,STDV)
      DIMENSION FOM(10,6),HEL(200),ANS1(20),BANS(4)
      COMMON /BLKA/COEF(400,20)
      DO 1 I=1,IFIO
      J=I*2-1
      COEF(J,1)=FOM(I,3)
      COEF(J,2)=FOM(I,4)
      COEF(J,3)=1.0
      COEF(J,4)=0.0
      COEF(J,5)=FOM(I,1)
      COEF(J+1,1)=FOM(I,4)
      COEF(J+1,2)=FOM(I,3)*(-1.0)
      COEF(J+1,3)=0.0
      COEF(J+1,4)=1.0
      COEF(J+1,5)=FOM(I,2)
    1 CONTINUE
      JK=IFIO*2
      NU=4
      CALL NORMAL(NU,JK,ANS1)
      DO 3 I=1,JK
      HEL(I)=0.0
      DO 3 J=1,NU
    3 HEL(I)=HEL(I)+COEF(I,J)*ANS1(J)
      DO 4 I=1,JK
      L=I+JK
      HEL(L)=HEL(I)-COEF(I,5)
    4 CONTINUE
      DO 5 I=1,NU
    5 BANS(I)=ANS1(I)
      STDV=0.0
      DO 6 I=1,JK
    6 STDV=STDV+HEL(I+JK)**2
      STDV= SQRT(STDV/(FLOAT(JK)-5.0))
      RETURN
      END
      SUBROUTINE GRUBER (OMEGA,PHI,AKAPPA,C)
      DIMENSION C(15,3)
      C(1,1)=TAN(OMEGA)
      C(1,2)=TAN(PHI)
      C(1,3)=TAN(AKAPPA)
      C(2,1)=SIN(OMEGA)
      C(2,2)=SIN(PHI)
      C(2,3)=SIN(AKAPPA)
      C(3,1)=COS(OMEGA)
      C(3,2)=COS(PHI)
      C(3,3)=COS(AKAPPA)
      C(4,1)=C(3,2)*C(3,3)
      C(5,1)=C(3,2)*C(2,3)*(-1.0)
      C(6,1)=C(2,2)
      C(10,1)=C(2,2)*C(3,3)*(-1.0)
```

```
      C(11,1)=C(2,2)*C(2,3)
      C(12,1)=C(3,2)
      C(10,2)=C(4,1)*C(2,1)
      C(11,2)=C(5,1)*C(2,1)
      C(12,2)=C(2,1)*C(2,2)
      C(10,3)=C(4,1)*C(3,1)*(-1.0)
      C(11,3)=C(5,1)*C(3,1)*(-1.0)
      C(12,3)=C(3,1)*C(2,2)*(-1.0)
      C(4,2)=C(3,1)*C(2,3)+C(12,2)*C(3,3)
      C(5,2)=C(3,1)*C(3,3)-C(12,2)*C(2,3)
      C(6,2)=C(2,1)*C(3,2)*(-1.0)
      C(4,3)=C(2,1)*C(2,3)+C(10,1)*C(3,1)
      C(5,3)=C(2,1)*C(3,3)+C(11,1)*C(3,1)
      C(6,3)=C(3,1)*C(3,2)
      DO 1 I=7,9
      C(I,1)=0.0
      C(I,2)=C(I-3,3) *(-1.0)
      C(I,3)=C(I-3,2)
      C(13,I-6)=C(5,I-6)
      C(14,I-6)=-C(4,I-6)
    1 C(15,I-6)=0.0
      RETURN
      END
      SUBROUTINE HELMT(A,XO,YO,XH,YH)
      DIMENSION A(15)
      XH=A(1)*XO+A(2)*YO+A(3)
      YH=A(1)*YO-A(2)*XO+A(4)
      RETURN
      END
      SUBROUTINE COEFF(DXG,DYG,DZG,XP,YP,FOCAL,D,E)
      DIMENSION D(15,3),E(2,9),F(4,3),P(2)
      K=4
      P(1)=XP
      P(2)=YP
      DO 1 I=1,4
      DO 1 J=1,3
      F(I,J)=D(K,1)*DXG+D(K,2)*DYG+D(K,3)*DZG
    1 K=K+1
      DO 4 I=1,2
      DO 2 J=1,4
    2 E(I,J)=(P(I)*F(J,3)+FOCAL*F(J,I))/F(1,3)
      DO 3 J=5,7
    3 E(I,J)=(P(I)*(-1.0)*D(5,J-4)-FOCAL*D(I+3,J-4))/F(1,3)
    4 E(I,8)=E(I,1)*(-1.0)
      RETURN
      END
      SUBROUTINE NORMAL(NU,NEQS,ANSWER)
      DIMENSION EN(20,20),ANSWER(20)
      COMMON /BLKA/COEF(400,20)
C     FORMATION OF NORMAL EQUATION FROM OBSERVATION EQS
```

```
      NP1=NU+1
      NM1=NU-1
      DO 9 I=1,NU
      DO 9 J=1,NP1
    9 EN(I,J)=0.0
      DO 1 I=1,NU
      DO 1 J=I,NP1
      DO 1 K=1,NEQS
    1 EN(I,J)=EN(I,J)+COEF(K,I)*COEF(K,J)
C     SOLUTION BY GAUSS ELIMINATION
      DO 2 I=1,NU
      SQR= SQRT(EN(I,I))
      DO 3 J=I,NP1
    3 EN(I,J)=EN(I,J)/SQR
      IF(I-NU) 4,5,5
    4 IP1=I+1
      DO 2 L=IP1,NU
      DO 2 J=L,NP1
    2 EN(L,J)=EN(L,J)-EN(I,L)*EN(I,J)
    5 EN(NU,NP1)=EN(NU,NP1)/EN(NU,NU)
      DO 6 I=1,NM1
      NMI=NU-I
      NMIP1=NMI+1
      DO 7 J=NMIP1,NU
    7 EN(NMI,NP1)=EN(NMI,NP1)-EN(J,NP1)*EN(NMI,J)
    6 EN(NMI,NP1)=EN(NMI,NP1)/EN(NMI,NMI)
      DO 8 I=1,NU
    8 ANSWER(I)=EN(I,NP1)
      RETURN
      END
      SUBROUTINE DCVECT(C,FL,X,Y,DCX,DCY,DCZ)
      DIMENSION C(15,3)
      VT=SQRT(X**2+Y**2+FL**2)
      XV=X/VT
      YV=Y/VT
      ZV=-FL/VT
      DCX=C(4,1)*XV+C(5,1)*YV+C(6,1)*ZV
      DCY=C(4,2)*XV+C(5,2)*YV+C(6,2)*ZV
      DCZ=C(4,3)*XV+C(5,3)*YV+C(6,3)*ZV
      RETURN
      END
      SUBROUTINE DMS (RAD,IDG, MINT,SC)
      IMINT=0
      IDEG=0
      S= ABS(RAD)*206264.806
   10 S=S-60.0
      IF(S.LT.0.0) GO TO 11
      IMINT=IMINT+1
      GO TO 10
   11 SC=S+60.0
```

```
12  IMINT=IMINT-60
    IF(IMINT.LT.0) GO TO 13
    IDEG=IDEG+1
    GO TO 12
13  MINT=IMINT+60
    MINT=IABS(MINT)
    SC=ABS(SC)
    IF(RAD.GE.0.0) GO TO 14
    IDG=IDEG*(-1)
    RETURN
14  IDG=IDEG
    RETURN
    END
    SUBROUTINE GRAD (RADAN,GRD)
    S=RADAN*200.0/3.14159265359
    GRD=S
    RETURN
    END
    SUBROUTINE PAGE(I,L,P)
    COMMON /BLKC/IPAGE
    COMMON /BLKE/AMODEL,BMODEL,CMODEL,DMODEL
    IF(MOD(I,L).EQ.0) GO TO 1
    P=0.0
    RETURN
1   WRITE(6,2) IPAGE,AMODEL,BMODEL,CMODEL,DMODEL
 2  FORMAT(1H1,2X*PAGE*I3,30X,4A10/)
    P=1.0
    IPAGE=IPAGE+1
    RETURN
    END
```

APPENDIX III

Program CURFIT: Least Squares polynomial curve-fitting routine

Input data deck for CURFIT program:

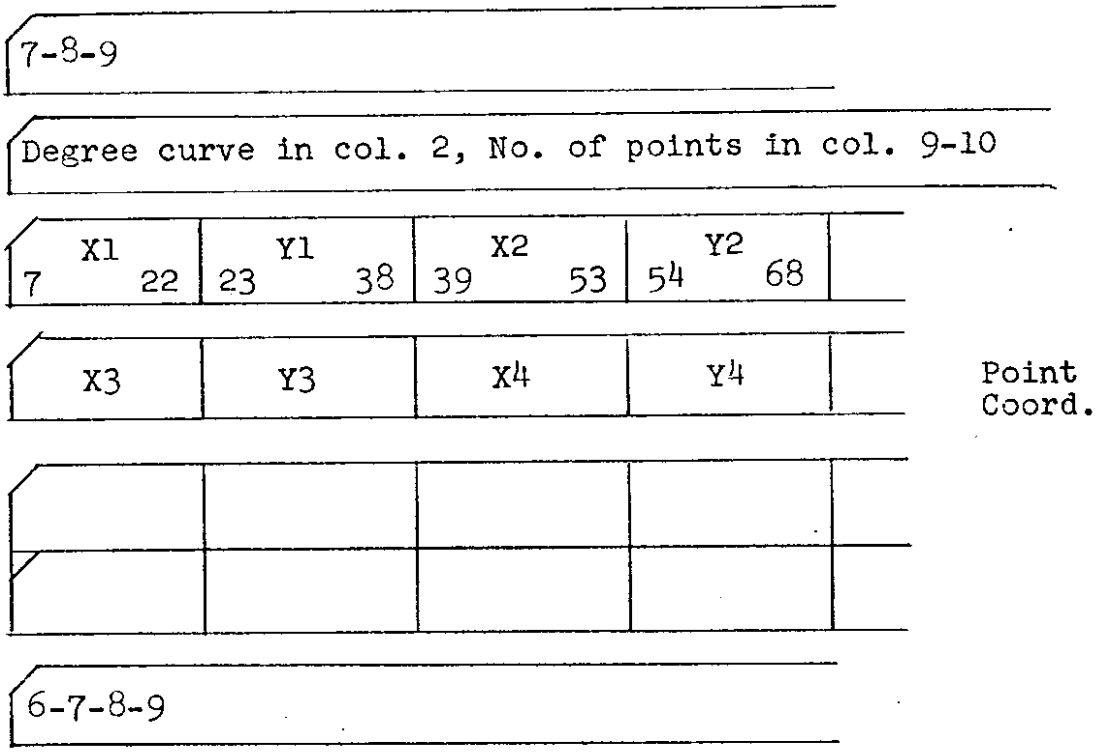

```
      PROGRAM CURFIT(INPUT,OUTPUT,TAPE5=INPUT,TAPE6=OUTPUT)
C     LEAST-SQUARES POLYNOMIAL CURVE FITTING BY TRIANGULATIO
     *                                                      N
C     (GAUSS ELIMINATION) AND USING ROW INTERCHANGES TO REDU
     *                                                      CE ERROR
C
      DIMENSION A(100),C(100),V(100,100),SP(200), X(1000),Y(
     *                                                      1000)
 1    READ(5,200) IDEG, NDATA
 1000 ID2 = 2*IDEG
      M = IDEG + 1
      WRITE(6,400) NDATA, IDEG
      WRITE(6,500)
      READ(5,100) (X(I), Y(I), I=1,NDATA)
 1112 WRITE(6,300) (X(I), Y(I), I=1,NDATA)
C     SUMS OF POWERS OF X(I), AND CONSTANTS OF EQUATIONS
 1111 DO 3 I=1,ID2
      SP(I) = 0.
      DO 3 J=1,NDATA
 3    SP(I) = SP(I) + X(J)**I
      C(1) = 0.
      DO 4 J=1,NDATA
 4    C(1) = C(1) + Y(J)
      DO 6 K=2,M
      C(K) = 0.
      DO 6 J=1,NDATA
 6    C(K) = C(K) + Y(J)*X(J)**(K-1)
C     A(I) ARE THE COEFFICIENTS OF THE DESIRED POLYNOMIAL
C THE V(I,J) ARE THE COEFFICIENTS OF THE A(I)IN THE SIMULTAN
     *                                                      EOUS
C EQUATIONS, AND ARE THE SP(I) OCCURRING AS A SYMMETRIC ARRA
     *                                                      Y
      DO 5 I=1,M
      DO 5 J=1,M
      K = I+J - 2
      IF(K.NE.0) GO TO 7
      V(1,1) = NDATA
      GO TO 5
 7    V(I,J) = SP(K)
 5    CONTINUE
C     ROW REARRANGEMENT TO MAXIMIZE DIAGONAL ELEMENTS
C     MAXIMIZE THE ABSOLUTE VALUE OF V(L,L) OVER THE REMAINI
     *                                                      NG M-L+1
C ROWS, L=1,M
      DO 20 I=1,IDEG
      L = I
      J = I + 1
      DO 8 K=J,M
 8    IF(ABS(V(L,I)).LT.ABS(V(K,I)))  L = K
C     INTERCHANGE ROWS IF NECESSARY
```

```
      IF(L.EQ.I)   GO TO 15
      DO 9 JJ=1,M
      TSTO = V(I,JJ)
      V(I,JJ) = V(L,JJ)
 9    V(L,JJ) = TSTO
      TSTO = C(I)
      C(I) = C(L)
      C(L) = TSTO
C     TRIANGULATION OF V(I,J) ARRAY
 15   DO 20 K=J,M
      Q = V(K,I)/V(I,I)
      DO 30 II=1,M
 30   V(K,II) = V(K,II) - Q*V(I,II)
 20   C(K) = C(K) - Q*C(I)
C     SOLVE FOR A(I) IN TRIANGULAR ARRAY
      A(M) = C(M)/V(M,M)
      DO 50 I=1,IDEG
      J = M - I
      K = J + 1
      S = 0.
      DO 40 L=K,M
 40   S = S + V(J,L)*A(L)
 50   A(J) = (C(J) - S)/V(J,J)
      WRITE(6,600) A(1)
      IF(IDEG.EQ.0) GO TO 2001
      DO 2000 I=2,M
      J= I - 1
 2000 WRITE(6,700) I, A(I), J
 2001 CONTINUE
      DIMENSION YC(1000)
      DO 44 J=1,NDATA
      YC(J) = A(1)
      DO 44 I=2,M
 44   YC(J) = YC(J) + A(I)*X(J)**(I-1)
       WRITE(6,299)
      WRITE(6,300) (Y(I), YC(I), I=1,NDATA)
      P = 0.
      DO 45 I=1,NDATA
 45   P = P + (Y(I) - YC(I))**2
      D = NDATA
      SEE = SQRT(P/D)
 46   WRITE(6,102) SEE, P
      GO TO 1
 102  FORMAT(1H0,30HSTANDARD ERROR OF ESTIMATE IS ,E12.4,/1X
     *                                          ,29HSUM OF
     1DEVIATIONS SQUARED IS ,E12.4 )
 100  FORMAT(6X,4F15.8)
 200  FORMAT(I2,4X,I4)
 299   FORMAT(1H0,1X,11H(Y) - INPUT ,3X,10HCALCULATED   )
```

```
300   FORMAT(1H ,/1H ,F12.7,2X,F12.7)
400  FORMAT(1H1, 5X,24HNUMBER OF DATA SETS IS  ,I4,17X,24HP
     *                                          OLYNOMIAL HA
     1S DEGREE    ,I2)
500   FORMAT(1H0,7X,1HX,13X,1HY)
600  FORMAT(1H0,13X, 8HA( 1) = , E16.8, 10X, 13HCONSTANT TE
     *                                       RM)
700  FORMAT(1H0,13X,2HA(,I2,4H) = ,E16.8,10X,18HCOEFFICIENT
     *                                        OF X**,I2)
      STOP
      END
```